UNIVERSITY OF OKLAHOMA

GRADUATE COLLEGE

ROLE OF ATP BINDING AND HYDROLYSIS IN ASSEMBLY OF MACAB-TOLC MACROLIDE TRANSPORTER

A DISSERTATION

SUBMITTED TO THE GRADUATE FACULTY

In partial fulfillment of the requirements for the

Degree of

DOCTOR OF PHILOSOPHY

By

SHUO LU

Norman, Oklahoma

2013

Downloaded from SHAREOK. Persistent Handle URL: https://hdl.handle.net/11244/318486

ROLE OF ATP BINDING AND HYDROLYSIS IN ASSEMBLY OF MACAB-TOLC MACROLIDE TRANSPORTER

A DISSERTATION APPROVED FOR THE
DEPARTMENT OF CHEMISTRY AND BIOCHEMISTRY

BY

_____

Dr. Helen I. Zgurskaya, Chair

_____

Dr. Valentin V. Rybenkov

_____

Dr. Susan J. Schroeder

_____

Dr. Jun Li

_____

Dr. Elizabeth A.Karr

© Copyright by SHUO LU 2013
All Rights Reserved

Acknowledgements

As time flies by, it finally becomes to the end of my Ph.D. life in the University of Oklahoma. Looking back at the past five and a half years, I have a very complicated feeling about this long and tough journey. I know that I cannot achieve any success without the help and support of so many people in my life.

I would like to express my sincere gratitude to my mentor and advisor Dr. Helen I. Zgurskaya for her support, advice and instruction through the years. Her optimistic attitude, rigorous thoughts and profound knowledge set a real model for me as a scientist. I cannot accomplish anything without her constant patience and motivation. I will always remember the time we spent together on discussing results, exchanging thoughts and planning new experiments. I must say that she has had the most indelible imprint on my life. I would also like to thank Dr. Valentin V. Rybenkov for his valuable suggestions and incisive criticisms about my research. I have learned from him that passion and creativity are the two key characters required to be successful as a true scientist. I am also grateful to all the people have been in my committee, Dr. Susan J. Schroeder, Dr. Elizabeth A. Karr, Dr. Jun Li, Dr. Philip E. Klebba and Dr. Ann West for their precious time and meaningful discussions during my general exams, annual evaluations and biochemistry seminars.

I would like to say thanks to all the members from Dr. Zgurskaya's and Dr. Rybenkov's lab with whom I have shared a great time in the past few the years. A special thank belongs to Dr. Elena Tikhonova for teaching me all the basic experimental skills at the beginning of my research and being continuously supportive especially when I met problems. I would also like to extend my thanks to Dr. Zoya Petrushenko, Dr. Zhiqiang

Sun, Dr. Yoichi Yamada and Dr. Ganesh Krishnamoorthy for their helpful suggestions and support. Thanks to all the people in the lab: Dr. Jon, Dr. Liang, Dr. Hang, Dr. Rupa, Dr. Sita, Abigail, Logan, April, Viridiana and Bijit for their friendships. We are a wonderful family and I really wish we could spend a lot of more time togehter.

Finally, I want to thank my parents who are now thousand miles away from me. They are the only persons who always unconditionally love and support me. I am very fortunate to be their child and I wish to have a long healthy life together with them.

Table of contents

Acknowledgements ..... **iv**

Table of contents ..... **vi**

List of Tables ..... **x**

List of Figures ..... **xi**

Abstract ..... **xiii**

I. Introduction **1**

I.1 Multiple-drug resistance (MRD) efflux complexes in bacteria. 3

I.2 The role of MacAB-TolC complex in macrolide resistance and toxin secretion in *E. coli* 6

I.3 Structural characterization of MacAB-TolC 8

I.3.1 MacB. 8

I.3.2 MacA. 12

I.3.3 TolC. 14

I.4 Functional characterization of MacAB-TolC 17

I.4.1 MacB. 17

I.4.2 MacA. 18

I.4.3 TolC. 20

I.5 Specific aims and goals of this dissertation. 21

II. Experimental Procedures **22**

II.1 Construction of plasmids. 22

II.2 Site-directed mutagenesis. 23

II.3 Protein assays. 24

II.3.1 SDS-PAGE and western blotting. 24

II.3.2 Protein concentration determination. 25

II.4 Purification of ApoA-I. 25

II.5 Purification of MacAB-TolC components. 26

II.6 Co-purification of MacAB-TolC complex. 28

II.7 ATPase assay. 28

II.8 Reconstitution of proteins into proteoliposomes and nanodiscs. 30

II.8.1 Reconstitution of proteins into proteiliposomes. 30

II.8.2 Reconstitution of proteins into nanodiscs. 31

II.9 Limited proteolysis. 32

II.10 Minimum Inhibitory Concentration (MIC) measurements. 33

II.11 Surface Plasmon Resonance (SPR). 33

Biotinylation. 33

Immobilization. 34

Data collection and normalization. 35

Data analysis. 36

II.12 Size-exclusion chromatography (SEC). 37

II.13 Lipid concentration determination. 38

II.14 Transmission electron microscopy (TEM). 38

Chapter 1: Characterization of the functionality of MacB variants. 40

1.1 MacB variants exhibit different basal ATPase activity level. 40

1.2 Different conformational states of MacB variants. 46

1.3 ATP binding induces conformational changes of MacB variants. 48

1.4 MacA stimulates the ATPase activity of MacB variants except for $MacB^{LPL}$. 51

1.5 Kinetic properties of MacB variants. 52

1.6 Mutations in MacB affect the macrolide drugs resistance of *E. coli* W4680AD (Δ*acrAB,* Δ*acrD*) cells. 57

Chapter 2: Investigation of the protein-protein interactions between MacA and MacB. 58

2.1 Immobilization of MacB and a binding assay development. 58

2.2 Immobilized MacB variants bind nucleotides. 64

2.3 $MacA^{WT}$ forms oligomer in solution. 69

2.4 $MacA^{WT}$ binds MacB with nanomolar affinity. 70

2.5 $MacA^{S}$ binds MacB but with lower affinity comparing with $MacA^{WT}$. 74

2.6 ATP binding increases MacA-MacB affinity. 75

Chapter 3: Investigation of the protein-protein interactions between MacAB and TolC……. 79

3.1 Immobilized TolC binds $MacA^{S}$ and $MacA^{WT}$. 79

3.2 TolC does not directly interact with MacB. 81

3.3 MacB is essential for the recruitment of TolC. 84

Chapter 4: Reconstitution of MacAB-TolC into nanodiscs. 87

4.1 Construction and purification of tag-less ApoA-I. 87

4.2 MacB and TolC can be reconstituted into nanodiscs. 90

4.3 MacB reconstituted into nanodiscs can hydrolyze ATP. 92

4.4 Immobilized MacB nanodiscs bind ATP. 95

4.5 $MacA^S$ binds MacB nanodiscs. 97

III. Discussion. 98

III.1 The interaction between MacA and MacB is not sensitive to either ATP hydrolysis or conformational changes of MacB. 99

III.2 TolC cannot directly interact with MacB. 101

III.3 The periplasmic loop of MacB is not required for MacA binding but is essential for MacA-mediated stimulation of MacB ATPase 102

III.4 The binding of ATP increases the affinity of MacA-MacB complex..... 104

III.5 The mechanism of complex assembly of MacAB. 106

III.6 Reconstitution of membrane proteins into lipid nanodiscs can be used to study MacAB-TolC system 107

Reference 110

Appendix A. List of strains and plasmids 115

Appendix B. List of primers.....117

List of Tables

Chapter 1: Characterization of the functionality of MacB variants

Table 1.1 Kinetic parameters of MacB ATPase and its derivatives 56

Table 1.2 Macrolide susceptibilities of *E. coli* W4680AD (Δ*acrAB,* Δ*acrD*) cells carrying plasmids producing MacA along with MacB variants (MIC, μg/mL). 58

Chapter 2: Investigation of the protein-protein interactions between MacA and MacB

Table 2.1 Kinetic parameters of MacA-MacB interactions in the presence of nucleotides……..73

List of Figures

I. Introduction

Figure I.1 Mechanisms of antibiotic resistance in bacteria..... 2

Figure I.2 Multiple-drug resistance (MDR) efflux pumps in Gram-positive and Gram-negative bacteria. 4

Figure I.3 Schematic model of the molecular construction of the ABC-type macrolide-specific drug exporter MacA-MacB system complexed with TolC in *E. coli*. 7

Figure I.4 Membrane topology of MacB 10

Figure I.5 The overall structure of MacB PCD.....11

Figure I.6 The overall structure of MacA 13

Figure I.7 The overall structure of TolC.. 15

Chapter 1: Characterization of the functionality of MacB variants

Figure 1.1 Specific ATPase activity of $MacB^{WT}$ and its derivatives..... 45

Figure 1.2 Trypsin digestion patterns of $MacB^{D}$, $MacB^{169}$, $MacB^{YC}$ and $MacB^{LPL}$ 48

Figure 1.3 Trypsin digestion patterns of $MacB^{D}$, $MacB^{169}$, $MacB^{YC}$ and $MacB^{LPL}$ in the presence or absence of nucleotides 50

Figure 1.4 Specific ATPase activity of MacB and MacAB proteoliposomes 52

Figure 1.5 Dependence of MacB ATPase activity on MacA 55

Figure 1.6 Dependence of ATP hydrolysis by MacB and MacAB in detergent micelles on the concentration of ATP 56

Chapter 2: Investigation of the protein-protein interactions between MacA and MacB

Figure 2.1 Biotinylation of $MacB^{WT}$ and its derivatives..... 62

Figure 2.2 Development of a binding assay..... 63

Figure 2.3 Gel filtration analysis of $MacB^{D}$, $MacA^{S}$ and $MacA^{WT}$ 66

Figure 2.4 Immobilized MacB binds ATP, ADP and AMP-PNP..... 69

Figure 2.5 $MacA^{WT}$ binds MacB variants..... 72

Figure 2.6 $MacA^{S}$ binds MacB variants 75

Figure 2.7 Dependence of k_{obs} of MacA on the concentrations of nucleotides..... 77

Figure 2.8 $MacA^{WT}$ binds MacB in the presence of nucleotides..... 79

Chapter 3: Investigation of the protein-protein interactions between MacAB and TolC

Figure 3.1 Immobilized TolC binds $MacA^{S}$ and $MacA^{WT}$..... 81

Figure 3.2 Immobilized TolC cannot bind MacB 82

Figure 3.3 $TolC^{WT}$ and $TolC^{\Delta Loop}$ cannot bind MacB..... 83

Figure 3.4 Co-purification of MacA and TolC with $MacB^{WT}$ and its derivatives..... 86

Figure 3.5 $MacB^{LPL}$ fails to recruit TolC. 86

Chapter 4: Reconstitution of MacAB-TolC into nanodiscs

Figure 4.1 Reconstituion of nanodiscs..... 89

Figure 4.2 MacB and TolC can be reconstituted into nanodiscs..... 92

Figure 4.3 Specific ATPase activity of nanodiscs..... 94

Figure 4.4 Immobilized MacB nanodiscs bind ATP 96

Figure 4.5 Immobilized MacB nanodiscs bind $MacA^{S}$. 97

III. Discussion

Figure III. 1 A proposed transport mechanism of MacAB–TolC..... 107

Abstract

In Gram-negative bacteria, intrinsic antibiotic resistance is provided by three component efflux transporters. In *Escherichia coli*, MacAB-TolC is the first experimentally described ATP-driven tripartite efflux pump responsible for macrolide resistance and enterotoxin secretion (Kobayashi, Nishino et al. 2001; Yamanaka, Kobayashi et al. 2008). In this complex, MacB is the inner membrane (IM) ABC-type (ATP-Binding Cassette) transporter which utilizes the energy from ATP hydrolysis for the transport of substrates. MacB functions together with a periplasmic membrane fusion protein (MFP) MacA. MacA stimulates the ATPase activity of MacB by inducing the closure of the nucleotide binding domains (NBD) of MacB (Modali and Zgurskaya 2011). TolC, as a versatile outer membrane (OM) channel, forms complex with MacAB to facilitate the extrusion of substrates into the exterior environment. Up to now it is still unclear how MacAB and TolC associate with each other contributing to the export of substrates, as well as how the presence of ATP and substrates affects the functions of this complex.

The first part of this dissertation focuses on understanding the mechanism of complex assembly of MacAB-TolC and the role of ATP in this process. We developed a real-time assay for the analysis of concurrent ATP hydrolysis and assembly of MacAB-TolC using surface plasmon resonance (SPR) technique. We found that MacB binds nucleotides with fast on- and off- rates and a low millimolar affinity. MacA-MacB forms a stable complex with nanomolar affinity and the binding of ATP increases the affinity of MacA-MacB interactions. These results strongly suggest that the binding of ATP brings MacB into a conformation with higher affinity towards MacA. Furthermore,

the MacA-MacB complex remains unchanged during ATP hydrolysis cycle. We also found that the large periplasmic loop (LPL) of MacB is required for the MacA-dependent stimulation of MacB ATPse and the recruitment of TolC into the complex by MacA. Based on these findings, we propose a mechanism of complex assembly of MacAB-TolC complex. MacA has a higher affinity towards the ATP-bound state of MacB and promotes the closed conformation of MacB NBD for ATP hydrolysis. The MacA-dependent stimulation of MacB ATPase is coupled to the recruitment of TolC by MacA through the interactions between MacA and MacB LPL.

The second part of this dissertation focuses on developing a new method for the study of membrane protein complex MacAB-TolC. For this purpose we reconstituted MacAB-TolC into lipid nanodiscs. We found that MacB containing nanodiscs can bind and hydrolyze ATP, suggesting that MacB is functional in nanodiscs. Interestingly, $MacB^{C56A/D643C}$, which only exhibits 60% MacB ATPase compared to that of $MacB^{WT}$ in detergent, shows ATPase activity similar to $MacB^{WT}$ in nanodiscs. We conclude that reconstitution of MacB into lipid nanodiscs provides a more native environmen to investigate the biological and physiological functions of MacB and the mechanism of assembly of MacAB-TolC complex.

I. Introduction

Since the discovery of the first antibiotic drug penicillin in 1928, many antibiotics have been found and manufactured to treat infectious diseases (Nikaido 2009). The discovery and usage of antibiotics had once been considered to be one of the most profound contributions to human life. However, in the past decade, an increasing number of bacterial pathogens have become resistant to antibiotics. The emergence of drug resistant pathogens leads to a serious problem that some therapeutic agents cannot be used for the treatment of infections anymore (Piddock 2006). The drug resistance phenomenon has been identified in micro-organisms, and also in mammalian cells recently (Sharma, Sharma et al. 2005). In addition, it spreads through cell populations rapidly (Higgins 2007). Nevertheless, it is more surprising that an increasing number of bacterial species show simultaneous resistance towards many structurally and chemically unrelated drugs, which is called the multiple-drug resistance (MDR) (Li and Nikaido 2009). This MDR phenomenon dramatically reduces the efficiency of antibiotics and restricts the clinical use of certain antibiotic families (Nikaido and Pages 2012). In order to maintain the drug efficiency and develop new antibiotic drugs, extensive studies have been done to explore the mechanisms of bacterial drug resistance.

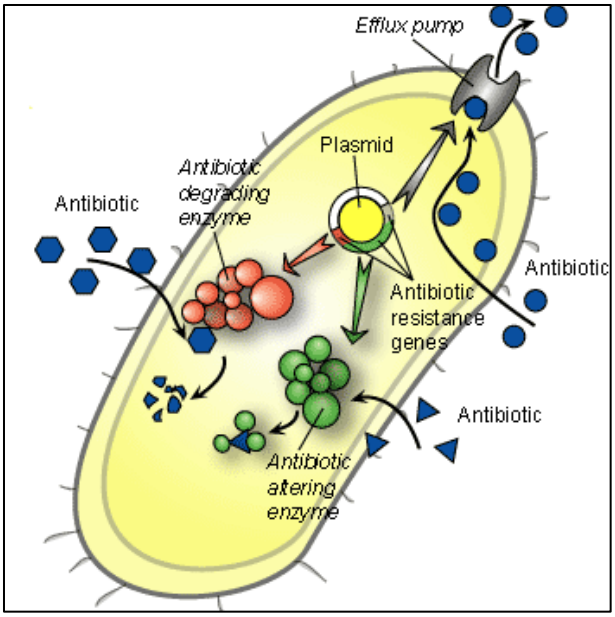


Figure I.1 Mechanisms of antibiotic resistance in bacteria. Figure Adopted from http://www.scq.ubc.ca/attack-of-the-superbugs-antibiotic-resistance.

The commonly accepted mechanisms of bacterial drug resistance include the alteration of target proteins, the inactivation of drugs, the decrease of membrane permeability and the expression of drug efflux pumps (Figure I.1) (Higgins 2007). Bacteria obtain these drug resistance abilities through acquired and intrinsic mechanisms (Alekshun and Levy 2007). The acquired mechanism is related to the introduction of mutations in antibiotic targeted genes, which is accomplished by exchanging resistant traits through the processes of transduction, conjugation and transformation between bacteria species (Levy and Marshall 2004). The intrinsic mechanism is the contribution of naturally occurring genes, such as genes encoding many multiple-drug resistance (MDR) efflux systems. The MDR efflux systems recognize and extrude a broad range of structurally and chemically unrelated compounds (Zgurskaya and Nikaido 2000) and are considered to be the primary reason for drug resistance in bacteria.

The following section will concentrate on the brief description of MDR efflux systems in bacteria and then focus specifically on the introduction of the structural and functional bases of *E. coli* macrolide efflux transport system MacAB-TolC.

I.1 Multiple-drug resistance (MRD) efflux complexes in bacteria.

Drug efflux complexes contain transport proteins which utilize the metabolic energy for the extrusion of multiform substrates from the cytosolic compartment of cells into the external environment. These proteins can be found not only in prokaryotic but also in eukaryotic organisms (Van Bambeke, Balzi et al. 2000) and they contribute significantly to the existing drug resistance phenomenon (Borges-Walmsley, McKeegan et al. 2003; Webber and Piddock 2003). Active drug efflux transporters can be specific to one substrate, and are often called single-drug or group-specific efflux transporters. In addition, efflux transporters can be versatile to multiple structurally and functionally dissimilar organic compounds, and are called multiple drug resistance (MDR) efflux transporters (Lubelski, Konings et al. 2007). The mammalian P-glycoprotein is an ATP-driven efflux pump and is the first described MDR transporter (Paulsen 2003). MDR efflux transporters are also widespread throughout the bacteria kingdom (Paulsen and Lewis 2001).

MDR efflux transporters can be classified into different superfamilies based on the energy source they use, the number of transmembrane (TM) helices they possess, the substrates they transport and the number of accessary protein they need (Piddock 2006). In bacteria, MDR transporters are commonly classified into two major groups based on the energy mode utilized for the extrusion of drugs (Lubelski, Konings et al. 2007):

primary active transporters and secondary active transporters. The primary active transporters contain the ATP-binding cassette (ABC) superfamily and utilize the energy from ATP hydrolysis to couple the drug export process against the drug concentration gradient. The secondary active transporters are energized by the proton motive force and are composed of superfamilies of H^+- and Na^+- antiporters (Paulsen, Brown et al. 1996; Webber and Piddock 2003). The MDR secondary transporters can be further divided into four major families based on the amino acid sequence homologies and predicted secondary structures (Figure I.2) (Piddock 2006):

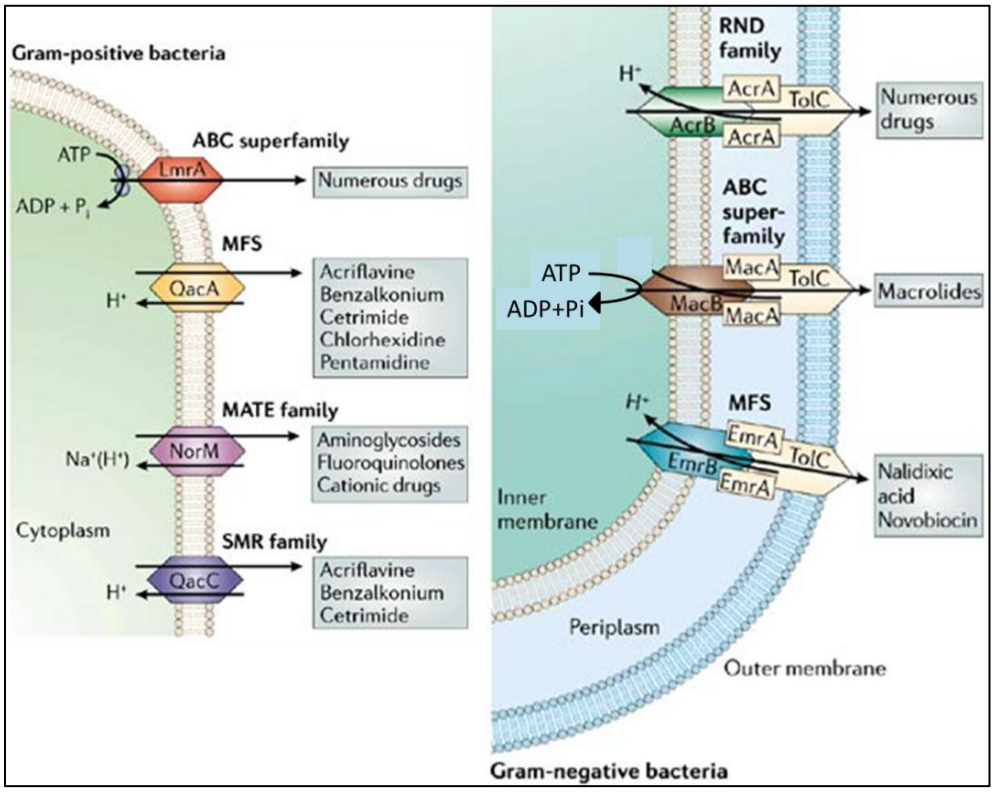


Figure I.2 Multiple-drug resistance (MDR) efflux pumps in Gram-positive and Gram-negative bacteria. Figure adopted and modified from (Piddock 2006)

(I) the Major Facilitator Superfamily (MFS) transporters, which form the largest

group of secondary active transporters (Pao, Paulsen et al. 1998) and are predicted to have 12 or 14 TM helices with a large cytoplasmic loop between helix 6/7 (Saier, Beatty et al. 1999), (II) the Multidrug and Toxic-compound Extrusion (MATE) transporters, which have comparable size to the MFS transporters and are predicted to have 12 TM helices (Jack, Yang et al. 2001), (III) the Small Multidrug Resistance (SMR) transporters, which are relatively small size transporters and are putatively folded into 4 TM helices (Paulsen, Brown et al. 1996) and (IV) the Resistance Nodulation Division (RND) transporters, which are much larger than MFS transporters and are predicted to possess 12 TM helices with large periplasmic or extracytoplasmic domains between helices 1/2 and helices 6/7 (Mao, Warren et al. 2002; Murakami, Nakashima et al. 2002). MDR efflux systems are widespread in both Gram-positive and Gram–negative bacteria. A single bacterial species can express MDR efflux pumps from more than one superfamily and/ or express more than one kind of efflux pumps from the same superfamily.

In Gram-negative bacteria, the presence of outer membrane bilayer and the expression of MDR efflux systems contribute to the intrinsic drug resistance (Lubelski, Konings et al. 2007). To allow the direct expulsion of drugs into the exterior environment, the majority of MDR efflux systems use the tripartite protein complexes to translocate drugs across both the inner and outer membranes (Nikaido 1996). These transport systems commonly consist of an inner membrane transporter, a membrane fusion protein (MFP) and an outer membrane protein channel (Borges-Walmsley, McKeegan et al. 2003). The inner membrane transporters belong to one of the three superfamilies of proteins: the RND, ABC and MFS. They utilize the energy generated by either ATP hydrolysis or proton motive force to translocate substrates. MFPs are anchored to the

inner membrane by a lipid moiety or a single α-helix and function as physical linkers between the inner membrane transporters and the outer membrane channels. MFPs can be found in the tripartite efflux systems involved in the exportation of small molecules, proteins, oligosaccharides and each transport system is tended to have its own adaptor MFP (Yoneyama, Ocaktan et al. 1998). The outer membrane channels are multifunctional proteins involved in the translocation of both small drug molecules and large polypeptide toxin and are interchangeable between different drug efflux systems. The assembly of three protein components facilitates the direct transport of substrates from the cytoplasm or cytoplasmic membrane into the extracellular environment (Zgurskaya and Nikaido 2000). MDR efflux systems in *E. coli* have been used as prototypes for the genetic and biochemical studies (Li and Nikaido 2004; Li and Nikaido 2009). As a result, the contributions of MDR to intrinsic and acquired resistance of *E. coli* have been explored in detail (Lubelski, Konings et al. 2007). In *E. coli*, MacB, as an ABC exporter, functions together with MacA and TolC (Kobayashi, Nishino et al. 2001). The following sections will be focused on structural and functional studies of the MacAB-TolC efflux pumps.

I.2 The role of MacAB-TolC complex in macrolide resistance and toxin secretion in *E.coli*.

The ABC transporter family is the largest in all paralogous protein families (Higgins 2001). In *E. coli*, five putative ABC-type transporters are identified in the genome. However, only one ABC exporter MacB has been found to be related to drug resistance in *E. coli* (Kobayashi, Nishino et al. 2001). MacB is the first ABC-type exporter

experimentally characterized in Gram-negative bacteria.

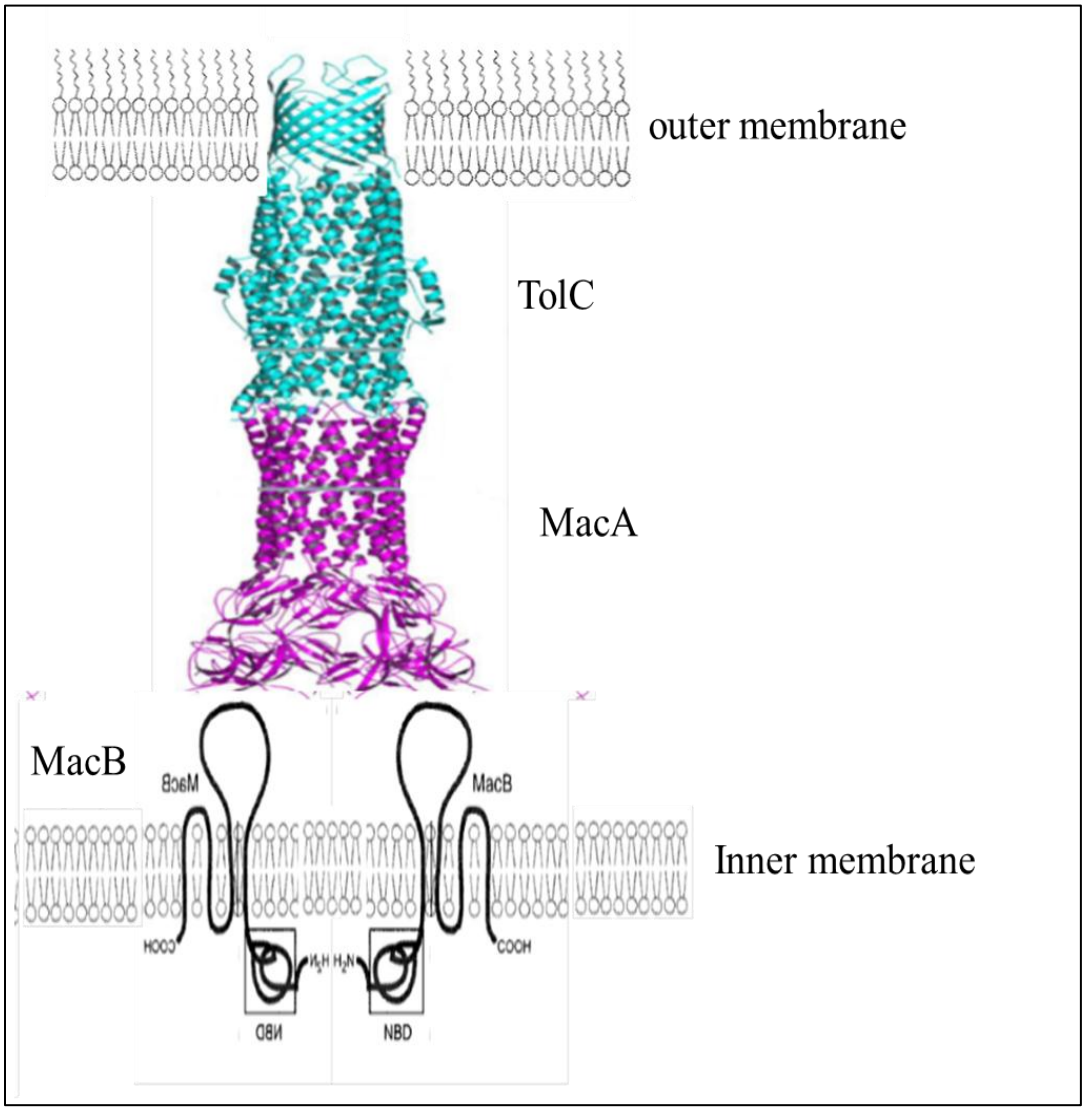


Figure I.3 Schematic model of the molecular construction of the ABC-type macrolide-specific drug exporter MacA-MacB system complexed with TolC in *E. coli*. Figure Adopted from (Kobayashi, Nishino et al. 2001; Xu, Song et al. 2011).

MacB confers resistance against erythromycin when overexpressed in a hypersensitive strain lacking the major MDR pump AcrAB-TolC (Kobayashi, Nishino et al. 2001). Erythromycin is classified as a macrolide antibiotic and functions as a protein

synthesis inhibitor (Tenson, Lovmar et al. 2003). MacB exhibits resistance against macrolides containing 14- and 15- membered lactones but no or weak resistance against 16-membered ones. To achieve the resistance against macrolides, MacB needs the assistance of two accessory proteins, the MFP protein MacA and the multifunctional outer membrane channel TolC (Tikhonova, Devroy et al. 2007). MacAB and TolC form tripartite complexes and utilize the energy generated by ATP hydrolysis to expel macrolides from the cytoplasm to the extracellular environment (Figure I.3). Recent studies indicate that the MacAB-TolC efflux system is also involved in the recognition and translocation of heat-stable enterotoxin STII from the periplasm to the exterior (Yamanaka, Kobayashi et al. 2008).

Even though MacAB is unique in *E. coli*, its homologs are widely identified in all bacteria with some of them implicated in secretion of toxins and siderophores (Dubern, Coppoolse et al. 2008; Zgurskaya, Yamada et al. 2009). In contrast, TolC is exclusive to Gram-negative bacteria and forms tripartite complexes with diverse inner membrane transporters.

I.3 Structural characterization of MacAB-TolC.

MacAB and TolC belong to different membrane protein families and they exhibit some distinctive structural features.

I.3.1 MacB.

MacB is a noncanonic ABC transporter with only one nucleotide binding domain

(NBD) (Kobayashi, Nishino et al. 2001). Unlike most of the half-type transporters whose NBD are located at the C-termini of proteins, the NBD of MacB is at the N-terminus. This structural arrangement of MacB is similar to that of the ABCG subfamily which is involved in the regulation of lipid trafficking mechanisms in eukaryotes or humans (Schmitz, Langmann et al. 2001). However MacB shows no sequence homology to any ABCG family proteins. The NBD of MacB incorporates three conserved motifs in ABC-type transporters: a Walker A motif, a Walker B motif and an ABC signature motif LSGGQ. These motifs are the characteristic features of ABC superfamily. In general, the Walker A motif binds the phosphate groups of the nucleotides; the Walker B motif provides a conserved glutamate residue that nucleophilically attacks ATP in the presence of water molecule; the ABC signature motif only contacts ATP in the ATP-bound state. Usually, two ATP molecules are sandwiched between the Walker A motif from one NBD and the LSGGQ motif from the other NBD.

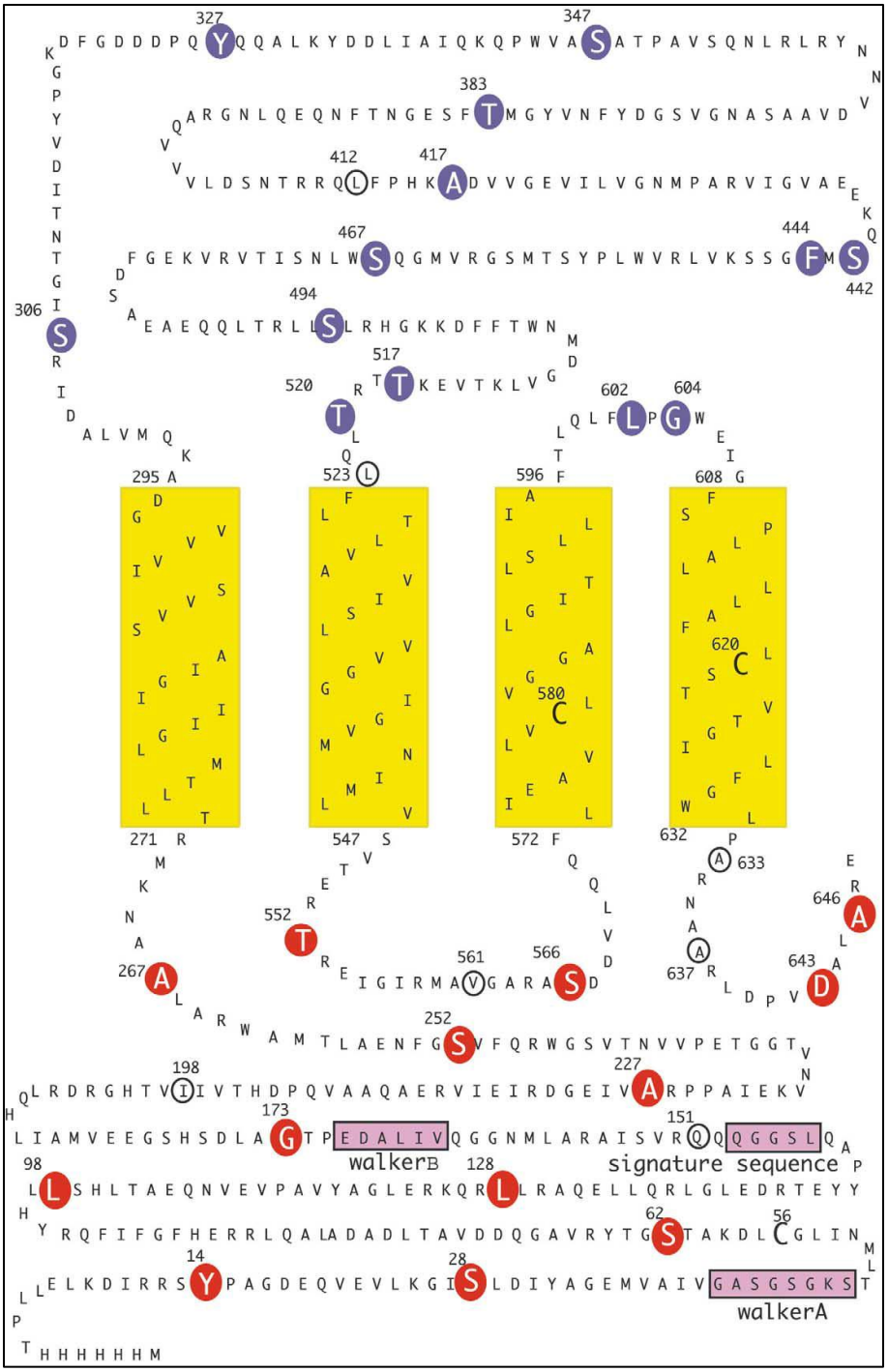


Figure I.4 Membrane topology of MacB. Figure adopted from (Kobayashi, Nishino et al. 2003). The putative transmembrane (TM) segments are shown in yellow squares. The Walker A, Walker B and signature sequence of MacB NBD are shown as pink rectangles.

MacB comprises four transmembrane (TM) segments and a large periplasmic domain formed by a loop connecting TM1 and TM2 (Kobayashi, Nishino et al. 2003) (Figure I.4). MacB has the least number of TM segments in half-type ABC transporters. Most ABC-type transporters have at least six TM segments and function as dimers with a total of 12 TM segments (Holland and Blight 1999). So far, the full length structure of MacB has not been solved. Nevertheless, the crystal structure of the periplasmic core domain (PCD) of the *Actinobacillus actinomycetemcomitans* (Aa)MacB is available (Xu, Sim et al. 2009).

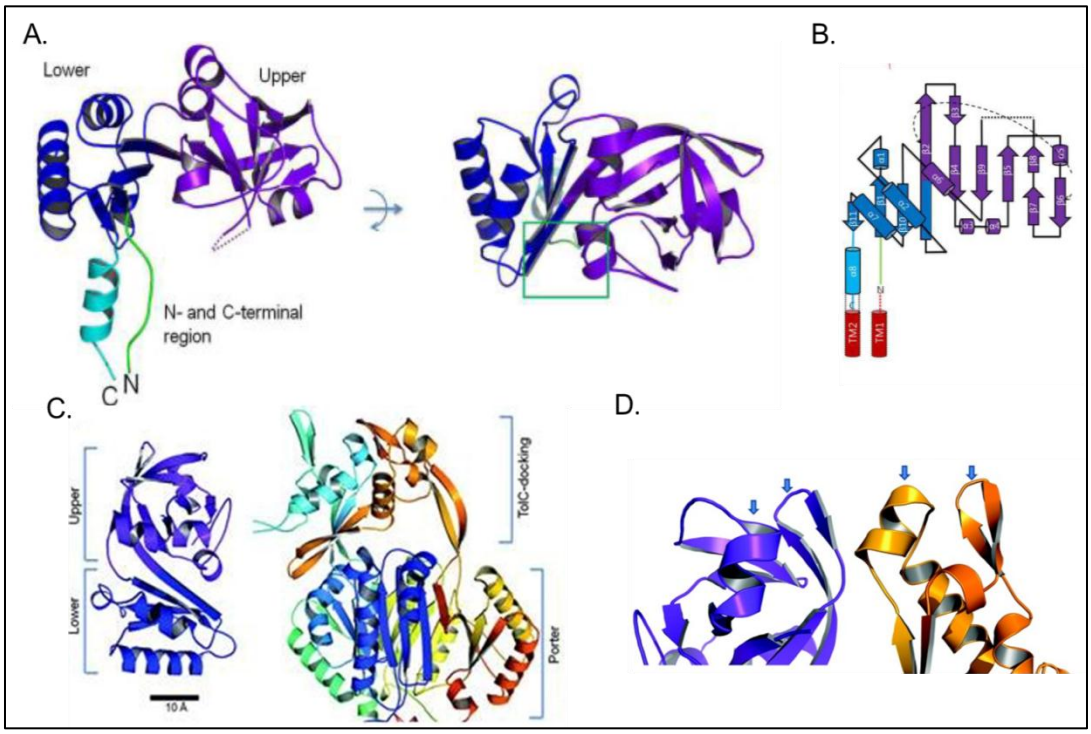


Figure I.5 The overall structure of MacB PCD. A. The side and top views of PCD are depicted. B. Folding topology of Aa MacB PCD. C. Secondary structures of the periplasmic regions of MacB (Left) and AcrB (Right). D.The periplasmic tip regions of MacB and AcrB. Figure adopted from (Xu, Sim et al. 2009).

There are two perpendicularly positioned components in Aa MacB PCD, a flexible N- and C- terminal regions and a rigid mixed αβ domain (Figure I.5 A). These two components are connected by flexible linkers and no physical interactions were observed between them. The mixed αβ domain is composed of a nine stranded β-sheet and three α-helices (Figure I.5 B). This domain is divided into the upper and lower subdomains by a shallow crevice in the middle (Figure I.5 A). In the full length MacB, the PCD is connected to the TM segments with the N- and C- terminal regions linked to TM1 and TM2, respectively. Structural comparison between the PCD of MacB and the periplasmic domain of the RND transporter AcrB reveals some similarities (Figure I.5 C). AcrB forms a homotrimer with the periplasmic domain composed of a TolC-docking domain and a porter domain (Murakami, Nakashima et al. 2002). The structure of the lower subdomain of MacB PCD is similar to that of the AcrB porter domain and the upper subdomain of MacB PCD shares some structural similarity to the tip region of the AcrB TolC-docking domain (Figure I.5 C, D). All these structural features of MacB could contribute to the substrate binding or complex assembly. The other putative periplasmic region between TM3 and TM4 of MacB cannot form any secondary structure and is not able to interact with PCD.

I.3.2 MacA.

MacA is a membrane fusion protein (MFP) with a TM segment at the N terminus, which is composed of 40 amino acid residues and anchors MacA to the inner membrane (Tikhonova, Devroy et al. 2007). Ec MacA was crystallized as a hexamer with a 3.0 Å resolution (Yum, Xu et al. 2009). The crystal structure shows three domains of MacA: the β-barrel domain, the lipoyl domain and the α-hairpin domain (Figure I.6 A). The

membrane proximal domain of MacA is not solved in this structure. MacA shares high structural similarity to other MPFs, such as Ec AcrA and its homologue *Pseudomonas aeruginosa* Pa MexA (Akama, Matsuura et al. 2004; Higgins, Bokma et al. 2004; Mikolosko, Bobyk et al. 2006). AcrA and MacA share 40% sequence similarity, but belong to different MFP subfamilies (Zgurskaya, Yamada et al. 2009). The coiled-coil α-hairpin of Ec MacA has six heptad repeats per helix and the length of the funnel stem of MacA is 11 Å longer than that of AcrA (Figure I.6 B). A superposition of the Ec MacA protomer onto Ec AcrA using the lipoyl domain as reference reveals that the α-hairpin domain and β-barrel domain of MacA differ from those of AcrA by 20 °.

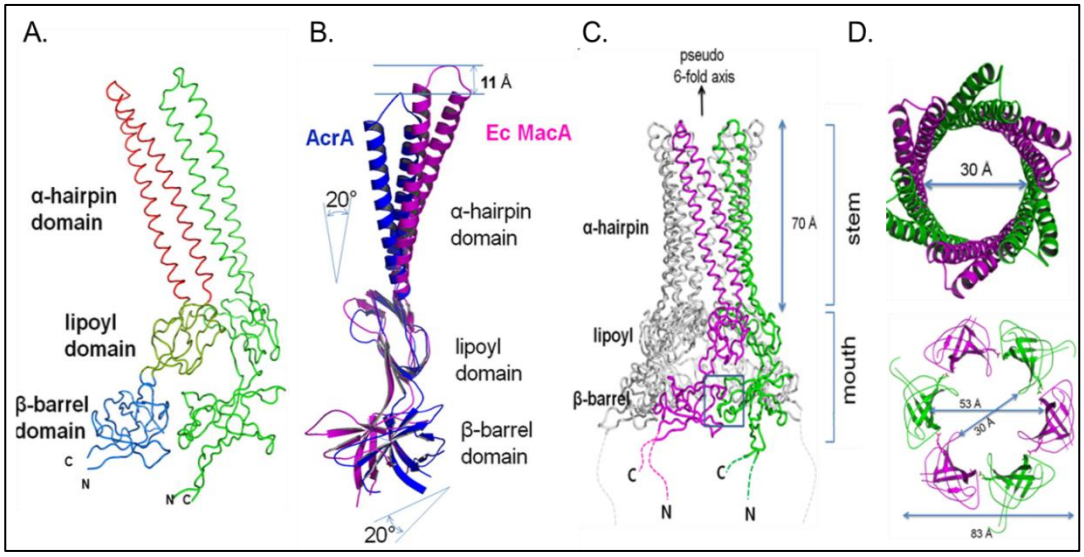


Figure I.6 The overall structure of MacA. A. The asymmetric unit of Ec MacA. B. Superposition of the Ec MacA protomer onto Ec AcrA using the lipoyl domain as reference. C. The hexameric structure of Ec MacA. D. The top and bottom views of the hexameric structure of Ec MacA. Figure adopted from (Yum, Xu et al. 2009).

The crystal structure of Ec MacA exhibits a funnel-like structure with a central

channel along the crystallographic pseudo-6-fold axis generated by a side-by-side packing interaction of six protomers (Figure I.6 C). The juxtaposition of the α-hairpin domains forms a 70 Å long and 30 Å wide stem and the lipoyl and β-barrel domains form a conical mouth with a 83 Å outside diameter (Figure I.6 D). The stem part of MacA hexamer is suggested to connect to the tip region of TolC (Xu, Song et al. 2011). Furthermore, MacB is suggested to be associated with the conical mouth of MacA.

I.3.3 TolC.

TolC, a versatile outer membrane channel, forms a conduit for the translocation of substrates across the outer membrane into the exterior. The crystal structure of Ec TolC was solved with a 2.1 Å resolution in 2000. It shows a mono-barrel homotrimer form (Koronakis, Sharff et al. 2000). Each of the three monomers contains four antiparallel β-strands and four antiparallel α-helical strands (Figure I.7 B). The overall structure of TolC is a tapered hollow cylinder with a length of 140 Å. It comprises a 40 Å long outer membrane β-barrel domain (the channel domain) and a contiguous 100 Å long α-helical barrel (the tunnel domain) projecting across the periplasmic space. A third domain, known as the equatorial domain, contains both α-helices and β-strands and situates around the midsection of the tunnel domain (Figure I.7 A). The structure of TolC provides a large solvent-filled interior cavity with a volume of 43,000 $Å^2$.

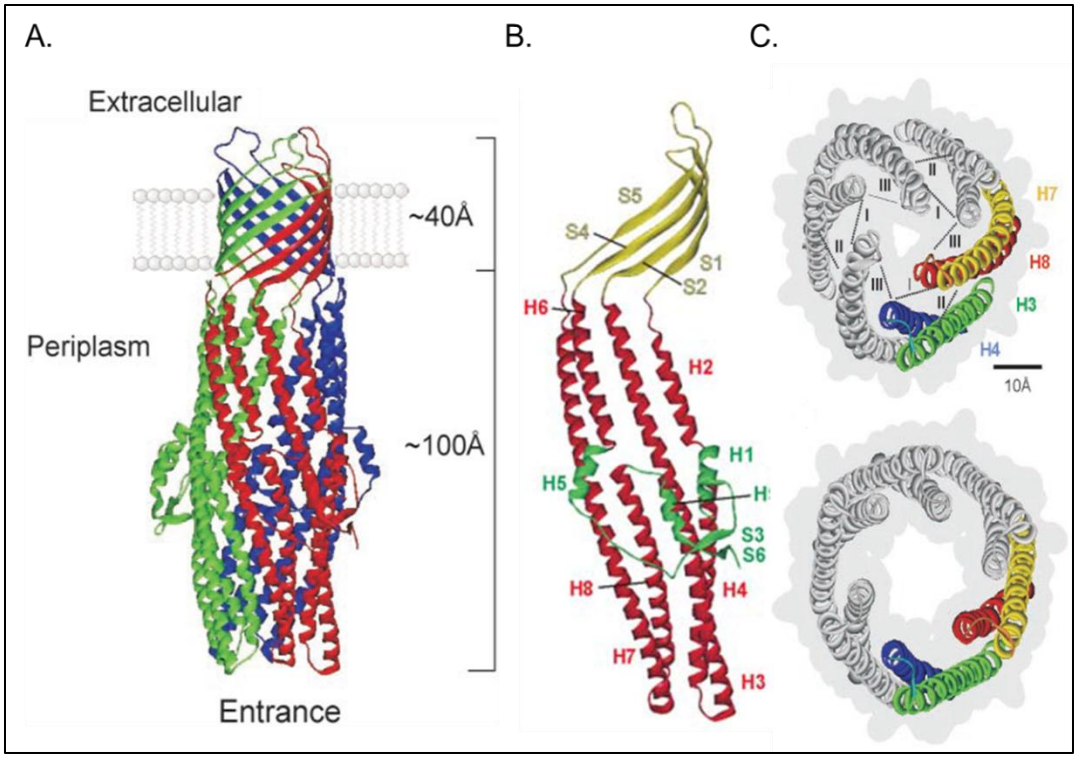


Figure I.7 The overall structure of TolC. A. The structure of a TolC trimer. B. The structure of a TolC protomer. C. The ribbon depictions close (up) and open (down) states of TolC tunnel entrance, viewed from the periplasm. The coiled-coils of one protomer are colored (H3/4 and H7/8; numbering taken from Koronakis, Sharff et al. 2000) and the constraining intramonomer (I and II) and intermonomer (III) links are shown. Figures adopted from (Andersen 2003; Koronakis, Eswaran et al. 2004).

Unlike other outer membrane proteins which contain one β-barrel per monomer, the channel domain of TolC exists as a distinct structure with 12 right-twisted β-strands forming a single β-barrel (Pautsch and Schulz 1998). To maintain the curvature of the β-barrel, small or unbranched amino acid side chains are tended to lie periodically on the inside of the barrel and residues with bulkier branched side chains lie on the outside of the

barrel. The outer membrane β-barrel of TolC is constitutively open to the exterior and the highly flexible small extracellular loops at the top are sites of colicin and bacteriophage attachment (German and Misra 2001).

The TolC α-helical barrel is contiguous with the β-barrel domain and extends extensively into the periplasm. 12 α-helices (H2, H3, H6 and H7 of each monomer) arrange antiparallel to form an almost uniform cylinder in the upper section (Figure I.7 B). The α-barrel structure finishes with the equatorial domain and continues with the long helices H3 and H7 pairing with helices H4 and H8, respectively. The 12 α-helices have a left-handed superhelical twist throughout the entire α-helical barrel, but tend to untwist at the distal end comparing with the conventional coiled coils. The long helix H3 is straight with H4 coiling around it. The H3 and H4 together form the inner pair of helices. The outer pair of helices (H7 and H8) forms a conventional antiparallel coiled-coil bending inward and is responsible for the tapering of the periplasmic end of TolC. The coiled coils are stabilized by an intermeshing of side chains, known as "knobs-into-holes" packing. The hydrogen bonds within and between the helices and the salt bridges formed at the interface of monomers may contribute to the assembly and the trimerization of TolC. The dense packing of the coiled-coils is proposed to keep the periplasmic opening of TolC in its closed conformation. The weakening of the intramonomer and intermonomer links relaxes the inner coiled-coils from their constrained position to form the open conformation (Koronakis, Sharff et al. 2000; Andersen, Koronakis et al. 2002) (Figure I.7 C)

I.4 Functional characterization of MacAB-TolC

MacAB-TolC efflux transport system is involved in the extrusion of macrolide antibiotics and heat stable enterotoxin STII. Each components of this tripartite complex has its own function.

I.4.1 MacB.

MacB functions as a dimer and can export macrolides and heat-stable enterotoxin STII across the membrane bilayer (Kobayashi, Nishino et al. 2001; Yamanaka, Kobayashi et al. 2008). MacB confers resistance against macrolide antibiotics composed of 14- and 15-membered lactones but no or weak resistance against 16-membered ones. As other ABC-type proteins (Davidson, Dassa et al. 2008), two ATP molecules are likely bound at the interface of MacB NBDs. The binding of nucleotides or nucleotide analogues to MacB can cause the same closed nucleotide-bound conformation of MacB. MacA is not needed for the binding of nucleotides to MacB (Modali and Zgurskaya 2011).

When solubilized in Triton X-100, purified MacB displays a basal ATPase activity with a K_M for ATP in a low millimolar range. The MacB ATPase activity is unresponsive to the putative substrate oleandomycin and the presence of accessory proteins MacA, TolC or both does not substantially affect the ATP hydrolysis of MacB (Tikhonova, Devroy et al. 2007). MacB lost all its ATPase activity in *n*-Dodecyl β-D-maltoside (DDM) micelles. Moreover, MacB ATPase is inhibited upon incorporation into the phospholipid bilayer. Furthermore, the basal ATPase activity of MacB in Triton X-100 is also diminished by lipids in all tested detergent/lipid ratio. It is suggested the formation of lipid bilayer leads to conformational changes in MacB.

In ABC transporters, K47 and D169 are the conserved catalytic residues located in the walker A and walker B motifs, respectively. Introducing either K47L or D169N substitution into MacB abolishes the ATPase activity of MacB completely. In addition, these variants fail to provide macrolide resistance to the drug hypersensitive strain, suggesting that MacB adopts a transport mechanism similar to that of the typical ABC transporters (Tikhonova, Devroy et al. 2007).

I.4.2 MacA.

MacA is the MFP in MacAB-TolC tripartite complex and it functions more than a physical linker between MacB and TolC. MacA is a hexameric protein that forms a tunnel-like structure connecting the peripalsmic domains of MacB and TolC. This hexamerization of MacA is essential for the fully function of MacAB-TolC efflux pump *in vivo* (Xu, Sim et al. 2009; Yum, Xu et al. 2009). MacA can directly bind TolC with (Tikhonova, Dastidar et al. 2009). The tip regions of the α-barrel of TolC and MacA interact in a tip-tip intermeshing cogwheellike manner (Xu, Song et al. 2011). MacA interacts with MacB and the presence of MacA increases the binding capacity of MacB towards erythromycin (Lin, Bavro et al. 2009).

The ATPase activity of MacB is significantly stimulated by MacA in proteoliposomes and this MacA-dependent stimulation of MacB ATPase only occurs when MacA and MacB are incorporated into the same phospholipid bilayer. Previous studies suggest that MacA and ATP act synergistically to induce the closed conformation of MacB NBDs (Modali and Zgurskaya 2011). The MacA stimulation of MacB ATPase is concentration dependent and the presence of putative substrate oleandomycin does not

further stimulate the ATPase activity of MacB. The ATPase activities of $MacB^{K47L}$ and $MacB^{D169N}$ are not restored by MacA and the MacA analogue AcrA fails to increase the ATP hydrolysis rate of MacB, suggesting that the MacA-dependent stimulation of MacB ATPase is specific to MacB (Tikhonova, Devroy et al. 2007). Even though the periplasmic domain of MacA is sufficient to bind MacB, the N-terminal TM segment of MacA is required not only for the MacB ATPase stimulation *in vitro* but also for the macrolide resistance *in vivo*. These results imply that the MacA-dependent stimulation of ATP hydrolysis by MacA is functionally linked to macrolide resistance *in vivo*.

The MP domains of MFPs are shown to play significant role in tripartite complex assembly (Ge, Yamada et al. 2009; Tikhonova, Yamada et al. 2011). In the MP domain of MacA, the C-terminal 70 amino acid residues are the most conserved residues between MFPs (Zgurskaya, Yamada et al. 2009). The MP domain of MacA plays a critical role in the stimulation of MacB ATPase by promoting the closed ATP-bound state of MacB NBDs. While assembling into the tripartite complex, the conformational transitions of the MacA MP domain modulate the ATPase activity of MacB. The MP domain of MacA acts as a switch in coupling the energy consumption by MacB to the extrusion of substrates outside the cell (Modali and Zgurskaya 2011). In agreement with previous studies of MFPs (Touze, Eswaran et al. 2004), MacA lacking the C-terminal end cannot bind MacB. Moreover, the C-terminal deletion mutant of MacA fails to stimulate the MacB ATPase and cannot facilitate the transport of macrolides. These results suggest that the function of MacB requires the MacA-MacB interactions on both sides of the membrane and within the membrane. Furthermore, all these studies imply that the MacB function is tighly regulated by MacA.

I.4.3 TolC.

TolC can form complexes with different transporters. It is involved in two distinct export systems, the type I protein secretion system and the multidrug efflux pumps that transport a wide range of substrates (Andersen 2003; Koronakis, Eswaran et al. 2004). To date, at least eight multidrug transporters belonging to different superfamilies have been reported to require TolC for the extrusion of drugs, which are AcrAB, AcrD, AcrF, MdtF and MdtB from the RND superfamily, EmrB and EmrY from the MFS superfamily and MacB from the ABC-type superfamily. TolC associates with AcrA-AcrB forming the dominant MDR efflux tripartite complex in Gram-negative bacteria, which contributes significantly to reducing the periplasmic antibiotic concentrations (Nikaido 2009).

The periplasmic entrance of TolC is believed to be opened upon association with the inner membrane complex (Zgurskaya, Krishnamoorthy et al. 2011). In addition, the binding of TolC to MFPs induces conformational changes in the MP domain of MFP, which could be required for the activation of the inner membrane transporters and the assembly of the tripartite complexes (Modali and Zgurskaya 2011; Tikhonova, Yamada et al. 2011).

The expression level of TolC has no restriction to the drug efflux capacity of bacteria (Zgurskaya, Krishnamoorthy et al. 2011). Inactivation of TolC elevates the susceptibility of enteric bacteria to a broad range of antimicrobial agents like antibiotics, detergents, dyes, organic solvents, and others (Sulavik, Houseweart et al. 2001). TolC is also an important component for the maintenance of the pathogenicity and virulence in Gram-negative bacteria. The loss of TolC or one of its homologues diminishes the bacterial survival and virulence (Koronakis, Sharff et al. 2000). Moreover, TolC may be

related to the expulsion of metabolites (Hantke, Winkler et al. 2011), the tolerance against acidity (Deininger, Horikawa et al. 2011) and the maintenance of membrane integrity (Dhamdhere and Zgurskaya 2010). So far, how TolC is involved in different transport systems and how different inner membrane transporters trigger the opening of TolC for the extrusion of substrates are still obscure.

I.5 Specific aims and goals of this dissertation.

In *E. coli*, MacAB-TolC tripartite efflux complex is involved in the extrusion of macrolides and enterotoxin STII. In addition, MacAB homologs are widely identified in all Bacteria kingdom. Understanding the transport mechanism of MacAB-TolC system will give us insights into the MDR phenomenon in bacteria and probably serve as a prototype for the study of MacAB homologs. The main goal of this study is to characterize the mechanism of complex assembly of MacAB-TolC. We want to investigate the protein-protein interactions between MacAB-TolC in the presence and absence of ATP using surface plasmon resonance (SPR) approach. To achieve this goal, first, we will characterize the mechanism of complex assembly of MacAB–TolC and the role of ATP in this process. Second, we will reconstitute MacAB-TolC complex into nanodiscs to understand the mechanism of complex assembly in this membrane-like environment.

II. Experimental Procedures

II.1 Construction of plasmids.

To construct pTYB-ApoA-I plasmid expressing apolipoprotein A-I (ApoA-I) protein containing N-terminal Intein-tag, the coding sequence of *apoA-I* gene was amplified by PCR using pNFXex plasmid (Ryan, Forte et al. 2003) as a template. The PCR product was then cloned into NotI and SpeI restriction sites of pTYB11 vector (New England Biolabs). The constructed pTYB-ApoA-I plasmid was transformed into BL 21(DE3) for protein expression.

In previous studies (Tikhonova, Devroy et al. 2007), *macAB* gene was cloned into pUC18 (Sigma) and pBAD/MycHis-C vectors (Invitrogen) to construct pUCMacAB and $pBAB^{his}$ plasmids, respectively. D169N and Y14C/C56A substitutions were then introduced into pUCMacAB and $pBAB^{His}$ plasmids to construct pUCMacABD169N and $pBABYC^{His}$ plasmids. In order to insert D169N and C56A/Y14C substitutions into $pBAB^{His}$ and pUCMacAB plasmids, both pUCMacABD169N and $pBABYC^{His}$ plasmids were treated with enzyme PsiI. PsiI cuts between amino acid position 322 in MacA and 343 in MacB. This enzyme treatment generated two fragments, a 1000 bp fragment containing the desired mutations and a larger fragment containing the rest portions of pUCMacABD169N and $pBABYC^{His}$ plasmids. The purified 1000 bp fragments from pUCMacABD169N and $pBABYC^{His}$ were then exchanged and ligated back with the corresponding larger fragments. The insertion of the correct gene sequence was confirmed by DNA sequencing (Oklahoma Medical Research Foundation Sequencing

Facility).

II.2 Site-directed mutagenesis.

D643C substitution was introduced into MacB using a QuickChange XL site-directed mutagenesis kit (Stratagene). The pBB^{His} plasmid (Tikhonova, Devroy et al. 2007) was used as a template for PCR. The resulting construct as sequenced in Oklahoma Medical Research Foundation Sequencing Facility to confirm the introduction of the desired substitution.

To construct $MacB^{LPL}$ mutant lacking the large periplasmic loop (LPL), DNA sequences encoding the N-terminal 1-301 amino acid and C-terminal 518-648 amino acid fragments of MacB were amplified by PCR using pBB^{His} plasmid as a template. The two DNA fragments were then ligated by PCR and the DNA product was cloned into NcoI and PstI restriction sites of pBAD/MycHis-C. The same deletion of MacB was also introduced into pUCMacAB and $pBAB^{His}$ plasmids. The DNA sequence of *macA* gene was amplified together with the DNA sequence encoding the N-terminal 1-301 amino acids of MacB by PCR using pUCMacAB plasmid as a template. The DNA sequence encoding the C-terminal 518-648 amino acids of MacB was also amplified by PCR using pUCMacAB plasmid as a template. The two DNA fragments were then ligated by PCR and the DNA product was cloned into NcoI and PstI restriction sites of pUCMacAB plasmids to construct pUCMacABLPL plasmid. The $pBABLPL^{His}$ plasmid was constructed following the same protocol.

In order to introduce the Y14C/C56A substitutions into pBAB^{His} plasmid, the DNA sequence of *macA* gene plus the DNA sequence encoding the first 20 amino acids of MacB was amplified by PCR using pBAB^{His} plasmid as a template with an Y14C substitution introduced in *macB* gene. The DNA sequence encoding the 21-648 amino acids of MacB was amplified by PCR using pBBYC^{His} plasmid as a template. The two DNA fragments were then ligated by PCR to obtain full length *macAB* gene containing C56A/Y14C substitutions. The DNA product was cloned into NcoI and PstI restriction sites of pBAD/MycHis-C to construct pBABYC^{His} plasmid.

II.3 Protein assays.

II.3.1 SDS-PAGE and western blotting.

Sodium dodecyl sulphate-polyacrylamide gel electrophoresis SDS-PAGE and immunoblotting were performed by standard methods (Tikhonova, Devroy et al. 2007). Samples pre-mixed with the sample buffer plus β-mercaptoethanol were boiled and separated by 12 % SDS-PAGE followed by Coomassie Brilliant Blue (CBB) staining or silver staining. For immunobloting analysis, proteins were transferred onto polyvinylidene difluoride (PVDF) membranes at 75 V for 1 hr. The membranes were kept in blocking buffer (5% dry milk) at 4 ℃ overnight or at Room Temperature (RT) for 1 hr and then incubated with either one of anti-MacB, anti-MacA or anti-TolC rabbit polyclonal antibodies (Tikhonova and Zgurskaya 2004; Tikhonova, Devroy et al. 2007) followed by alkaline-phosphatase-conjugated anti-rabbit IgG antibody (Sigma). The proteins of interest were further visualized by substrates 5-bromo-4-chloro-3-indoyl

phosphate (BCIP) and nitro blue tetrazolium (NBT).

To confirm the biotinylation of proteins, proteins were separated by 12% SDS-PAGE, transferred onto the PVDF membrane, incubated with streptavidin-alkaline -phosphatase (Sigma) and visualized by BCIP and NBT.

II.3.2 Protein concentration determination.

Protein concentrations were determined using Bradford Protein Assay (Bio-Rad) or DC Protein Assay (Bio-Rad) with bovine serum albumin (BSA) as a standard. To determine the concentrations of proteins reconstituted into proteoliposomes or lipid nanodiscs, the protein samples and increasing concentrations of BSA were boiled and separated by 12% SDS-PAGE. Gels were stained with CBB and scanned using CanoScan D1230U scanner. Protein intensities were analyzed by ImageQuant Program (Molecular Dynamics) or Image Processing and Analyzing in Java (Image J). The quantitative data of BSA intensities were then plotted as a function of BSA concentrations to generate a standard curve for the calculation of protein concentrations. The concentrations of proteins were then determined using this standard curve.

II.4 Purification of ApoA-I.

E. coli ER2566 cells bearing the pTYB-ApoA-I were cultured in 4 L Luria-Bertani (LB) broth medium (+ 100 μg/ mL ampicillin) at 37 ℃. When the culture OD_{600} reached about 0.7, the expression of Intein-apoA-I fusion protein was induced by the addition of

Isopropyl β-D-1-thiogalactopyranoside (IPTG) to a final concentration of 0.4 mM at 12℃ for 20 hrs. Cells were collected by low speed centrifugation and resuspended in buffer 20 mM Tris-HCl (pH, 8.5), 5 mM Ethylenediaminetetraacetic acid (EDTA), 1 mM phenylmethane-sulfonylfluoride (PMSF), 5 mM $MgCl_2$ and 0.05 mg/mL Deoxyribonuclease I (DNAase I). French Press was used to disrupt cells and unbroken cells were removed by low speed centrifugation. The cell lysate was mixed with 3 times volume of 20 mM Tris-HCl (pH, 8.5), 500 mM NaCl, 1 mM PMSF (buffer A) supplemented with 2% Triton X-100 (TX-100) and the diluted cell lysate was mixed at 4℃ overnight to solubilize Intein-apoA-I. Next day, the cell lysate was centrifuged at 86,399 g for 40 min at 4℃ and the supernatant was applied onto a chitin column equilibrated with buffer A supplemented with 0.2% TX-100. The column was flushed with 10 bed volumes of buffer A supplemented with 0.2% TX-100 followed by 10 bed volumes of buffer A. Induction of the on column cleavage was conducted by quickly flushing the column with 3 bed volumes of buffer A supplemented with 50 mM Dichlorodiphenyltrichloroethane (DTT) and keeping the column at RT for 16 hrs. The column was washed with fresh cleavage buffer and ApoA-I protein was eluted from the column. The DTT induced column cleavage can be repeated 3-4 times until the majority of ApoA-I protiens were self-cleaved from the column. Purified ApoA-I was kept at 0℃ in 20 mM Tris-HCl (pH 8.0), 150 mM NaCl and 1 mM PMSF buffer for further usage.

II.5 Purification of MacAB-TolC components.

All proteins used in this study contained C-terminal 6-His-tags. MacA, MacB, TolC, $MacA^S$ and their derivatives were purified as described before (Zgurskaya and Nikaido

1999; Tikhonova and Zgurskaya 2004).

For MacA and MacB purification, *E. coli* cells carrying corresponding plasmids for expression were cultured in LB medium at 37℃ and induced by 0.1% arabinose when OD_{600} reached 0.6. After three hours, cells were collected by low speed centrifugation and resuspended in buffer containing 20 mM Tris-HCl (pH, 8.0), 5 mM EDTA, 1 mM PMSF, 100 μg/mL lysozyme (Sigma). Sonication was used to lyse the cells and unbroken cells were removed by low speed centrifugation. Membrane fractions of $MacA^{WT}$ and MacB variants were collected at 163,348 g and 194,398 g at 4℃ for 1.5 hrs, respectively. The membrane fractions of MacB and MacA were then solubilized by incubating in 20 mM Tris-HCl (pH 7.0), 200 mM NaCl, 1 mM PMSF, 0.1 mM β-mercaptoethanol, 5 mM imidazole buffer (MacB buffer) supplemented with 5% TX-100 and 20 mM Hepes-KCl (pH 7.7), 200 mM NaCl, 1 mM PMSF and 5 mM imidazole buffer (MacA buffer) supplemented with 5% TX-100 at 4℃ overnight, respectively. The next day, insoluble proteins were separated at 86,399 g for 40 min at 4℃ and the supernatant was loaded onto Cu^{+2}-charged NTA column (Novagen) equilibrated with MacB or MacA buffer supplemented with 0.2% TX-100. The majority of proteins were eluted by MacA or MacB buffer supplemented with 100-500 mM imidazole. Imidazole was removed by dialysis.

For TolC purification, *E. coli* cells carrying corresponding plasmids for expression were cultured in LB medium at 30℃ and induced overnight by 0.4 mM IPTG when OD_{600} reached 0.3-0.5. French Press was used to lyse the cells and the membrane fractions were separated at 163,348 g for 1.5 hrs at 4℃. The isolated membrane pellet was resuspended and incubated in 20 mM Tris-HCl (pH 7.5), 100 mM NaCl, 1 mM

PMSF, 20 mM $MgCl_2$ and 0.5% TX-100 buffer for 30 min to remove inner membrane and membrane associating proteins. The outer membrane fraction was separated at 86,399 g for 2 hrs at 4℃ and solubilized in 20 mM Tris-HCl (pH 7.5), 100 mM NaCl, 1 mM PMSF buffer supplemented with 5% TX-100 at 4℃ overnight. The purification procedure was the same as that of MacB.

For $MacA^S$ purification, cytoplasmic fraction of the cell lysate was separated at 86,399 g for 40 min at 4℃ and loaded directly onto Cu^{+2}-charged NTA column (Novagen). $MacA^S$ was purified as MacB but without the presence of TX-100.

II.6 Co-purification of MacAB-TolC complex.

The pBB^{His} plasmid expressing 6-His-tagged $MacB^{His}$ and its derivatives or $pBAB^{His}$ plasmids expressing $MacA^{WT}$ together with $MacB^{His}$ variants were transformed into *E.coi* W4680AD (*ΔacrAB, ΔacrD*) strain. Cells were cultured in 200 mL LB medium supplemented with 100 μg/mL ampicillin at 30℃ and induced for 3 hrs by adding L-arabinose to final concentration 0.1% when OD_{600} reached 0.7. Protein purification procedure was the same as that of MacB described above. The 100 mM imidazole fractions were used for further analysis.

II.7 ATPase assay.

To characterize the ATPase activity of MacB in detergent solution at different pH, 20 mM HEPES-KOH (pH 7.0), 5 mM DTT, 50 mM KCl, 0.2% TX-100 buffer and 20 mM MES-KOH (pH 6.0), 100 mM NaCl, 0.2% TX-100 buffer were used as the reaction

buffers for the measurements of the ATP hydrolysis rate of MacB. 0.2-0.42 μM of purified $MacB^{His}$ and its derivatives were added to the reaction mixture prepared with buffers of different pH. The ATP hydrolysis was measured at both 20 ℃ and 37 ℃. The ^{32}P γ-phosphate labelled ATP (3000 Ci $mmol^{-1}$, Amersham) was pre-mixed with unlabelled Mg-ATP and then added at the concentrations indicated in the corresponding figures. At time points of 0, 4, 8, 12, 16 min, one microlitre aliquots were removed from the reaction and mixed with 10 μL of the stop buffer containing 50 mM Tris-HCl (pH 8.0), 20 mM EDTA (pH 8.0), 0.5% SDS, 200 mM NaCl, 0.5 mg/mL proteinase K. The samples were incubated for at least 20 min at 55 ℃ to stop the reaction and then one microlitre of sample was spotted on PEI-F cellulose. The separation of components in each reaction was carried out by thin-layer chromatography (TLC) running in 10% formic acid and 0.5 mM LiCl. The amounts of the free Pi were quantified using Storm PhosphoImager and ImageQuant Software (Molecular Dynamics). The ATP hydrolysis rates or specific ATPase activities of MacB variants were calculated. When indicated, $MacA^{WT}$ was pre-mixed with MacB variants for 15 min before adding into the reaction mixture.

For kinetic measurements of MacA-dependent ATP hydrolysis, increasing concentrations of ATP were added into reactions. The rate of ATP hydrolysis was plotted as a function of ATP concentrations and the data were fit into Michaelis-Menten equation using Origin 8. The Michaelis-Menten equations are given below:

$$v = \frac{V_{max}[S]}{K_M + [S]} \qquad V_{max} = k_{cat}[E_t]$$

Here, V_{max} represents the maximum rate achieved by the system, K_M is the substrate concentration at which the reaction rate is half of V_{max}, k_{cat} measures the number of

substrate molecules turned over per enzyme molecule per second, k_{cat}/K_M, this ratio is often thought of as a measure of enzyme efficiency.

II.8 Reconstitution of proteins into proteoliposomes and nanodiscs.

II.8.1 Reconstitution of proteins into proteiliposomes.

E. coli polar lipids (Avanti) were resuspended in the reconstitution buffer containing 20 mM HEPES-KOH (pH 7.0), 5 mM DTT to the final concentration of 20 mg/mL. Lipids were destabilized with TX-100 in the final concentration of 0.45% and incubated at RT for 15 min. The reconstitution of proteins into liposomes was done by slowly adding a 25-50 μg protein sample into the destabilized liposome suspension, followed by incubation at RT for 30 min and slow removal of TX-100 with Biobeads SM-2 (Bio-Rad). After removing excess of beads with low speed centrifugation, proteoliposomes were diluted two times with reconstitution buffer (20 mM HEPES-KOH pH 7.0, 5 mM DTT) and collected by ultracentrifugation at 53,9994 g for 1 hr at 4℃. The pellet was resuspended in reaction buffer (20 mM HEPES-KOH pH 7.0, 5 mM DTT, 50 mM KCl) and then briefly sonicated. The resulting proteoliposomes were analyzed by quantitative SDS-PAGE to determine protein concentrations and used for assays within 2-3 days.

The ATP hydrolysis activities of MacB and MacAB in proteoliposomes were analyzed as described in section II.6 with following modifications. The final concentration of MacB in reactions was kept at 0.3-0.7 μM. The corresponding concentration of MacA in MacAB proteoliposomes was around 0.75-3.85 μM with calculated MacB/MacA ratio between 1:2.5 and 1:5.5. All the reactions were carried out in the reaction buffer without TX-100. To load ATP into proteoliposomes, the samples

were quickly frozen in liquid N_2 and sonicated after addition of ATP to reaction mixture. After three rounds of freezing and sonication, the samples were briefly pelleted down and immediately placed at 37℃. Reactions were carried out at 37℃ and the amounts of the released Pi were analyzed by thin-layer chromatography as described in section II.6.

II.8.2 Reconstitution of proteins into nanodiscs.

E. coli polar lipids (Avanti) were resuspended in the reconstitution buffer containing 20 mM Tris-HCl (pH 8.0), 0.5 mM EDTA, 5 mM DTT to the final concentration of 20 mg/mL. Lipids was solubilized by addition of 10% TX-100 to the final concentration 3% and incubation 37℃ for 1 hr. 60-120 μg of the purified MacB was slowly added into destabilized lipids and incubated at 37℃ for 1 hr. ApoA-I was then added to the protein/lipids mixture and incubated at 37℃ for 1 hr. The final concentration of each component was 80 μM ApoA-I, 5.6 mM lipids, 14 mM TX-100 and 8 μM MacB corresponding to the molar ratio 1:70:175:0.1. To remove TX-100, samples were extracted with Bio-Beads SM-2 (BioRad), resulting in the formation of MacB-containing nanodiscs (MacB nanodiscs). For reconstitution of empty nanodiscs, ApoA-I was added to lipid/TX-100 mixture immediately after the solubilizaiton step with the same molar ratio as above.

After reconstitution of MacB nanodiscs, the MacB nanodiscs were further purified by loading onto Ni^{2+}-charged NTA column equilibrated with the washing buffer containing 20 mM Tris-HCl (pH 8.0) and 100 mM NaCl. MacB nanodiscs were eluted by the washing buffer supplemented with 500 mM Imidazole. The eluted fractions were analyzed by 12% SDS-PAGE followed by silver staining. Fractions containing MacB nanodiscs were dialyzed against the reconstitution buffer to remove imidazole. The same

protocol was used to reconstitute TolC nanodiscs, but DDM was used as a detergent instead of TX-100. For the immobilization of empty nanodiscs, Cap-Biotin-PEG-PE (Avanti) was premixed with *E. coli* polar lipids in the molar ration 1:20 Cap-PE to *E. coli* and empty nanodiscs were reconstituted as described above.

ATP hydrolysis of MacB in nanodiscs was measured as described in Section II.6 except detergent TX-100 was omitted from the reaction buffer. $MacA^S$ or TolC nanodiscs were pre-mixed with MacB nanodiscs and incubated for 15 min prior to addition into the reaction mixture. Reactions were carried out at 37 ℃ and the amounts of released Pi were analyzed by thin-layer chromatography as described in Section II.6.

II.9 Limited proteolysis.

For proteolysis *in vitro,* 0.42 μg of purified MacB variants were pre-mixed with MES buffer (pH 6.0) (20 mM MES-KOH pH 6.0, 100 mM NaCl, 0.2% TX-100, 8 mM $MgCl_2$) or HEPES buffer (pH 7.0) (20 mM HEPES-KOH pH 7.0, 100 mM NaCl, 0.2% TX-100, 8 mM $MgCl_2$) supplemented with 4 mM nucleotide when indicated and incubated on ice for 5 min to allow the nucleotide binding. Proteolysis was carried out in the presence of increasing concentrations of trypsin (0.01, 0.1, 1.0, 10 μg/mL) in MES buffer (pH 6.0) or HEPES buffer (pH 7.0) at 37 ℃ for 15 min. Reactions were terminated by boiling in the SDS-sample buffer for 5 min. MacB fragments were resolved on 12% SDS-PAGE and visualized by anti-MacB immunoblotting.

II.10 Minimum Inhibitory Concentration (MIC) measurements.

MICs of oleandomycin and erythromycin were determined in 96 well plates as described previously (Tikhonova and Zgurskaya 2004). pUCMacAB plasmids were transformed into *E. coli* W4680AD (*ΔacrAB, ΔacrD*) cells. Approximately 10^5 exponentially growing cells (OD_{600} 0.4-0.6) were inoculated into LB medium supplemented with two-fold increasing concentrations of drugs. The cell growth was visualized after incubation at 30 ℃ overnight. The MICs of the drugs were determined as the lowest concentration of drugs that completely inhibits cell growth.

II.11 Surface Plasmon Resonance (SPR).

BIAcore 3000 biosensor and SensiQ Pioneer systems were used to characterize binding reactions (Tikhonova, Dastidar et al. 2009; Tikhonova, Yamada et al. 2011).

Biotinylation.

Tris [2-carboxyethyl] phosphine hydrochloride (TCEP) disulfide reducing gel was used to reduce the disulfide bonds formed in MacB-Cys variants. 200 µL of 0.5-0.9 mg/mL proteins were loaded onto an equal volume of the TCEP gel equilibrated with buffer containing 20 mM Tirs-HCl (pH 7.0), 150 mM NaCl, 5 mM EDTA, 0.2% TX-100 and incubated at RT for 45 min. The proteins were then eluted from the column with the same buffer in the first two or three fractions. The protein concentrations were determined by Bradford assay using BSA as a standard. 20 mM Maleimide-Polyethylene

glycol (PEG_2)-Biotin (MP-biotin) in phosphate buffered saline (PBS) buffer was freshly prepared. Reduced proteins were mixed with biotin solution to a 20:1 MP-biotin to protein molar ratio and the mixtures were incubated on ice for 2 hrs. To remove excessive thio-reagent, the biotin-protein mixtures were loaded onto NAP-5 column (GE HealthCare, Sephadex G-25) equilibrated with elution buffer containing 20 mM Tirs-HCl (pH, 7.0), 150 mM NaCl, 5 mM EDTA, 0.2% TX-100. Proteins were eluted with the elution buffer and the 0.5 mL fractions were collected. To ensure the removal of free biotin from the biotinylated proteins, the biotinylated protein samples were dialyzed against the elution buffer. The biotinylation of MacB variants as further confirmed using 12% SDS-PAGE followed by western blotting.

Immobilization.

Surface activation and protein immobilization procedures were performed as reported (Tikhonova et al., 2009, 2011). The Biacore system and a Streptavidin-coated SA biosensor chip (Biacore) were primed in the HEPES running buffer (pH 7.4) containing 20 mM HEPES-KOH, 150 mM NaCl, 0.2% TX-100. In order to clean up the surface, 50 mM NaOH and 1 M NaCl buffer were injected over the surfaces at a 40 μL/min flow rate for 1 min three times followed by 500 mM $MgCl_2$ at a 40 μL/min flow rate for 1 min. Approximately 0.01 μg/mL of biotinylated proteins were injected for 4 min at a low rate of 10 μL/min into a flow cell. The injection was stopped when desired concentrations of proteins were immobilized onto the surfaces. A protein-free flow cell prewashed with NaOH/NaCl solution and $MgCl_2$ was used as a control. $TolC^{A269C}$ was immobilized onto a $COOH_2$ chip using a previously described thiol-coupling protocol (Tikhonova, Dastidar et al. 2009).

Data collection and normalization.

The analyte samples were prepared in the appropriate running buffer and filtered to remove protein aggregates. The concentrations of proteins were determined by Bradford or DC Protein Assay using BSA as a standard. All experiments were performed in MES running buffer (pH 6.0) containing 20 mM MES-KOH, 150 mM NaCl, 0.2% TX-100 or HEPES running buffer (pH 7.0) containing 20 mM HEPES-KOH, 150 mM NaCl, 0.2% TX-100. 8 mM $MgCl_2$ was added into the running buffers when indicated. For kinetic study, 5-6 two fold serial dilutions of analytes (proteins, nucleotides and $MgCl_2$) were prepared and injected over the surfaces at a 50 μL/min flow rate for 2 min. The samples were injected over MacB and control surfaces simultaneously. Nucleotides were pre-mixed with proteins before injections when indicated. The surfaces were regenerated between each analyte injection by injecting regeneration buffer containing 500 mM $MgCl_2$, 20 mM Tris-HCl (pH 8.0), 150 mM NaCl, 0.2% TX-100 for 2 min. In order to wash out the remaining $MgCl_2$, the running buffer was injected over the surfaces for 1 min after each regeneration step. To acquire a response signal specific to the analyte-ligand interaction, the injection start time for the original sensorgrams was aligned and the signal on the control surface was subtracted from the total response on the ligand surface. To account for instrumental noise and discrepancy in buffer compositions, the running buffer was injected over the surfaces. Furthermore, the signal from the running buffer was also subtracted from the total response on the ligand surface as referred to the double referencing step.

Data analysis.

To determine the kinetic parameters, the BIAevaluation (GE Healthsciences) software was used to fit data into several common bimolecular interaction models. Due to the fast association and dissociation rates, the binding curves of nucleotides to MacB could not be fit into any kinetic models. The normalized steady state binding responses of nucleotides were plotted as a function of nucleotide concentrations.

The binding curves of MacA to MacB were fit globally into Two-State reaction (TS) model. Schematic representation and equations relevant to this model are given below:

$$(1) A + B \underset{k_{-1}}{\overset{k_1}{\rightleftarrows}} A \cdot B \underset{k_{-2}}{\overset{k_2}{\rightleftarrows}} \left[A \cdot B^* \right]$$

$$(2) \frac{\partial (A \cdot B)}{\partial t} = k_1 [A][B] - \left(k_{-1} [A \cdot B] - k_{-2} \left[A \cdot B^* \right] \right)$$

$$(3) \frac{\partial (A \cdot B^*)}{\partial t} = k_2 \left[A \cdot B^* \right] - k_{-2} \left[A \cdot B^* \right]$$

$$(4) R_t = [A \cdot B] + \left[A \cdot B^* \right]$$

The equilibrium dissociation constant for this model is:

$$(5) K_D = \frac{k_{-1} k_{-2}}{k_1 k_2}$$

where [A] is the concentration of analyte; [B] is the ligand binding capacity; [A B] and [A B*] are intermediate and final complexes, respectively; k_{-1}, k_{-2}, k_1, and k_2 are microscopic rate constants; and R_t is the total SPR response, which is directly proportional to [A B] + [A B*].

The observed rate constant is:

$$(6)\ k_{obs} = k_a \cdot [A] + k_d$$

where k_a is the rate constant for association, k_d is the rate constant for dissociation and [A] is the analyte concentration determined by fitting sensorgrams locally into a simple bimolecular interaction model using BIAevaluation software.

II.12 Size-exclusion chromatography (SEC).

High-performance liquid chromatography (HPLC) was used to further purified homogeneous nanodiscs or MacB/TolC nanodiscs. The nanodiscs samples were loaded onto YMC-Pack Diol-300 size exclusion column with a flow rate of 1 mL/min. The presence of protein was detected by absorbance at 280 nm and fractions were collected every 0.5 min. The protein composition of each fraction was determined using 12% SDS-PAGE followed by silver staining. To determine the size of the nanodisc particles, samples were pre-mixed with a standard containing carbonic anhydrase (CA, 29 kD, R_M=2.01 nm), bovine serum albumin (BSA, 66 kD, R_M=3.61 nm), alcohol dehydrogenase (AD, 150 kD, R_M=4.65 nm), thyroglobulin (Tg, 440 kD, R_M=8.58 nm) and loaded onto the column. The MWs of standard proteins were plotted as a function of protein radii. The radii of nanodisc particles were calculated from the standard curve. To further confirm the homogeneity of nanodisc particles, the samples were reloaded onto the SEC column running at 0.1 mL/min and the presence of protein was detected by absorbance at 280 nm.

To determine the oligomeric state of MacA and MacB, 5-10 μg of purified $MacA^S$, $MacA^{WT}$ and MacB were pre-mixed with a similar amount of a standard containing BSA (66 kD), alcohol dehydrogenase (150 kD) and ferritin (440 kD). The mixtures were

loaded onto self-packed 1 mL Sephacryl ^{TM} S-300 column equilibrated with MES (pH 6.0) running buffer with or without 8 mM $MgCl_2$. Fractions were collected and analyzed on 12% SDS-PAGE followed by silver staining. The intensity of protein bands on SDS-PAGE was further analyzed by Image J and plotted against fraction number.

II.13 Lipid concentration determination.

To analyze reconstituted nanodiscs, the lipid concentration was determined by measuring the inorganic phosphorus concentration as described in (Fiske and Subbarow 1925; Chen, Toribara et al. 1956) . A standard containing 1, 3, 5, 7 and 9 mM KH_2PO_4 was prepared. 10-100 μL of each sample were placed into a new glass tube followed by addition of 20 μL 10% $Mg(NO_3)_2$ in ethanol and were dried to ashes in a flame. 300 μL of 0.5 M HCl were added after tubes cooled down and samples were boiled a water bath for 15 min. Six parts of 0.42% $(NH_4)_6$ Mo_7O_{24} in 1 M H_2SO_4 and one part of 10% $C_6H_8O_6$ were mixed together before use. 700 μL of this mixture were added into the sample tubes and samples were incubated at 37 ℃ for 1 hr. Absorbance of each sample at 820 nm was determined by spectrophotometer (SHIMADZU, UV-1601) and the final concentration of lipid was calculated from a plot of the absorbance at 820 nm as a function of phosphorus concentrations.

II.14 Transmission electron microscopy (TEM).

Reconstituted rHDL and purified MacB nanodiscs samples were adsorbed onto carbon-coated copper grids at RT for 2 min. Then the grids were washed with double

distilled water and stained with 2% phosphotungstic acid (PTA) (pH 7.1) (Wlodawer, Segrest et al. 1979). Electron micrograph images of empty nanodiscs and MacB nanodiscs were recorded with a JEOL 2000-FX transmission electron microscope (TEM) operated at 100 Kv.

Chapter 1: Characterization of the functionality of MacB variants.

1.1 MacB variants exhibit different basal ATPase activity level.

In order to characterize the mechanism of complex assembly of MacAB-TolC, we wanted to investigate the kinetic of MacAB-TolC assembly and the role of ATP in this process. For this purpose, we intended to develop a real time assay using surface plasmon resonance (SPR) approach to monitor the kinetic association between MacAB and TolC. The first critical step of SPR method is to immobilize target proteins onto the surface. In our study we decided to immobilize inner membrane transporter MacB onto the surface. The general transport mechanism of ABC-type transporters starts with the binding of ATP and substrates (Davidson, Dassa et al. 2008). To investigate the assembly of MacAB-TolC tripartite complex during transport process, MacB, as the substrates and ATP binding protein, is a good candidate for immobilization. In addition, immobilization of MacB onto the surface can provide us an opportunity to understand the kinetics of MacA-MacB bipartite complex assembly and the role of ATP in this process.

In order to immobilize homogeneous and functional MacB onto the surface, we wanted to use streptavidin-coated SA chip. Streptavidin on the surface captures biotinylated proteins with high affinity and all the biotinylated proteins can be immobilized in a known and uniform orientation on the surface. In our expectation, the interaction between biotin and streptavidin could keep all immobilized MacB in an up and down orientation. Another advantage of using a SA chip is the neutral pH of the immobilization buffer. Both the amine and thiol coupling procedures require low pH (pH

4.8) during immobilization. Some proteins are unstable under such conditions and might aggregate or become inactive on the surface.

For biotinylation purposes, we wanted to introduce a single cysteine substitution at either N- or C- terminal end of MacB, which could react with Maleimide-Polyethylene glycol (PEG_2)-Biotin (MP-biotin). In the amino acid sequence of MacB, there are three intrinsic cysteine residues, at positions 56, 580 and 620 (Figure I.4). C580 and C620 are located in the hydrophobic TM region of MacB and are not accessible to N-ethyl maleimide (NEM) (Kobayashi, Nishino et al. 2003). C56, on the other hand, is located in the first putative loop region of MacB NBD and could react with MP-biotin. To avoid undesired biotinylation at position 56, we mutated this cysteine into alanine. We then introduced a D643C mutation into the C-terminal end of $MacB^{WT}$ and $MacB^{C56A}$, respectively (Figure I.4). D643 is located at the cytoplasmic end of MacB. Overexpression of $MacB^{D643C}$ confers resistance to erythromycin upto $MacB^{WT}$ level, indicating D643C is a functional silent substitution (Kobayashi, Nishino et al. 2003).

Previous studies (Tikhonova, Devroy et al. 2007) suggest that both the cytoplasmic and periplasmic portions of MacB are important for the interaction with MacA and for the stimulation of MacB ATPase activity by MacA. We next constructed MacB variants with substitutions in both the cytoplasmic and periplasmic regions of MacB, which could disrupt different ATP hydrolysis steps MacB (Figure 1.1 A). D169, a highly conserved residue in the Walker B region of NBDs, is responsible for ATP hydrolysis by acting as a general base (Geourjon, Orelle et al. 2001). $MacB^{D169N}$ completely loses its ATPase activity and fails to complement the hypersensitivity of *E. coli* W4680 (Δ*acrAB,* Δ*acrD*) strain to macrolides (Tikhonova, Devroy et al. 2007). Thus, $MacB^{D169N}$ was used as the

catalytical inactive MacB. To disrupt the interaction between MacA and MacB in the periplasmic regions, we deleted the large periplasmic loop (LPL) between TM1 and TM2 of MacB to construct $MacB^{LPL}$ mutant. This LPL region of MacB is proposed to be significant for the interaction between MacA-MacB and probably required for MacB-TolC interactions (Yum, Xu et al. 2009). For immobilization purposes, we introduced D643C point mutation into $MacB^{LPL}$ and $MacB^{D169N}$. The $MacB^{LPL}$ and $MacB^{169}$ discussed below are $MacB^{LPL}$ and $MacB^{D169N}$ with D643C substitution at the C-terminal end of MacB. Finally, to disrupt the binding of nucleotides, we mutated the highly conserved residue Y14 in the A-loop of MacB NBD. This Y14 stacks against the adenine ring of ATP and contributes to the nucleotide-binding affinity of NBDs in well characterized ABC transporters (Geourjon, Orelle et al. 2001; Carrier, Urbatsch et al. 2007). We introduced cysteine at postion Y14 into $MacB^{C56A}$ to construct $MacB^{YC}$ mutant.

In order to determine how the sunstitutions in MacB affect the ATP hydrolysis of MacB, we measured the ATPase activities of these MacB variants *in vitro*. All MacB variants were purified under the same condition as described in Experimental Procedures II.5. The concentrations of MacB variants were measured by Bradford or DC assay. The quality of proteins was verified using SDS-PAGE followed by CBB staining (Figure 1.1 B). The ATPase assay was carried out in HEPES buffer (pH 7.0) containing 20 mM HEPES-KOH, 5 mM DTT, 50 mM KCl at 37 ℃. 0.42 μM purified MacB variants and 1 mM Mg-ATP were added into reactions. Measured specific ATPase activities are shown in Figure 1.1 C.

$MacB^{D643C}$ showed ATPase activity similar to that of $MacB^{WT}$, indicating that

D643C substitution does not affect MacB function.

$MacB^{C56A}$ lost about 60% of MacB ATPase activity when compared to $MacB^{WT}$, indicating that position C56 is detrimental to the MacB ATPase. C56 is located eight positions down-stream from the Walker A motif of MacB. This result demonstrates that C56 in the NBD domain of MacB might contribute to the ATP binding, hydrolysis or both activities.

$MacB^{C56A/D643C}$ showed comparable ATPase with $MacB^{C56A}$, confirming that D643C has no effect on MacB function.

On the other hand, the Y14C substitution further diminished the ATPase activity of $MacB^{C56A}$ about three-fold. Since Y14 is involved in nucleotide binding to MacB, the loss of ATPase activity of $MacB^{YC}$ could be due to the defect in ATP binding of MacB. It is also possible that Y14 may also contribute to the ATP hydrolysis of MacB.

Moreover, in agreement with previous studies (Tikhonova, Devroy et al. 2007), $MacB^{D169N}$ lost the ability to hydrolyze ATP, confirming that D169N substitution completely inactivates MacB.

Surprisingly, $MacB^{LPL}$ retained its ATPase activity, which was only about 40% lower than that of $MacB^{D}$. The persistence of ATPase activity of $MacB^{LPL}$ suggests that the large periplasmic loop of MacB does not play a significant role in MacB ATP hydrolysis.

Previous studies suggest that the assembly of AcrAB-TolC tripartite complex is modulated by pH and the complexes are highly stable at pH 6.0 (Tikhonova, Dastidar et al. 2009; Tikhonova, Yamada et al. 2011). In order to capture the stable complexes of MacAB-TolC on the surface, we intended to use the MES buffer (pH 6.0) for our SPR

study. Since the ATPase assay above was carried out in HEPES buffer (pH 7.0), next we investigated whether MacB variants can hydrolyze ATP at pH 6.0 and how the ATPase activities of these MacB variants are affected by this pH change. For this purpose, we measured the ATPase activity of MacB variants in MES running buffer (pH 6.0) containing 20 mM MES-KOH (pH 6.0), 150 mM NaCl, 0.2% Triton X-100. All the measurements were carried out at 37 ℃ with 0.42 μM MacB and 1 mM Mg-ATP in each reaction (Figure 1.1 D).

Shift in pH from 7.0 to 6.0 decreased the ATPase activity of $MacB^{WT}$ and $MacB^{D}$ by about 50%. However, $MacB^{D}$ still showed ATPase activity similar to that of $MacB^{WT}$ at pH 6.0. This result confirms that $MacB^{D}$ is functional as $MacB^{WT}$ at pH 6.0.

In agreement with the measured ATPase activity at pH 7.0, $MacB^{YC}$ was defective in ATP hydrolysis at pH 6.0. The ATPase activity of $MacB^{YC}$ was about four fold lower than that of $MacB^{WT}$.

Surprisingly, the specific ATPase activity of $MacB^{LPL}$ at pH 6.0 is comparable to that of $MacB^{WT}$, indicating that at pH 6.0 $MacB^{LPL}$ can hydrolyze ATP with the same efficiency as $MacB^{WT}$.

These results suggest that $MacB^{D}$ functions as $MacB^{WT}$, whereas $MacB^{YC}$ is defective in hydrolyzing ATP. In addition, $MacB^{LPL}$ is functional more like $MacB^{WT}$ at pH 6.0.

Taken together, we are able to construct MacB variants with different ATP hydrolysis activities: $MacB^{D}$, a functional ATPase, $MacB^{LPL}$, a conditionally functional ATPase, $MacB^{YC}$, an ineffective ATPase and $MacB^{169}$, an inactive ATPase.

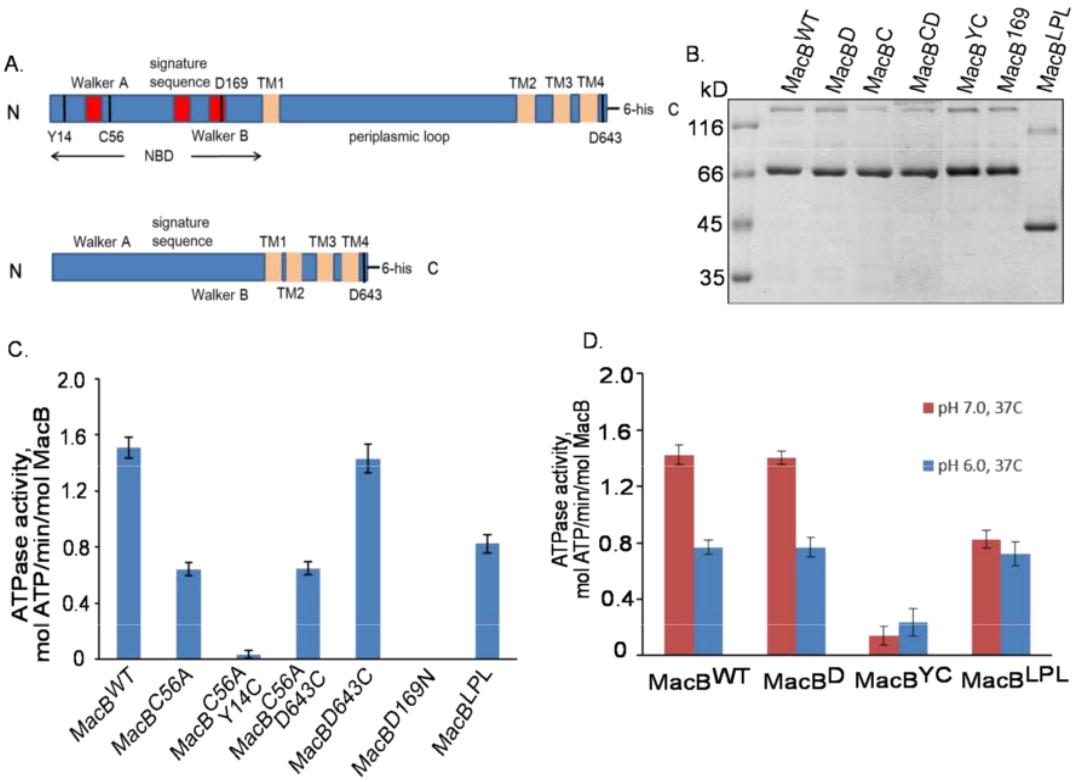


Figure 1.1 Specific ATPase activity of MacB^{WT} and its derivatives. A. Schematic representation of the secondary structures of MacB variants. The TMS, NBD, PCD domains of MacB and the walker A, signature sequence, walker B ranges of MacB NBD are indicated. Point substitutions are highlighted with black lines. B. 1 μg purified MacB^{WT} and MacB variants were separated by 12% SDS-PAGE and stained with CBB. C. Specific ATPase activity of MacB^{WT} and its derivatives measured in HEPES buffer (pH 7.0). Reactions contained 0.42 μM MacB and were carried out at 37 ℃ in the presence of 1 mM Mg-ATP. Error bars are SDs (n = 3). D. Specific ATPase activity of MacB^{WT} and its derivatives measured in HEPES buffer (pH 7.0) and in MES buffer (pH 6.0). The composition of reactions is the same as A and measurements were carried out at 37 ℃.

1.2 Different conformational states of MacB variants.

The above results show that MacB variants differ in their ATPase activities. One possible reason could be due to the conformational changes in MacB that affects the ATP binding and hydrolysis of MacB variants. To compare the conformational status of MacB variants, we used *in vitro* limited proteolysis. For this purpose, purified MacB variants were treated with increasing concentrations of trypsin in MES running buffer (pH 6.0) at 37℃ for 15 min and MacB digestion fragments were visualized by anti-MacB immunoblotting. As shown in Figure 1.2 A, at 10 μg/mL trypsin concentration, all three MacB variants were completely digested into 35, 34, 33 and 31 kD fragments. But the lower concentrations of trypsin revealed certain differences between proteins. The proteolytic patterns of $MacB^{D}$ and $MacB^{169}$ were identical with most of proteins digested into 35 kD fragment at 1μg/mL trypsin concentration. This result suggests that $MacB^{D}$ and $MacB^{169}$ adopt the same conformation in detergent. However, $MacB^{YC}$ showed a digestion profile different from that of $MacB^{D}$ and $MacB^{169}$. $MacB^{YC}$ was more resistant to trypsin as seen from the presence of the whole length $MacB^{YC}$ and its 60 and 50 kD fragments at 1 μg/mL trypsin. A 42 kD fragment was only detected in $MacB^{YC}$ proteolytic profile further suggesting that $MacB^{YC}$ adopts a conformation different from that of $MacB^{D}$ and $MacB^{169}$. Whereas, in the case of $MacB^{LPL}$, only two minor digested fragments of $MacB^{LPL}$ were produced and none of them matched the fragments from the full length MacB variants. This is most likely because of the absence of trypsin digestion sites in MacB LPL.

Since the ATPase activities of MacB variants were sensitive to pH, we also checked the proteolytic profiles of MacB variants in HEPES buffer (pH 7.0). Even though the

digestion patterns of $MacB^{D}$, $MacB^{169}$ and $MacB^{YC}$ at pH 7.0 were similar to those at pH 6.0, proteins were more resistant to trypsin as seen in the presence of the full length proteins and its 50 kD fragment at 1 μg/mL trypsin. In agreement with the digestion profiles at pH 6.0, no differences were detected between $MacB^{D}$ and $MacB^{169}$. However, $MacB^{YC}$ digestion profile did not show the 38 kD fragment but extra fragments 33 and 31 kD were present at 1 μg/mL trypsin, indicating that $MacB^{YC}$ is more sensitive to trypsin than $MacB^{D}$ and $MacB^{169}$ at pH 7.0. The 42 kD fragment was still unique to $MacB^{YC}$. This result confirms that $MacB^{YC}$ exhibits a different conformation from that of $MacB^{D}$ and $MacB^{169}$. The conformational difference of $MacB^{YC}$ could be one of the reasons for the loss of $MacB^{YC}$ ATPase activity. In contrast, inactive $MacB^{169}$ is caused by the disability of binding or hydrolyzing ATP rather than a structure defect.

Comparison of the trypsin digestion profiles of MacB variants in Figure 1.2 revealed that $MacB^{YC}$ showed opposite trend of resistance toward trypsin comparing with that of $MacB^{D}$ and $MacB^{169}$ at different pH. Interestingly, this trend was also seen in the ATPase activities of $MacB^{D}$ and $MacB^{YC}$ (Figure 1.2 D). $MacB^{YC}$ exhibited higher ATPase activity at pH 6.0 than that at pH 7.0. However, the ATPase activities of $MacB^{D}$ reduced about 50% from pH 7.0 to pH 6.0. These results suggest that $MacB^{YC}$ is more stable at pH 6.0 but $MacB^{D}$ is destabilized at pH 6.0.

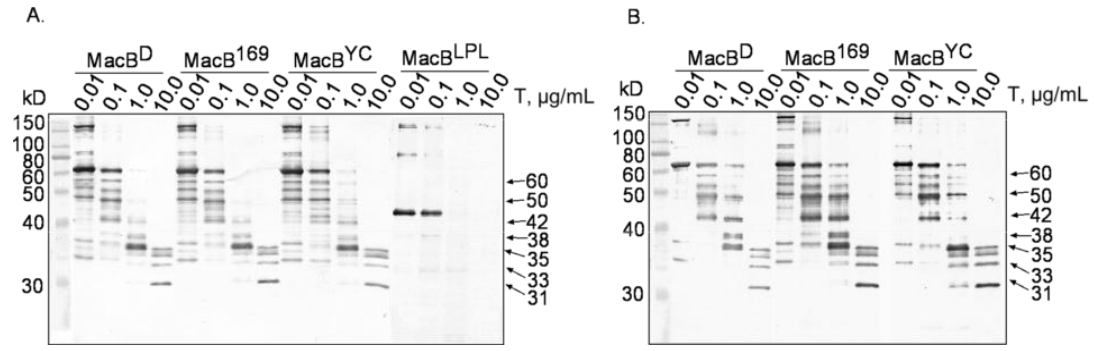


Figure 1.2 Trypsin digestion patterns of MacB^{D}, MacB^{169}, MacB^{YC} and MacB^{LPL}. A. 0.42 μg of purified MacB variants were treated with increasing concentrations of trypsin (0.01, 0.1, 1.0, 10 μg/mL) in MES running buffer plus 8 mM $MgCl_2$ (pH 6.0) and incubated at 37℃ 15 min. Reactions were terminated by boiling in SDS-sample buffer for 5 min. MacB fragments were resolved on 12% SDS-PAGE and visualized by anti-MacB immunoblotting. The numbers on the right are the molecular weight (MW) of digestion products in kD calculated based on the mobility of fragments as compared to the standard protein marker. B. The same as A but reactions were carried out in HEPES running buffer (pH 7.0).

1.3 ATP binding induces conformational changes of MacB variants.

Previous studies show that MacB is more resistant to trypsin in the presence of nucleotides *in vivo* (Modali and Zgurskaya 2011). This finding is in agreement with the model that the binding of nucleotides to MacB triggers the closure of NBDs. To further explore the reasons for deactivation of MacB variants, we investigated the *in vitro* trypsin digestion patterns of MacB variants in the presence of nucleotides.

For this purpose, purified MacB variants were pre-mixed with 4 mM Mg-ATP, 4 mM Mg-ADP or 4 mM Mg-AMPPNP and incubated on ice for 5 min to allow the binding of

nucleotides before addition of increasing concentrations of trypsin. MacB fragments were visualized by anti-MacB immunoblotting. At 1 μg/mL trypsin and pH 6.0 (Figure 1.3), the whole length proteins of $MacB^{D}$ and $MacB^{169}$ were detected in the presence not in the absence of nucleotides, suggesting that the binding of nucleotides notably protected these MacB variants from digestion. The protection against trypsin in the presence of nucleotides could also be seen for $MacB^{YC}$ but with a significantly less level than that of $MacB^{D}$ and $MacB^{169}$. At 1 μg/mL trypsin the proteolytic pattern of $MacB^{YC}$ in the absence of nucleotides was similar to that of $MacB^{D}$ or $MacB^{169}$ in the presence of nucleotides. This result suggests that the NBDs domains of $MacB^{YC}$ are likely to be in a semi-open conformation which could lead to a reduced affinity towards nucleotides. Similarly, $MacB^{LPL}$ was also more resistant to trypsin in the presence of nucleotides, meaning the closure of NBDs does not need the presence of periplasmic loop of MacB. Since ATP, ADP and AMP-PNP all resulted in the same protective changes of MacB variants against trypsin, we can conclude that the binding of nucleotides induce the same conformational changes in MacB variants.

At 1 μg/mL trypsin and pH 7.0 (Figure 1.3), the disappearance of full length proteins and 60, 50, 38 kD fragments indicated that $MacB^{D}$, $MacB^{YC}$ and $MacB^{169}$ were more susceptible to trypsin in the presence of nucleotides. The 42 kD fragment of $MacB^{YC}$ in the nucleotide bound state can be clearly detected at 0.1 μg/mL trypsin. This result confirms that the $MacB^{YC}$ has a conformation that is distinct from the nucleotide bound conformation of $MacB^{D}$ and $MacB^{169}$. Taken together, these results suggest that $MacB^{YC}$ adopts a different conformational state from that of $MacB^{D}$ and $MacB^{169}$. Furthermore, the binding of nucleotides induces the closed conformation of MacB NBDs.

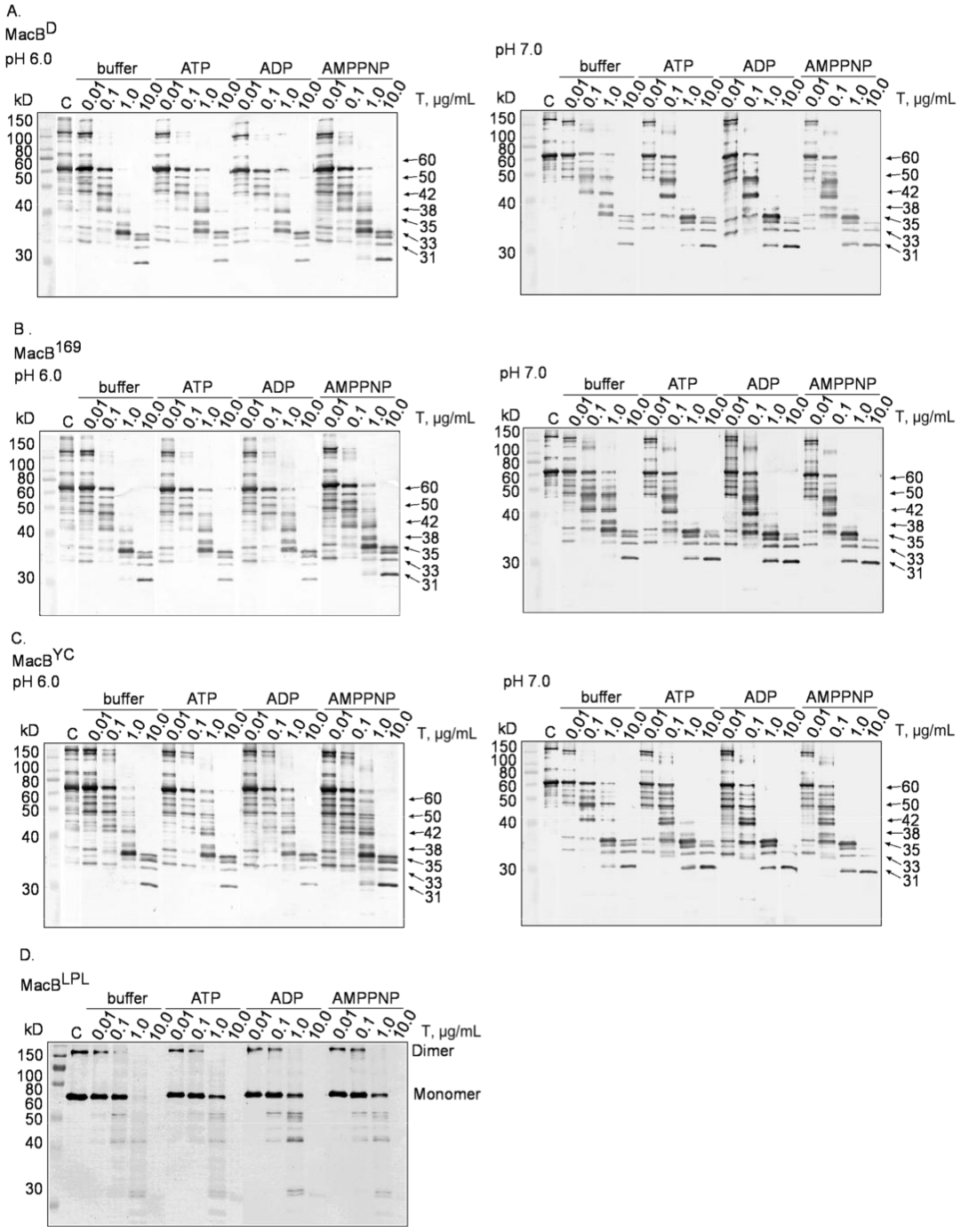


Figure 1.3 Trypsin digestion patterns of MacB^{D}, MacB^{169}, MacB^{YC} and MacB^{LPL} in the presence or absence of nucleotides. A. 0.42 μg of purified MacB^{D} were pre-mixed with 4 mM Mg-ATP, 4 mM Mg-ADP and 4 mM Mg-AMPPNP when indicated. Reactions were incubated on ice for 5 min to allow the binding of nucleotides.

Proteolysis was carried out with indicated concentrations of trypsin in MES running buffer supplemented with 8 mM $MgCl_2$ (pH 6.0) and HEPES running buffer (pH 7.0). Reactions were incubated at 37℃ for 15 min. MacB fragments were visualized by anti-MacB immunoblotting. B. The same as A but with 0.42 μg $MacB^{169}$. C. The same as A but with 0.42 μg $MacB^{YC}$. D. The same as A but with 0.42 μg $MacB^{LPL}$ in MES running buffer supplemented with 8 mM $MgCl_2$ (pH 6.0).

1.4 MacA stimulates the ATPase activity of MacB variants except for $MacB^{LPL}$.

Previous studies showed that MacA significantly stimulates MacB ATPase activity significantly when reconstituted together with MacB into proteoliposomes (Tikhonova, Devroy et al. 2007; Modali and Zgurskaya 2011). In order to investigate whether introducing mutations into MacB affect the MacA-dependent stimulation of MacB ATPase activity, we measured the ATPase activities of MacB variants in the presence or absence of MacA reconstituted into proteoliposomes. Purified $MacB^{WT}$ and its derivatives were reconstituted into proteoliposomes alone or together with MacA. 0.42 μM MacB in proteoliposomes and 1 mM Mg-ATP were added into each reaction and all measurements were carried out in HEPES buffer (pH 7.0) at 37℃ (Figure 1.4). In agreement with previous studies (Tikhonova, Devroy et al. 2007), MacA stimulated by 25 fold the ATPase activities of both $MacB^{D}$ and $MacB^{WT}$. Thus, in proteoliposomes $MacB^{D}$ functions as $MacB^{WT}$. $MacB^{C56A}$, $MacB^{C56A/D643C}$ and $MacB^{YC}$ alone in proteoliposomes still showed defect in hydrolyzing ATP comparing to that of $MacB^{WT}$. However, MacA reconstituted together with MacB variants into proteoliposomes managed to rescue the

loss of ATPase activities of MacB variants but not to the same extent as that of $MacB^{WT}$. This result suggests that introducing these substitutions in the NBDs of MacB cause minimal disruptions of the interaction between MacA and MacB. Interestingly, MacA failed to activate $MacB^{LPL}$ in proteoliposomes with less than two fold increase in MacB ATPase, suggesting that the large periplasmic loop of MacB is involved in MacA-dependent stimulation of MacB ATPase.

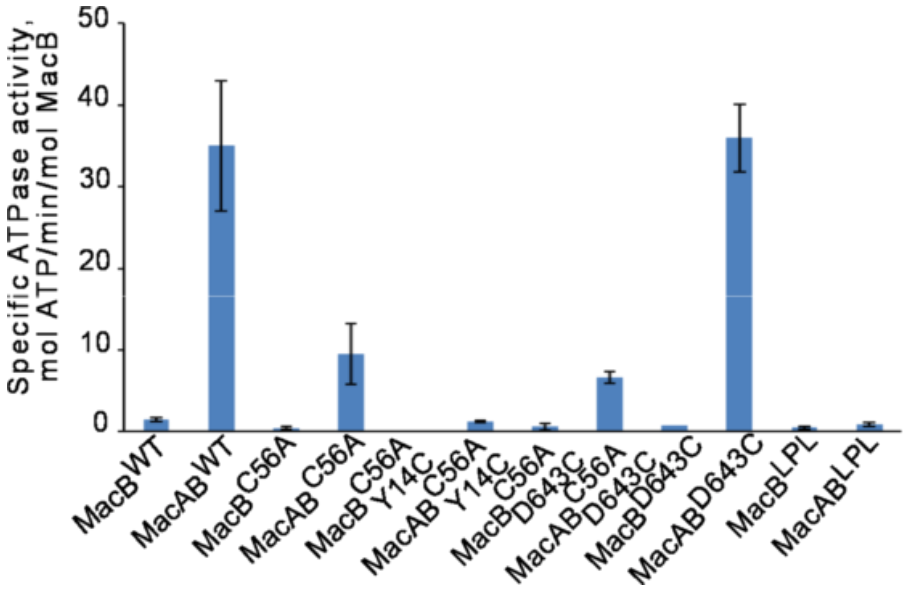


Figure 1.4 Specific ATPase activity of MacB and MacAB proteoliposomes. Proteoliposomes containing 0.42 μM MacB and 1 mM Mg-ATP were used in all reactions. Measurements were carried out at 37 ℃ in HEPES buffer (pH 7.0). Error bars are SDs (*n* = 3).

1.5 Kinetic properties of MacB variants.

Even though the MacA-dependent stimulation of MacB ATPase is not as strong as in detergent, about 40% increase can be detected with 3:1 MacA to MacB molar ratio in

reaction (Tikhonova, Devroy et al. 2007). In order to investigate how the ATPase activities of MacB variants were stimulated by MacA in MES buffer (pH 6.0), we measured the ATP hydrolysis rate of MacB variants with different MacA to MacB ratio (Figure 1.5). All reactions contained 0.42 μM MacB and 1 mM Mg-ATP and were carried out in MES buffer (pH 6.0) at 20 ℃ with different MacA to MacB ratio in each reaction. The ATP hydrolysis rate of $MacB^{WT}$ and $MacB^{D}$ increased about 30-40% at 3:1 MacA to MacB molar ratio and slightly decreased at higher MacA to MacB molar ratio. Even though the ATP hydrolysis rate of $MacB^{YC}$ is four-fold lower than that of $MacB^{D}$, the stimulation by MacA showed the same trend. This result implies that $MacB^{YC}$ interacts with MacA the same way as MacBWT and MacBD. In agreement with the result in proteoliposomes, $MacB^{LPL}$ had no response to the presence of MacA and no stimulation by MacA was detected, confirming that the periplasmic loop is important for MacA-dependent stimulation of MacB ATPase.

To further characterize the kinetic properties of MacB and MacAB ATPase, we measured the ATP hydrolysis rate of MacB and MacAB variants in the presence of increasing concentrations of ATP. All reactions contained 0.42 μM MacB and MacA to MacB molar ratio was kept at 3:1. 0.1-6 mM Mg-ATP was added into reactions. To get kinetics parameters for $MacB^{WT}$ and its derivatives, the MacB ATP hydrolysis rates were plotted as a function of ATP concentrations and data points were fit into Michaelis-Menten equation (Figure 1.6 & Table 1.1). Similar to $MacB^{WT}$, $MacB^{D}$ hydrolyzed 4 ATP molecules per min, suggesting $MacB^{D}$ has the same kinetic properties as $MacB^{WT}$ in pH 6.0. $MacB^{YC}$, on the other hand, could only hydrolyze less than one ATP per min. The V_{max} value of $MacB^{YC}$ decreased about 70%-80% compared to those of

$MacB^{WT}$ and $MacB^{D}$. These results indicate that $MacB^{YC}$ is a slower ATPase than $MacB^{D}$. The presence of MacA increased the V_{max} values of $MacB^{WT}$, $MacB^{D}$ and $MacB^{YC}$, suggesting that MacA is able to stimulate the ATPase activities of MacB variants.

K_M represents the substrate concentration at which the reaction rate is half of V_{max} and is considered to reflect the binding affinity of substrates towards enzymes. The K_M values of $MacB^{D}$ and $MacB^{YC}$ were comparable but 40% lower than that of $MacB^{WT}$, indicating that ATP has similar affinity towards $MacB^{D}$ and $MacB^{YC}$. This result is in conflict with our prediction that $MacB^{YC}$ is defective in ATP binding. Since the ATP hydrolysis rates of $MacB^{YC}$ measured in pH 6.0 at 20℃ were considerably low, any experimental error could cause this deviation. On the other hand, the purified $MacB^{D}$ could be inactivated for some reasons leading to reducing in ATP binding affities. In the presence or absence of MacA the K_M values of $MacB^{WT}$ and $MacB^{D}$ were similar, suggesting the presence of MacA does not significantly affect the MacB binding affinity toward ATP.

The k_{cat}/K_M parameter evaluates the enzyme efficiency. As shown in Table 1.1, despite the difference in ATP hydrolysis stages, MacA elevates the ATP hydrolysis efficiencies of all MacB variants expect for $MacB^{LPL}$. This result further suggests that the interaction between MacA and MacB variants remains the same.

Taken together, $MacB^{D}$ functions as $MacB^{WT}$ and $MacB^{YC}$ is a slower ATPase than $MacB^{D}$ and $MacB^{WT}$. Despite the differences in ATP hydrolysis abilities of $MacB^{D}$, $MacB^{WT}$ and $MacB^{YC}$, MacA can stimulate the ATPase activities of all three MacB variants. $MacB^{LPL}$ cannot be stimulated by MacA in both proteoliposomes and detergent, suggesting the LPL domain of MacB plays a significant role in MacA-dependent

stimulation of MacB ATPase.

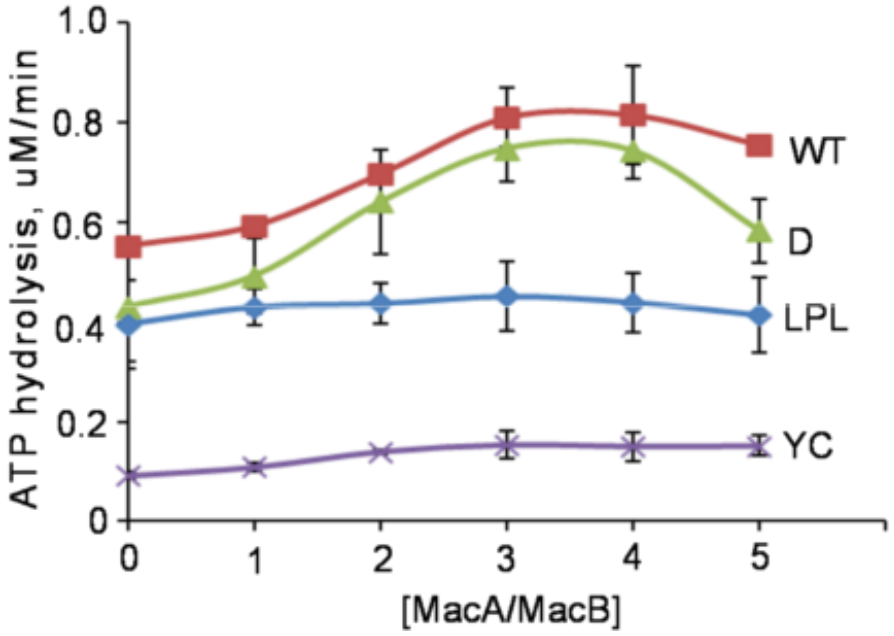


Figure 1.5 Dependence of MacB ATPase activity on MacA. All reactions contained 0.7 μM MacB and 1 mM Mg-ATP and were carried out at 20 ℃ in MES buffer (pH 6.0). Error bars are SDs (n = 3).

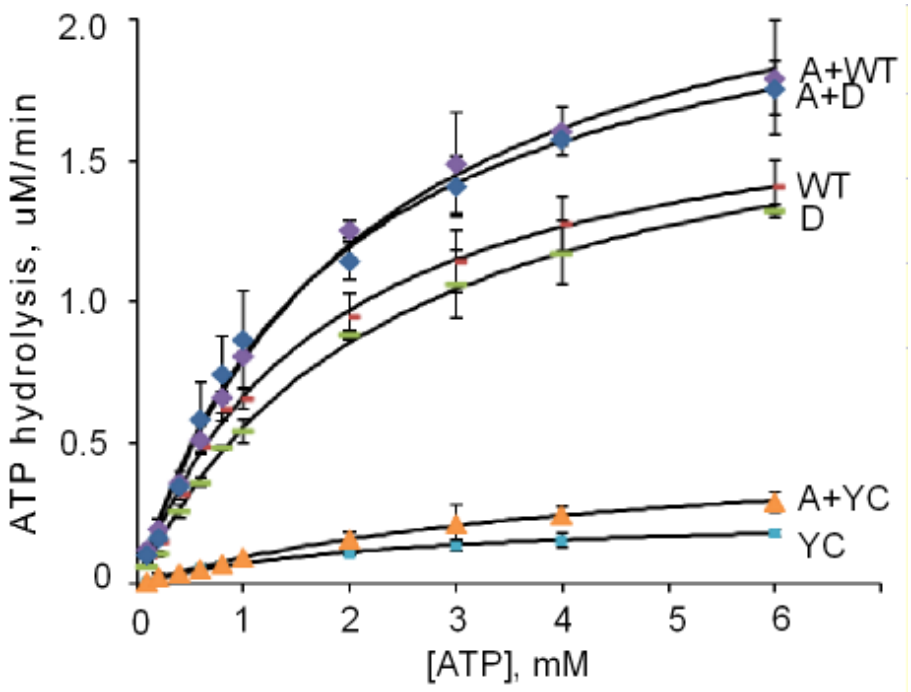


Figure 1.6 Dependence of ATP hydrolysis by MacB and MacAB in detergent micelles on the concentration of ATP. All reactions contained 0.42 μM MacB and were carried out at 20℃ in MES buffer (pH 6.0). Data were fit into Michaelis-Menten equation. The MacA: MacB molar ratio was 3:1. Error bars are SDs (n = 3).

Table 1.1 Kinetic parameters of MacB ATPase and its derivatives.

Protein	K_M (mM)	V_{max} (μM/min)	k_{cat} (s^{-1})	k_{cat}/K_M ($M^{-1}s^{-1}$)
$MacB^{WT}$	1.74 ±0.1	1.82 ±0.05	0.072 ±0.001	41.5 ±0.57
$MacAB^{WT}$	1.84 ±0.16	2.29 ±0.08	0.091 ±0.002	49.4 ±1.08
$MacB^{D}$	2.41 ±0.15	1.88 ±0.05	0.074 ±0.002	30.9 ±1.24
$MacAB^{D}$	2.11 ±0.14	2.47 ±0.06	0.098 ±0.001	46.5 ±0.47
$MacB^{YC}$	2.5 ±0.32	0.25 ±0.014	0.01 ±0.0003	3.97 ±0.12
$MacAB^{YC}$	4.7 ±0.43	0.52 ±0.028	0.021 ±0.0007	4.39 ±0.15

1.6 Mutations in MacB affect the macrolide drugs resistance of *E. coli* W4680AD (Δ*acrAB,* Δ*acrD*) cells.

MacAB-TolC efflux pumps use the energy generated from ATP hydrolysis to transport macrolides across the membrane. Thus, functional MacB is required in this process as the motor. Since MacB variants are in different ATP hydrolysis state, we next investigated whether $MacB^{WT}$, $MacB^{169}$, $MacB^{YC}$ and $MacB^{LPL}$ are functional in transport of macrolides. For this purpose, we measured the minimal inhibitory concentrations (MIC) of *E. coli* W4680AD (Δ*acrAB,* Δ*acrD*) cells carrying plasmids that produce MacA and MacB variants (Table 1.2). The major MDR transporter *acrAB* gene in *E. coli* W4680AD (Δ*acrAB,* Δ*acrD*) strain is deleted from the chromosome. As a result, this strain is highly susceptible to macrolides and other antibiotics. When overproduced in this strain, MacAB confers resistance to macrolide drugs erythromycin and oleandomycin (Kobayashi, Nishino et al. 2001; Tikhonova, Devroy et al. 2007). In agreement with previous studies, $MacAB^{WT}$ was able to complement the macrolide susceptibility of *E. coli* W4680AD cells upto 32 μg/mL of erythromycin and 78 μg/mL of oleandomycin. Inactive $MacB^{169}$ failed to complement the macrolide susceptibility. On the other hand, $MacB^{YC}$ could provide some resistance to macrolides but with about 8 folds decrease comparing to that of $MacB^{WT}$. These results demonstrate that $MacB^{YC}$ retains some activities and can still form complex with MacA-TolC for the transportation of macrolides. Furthermore, the ATP hydrolysis rate of MacB is directly related to the transport function of MacB. However, $MacB^{LPL}$ failed to rescue the hypersusceptibility of *E. coli* W4680AD cells, suggesting that $MacB^{LPL}$ cannot couple the ATP hydrolysis to the transportation of macrolides probably due to the lack of periplasmic loop of MacB.

These results further imply that the efficient transport of macrolides by MacAB-TolC complex not only requires the active MacB ATPase but also the proper assembly of MacAB-TolC complex.

In summary, we constructed MacB variants in different functional states. $MacB^{D}$ hydrolyzes ATP and interacts with MacA as $MacB^{WT}$. The ATPase activity of $MacB^{LPL}$ is comparabe to $MacB^{D}$, but MacA fails to stimulate $MacB^{LPL}$ ATPase activity. Even though $MacB^{YC}$ is defective in ATP hydrolysis and adopt a different confirmation, MacA can still stimulate $MacB^{YC}$ activity to some degree. $MacB^{169}$ is completely inactive but has the same conformation as $MacB^{D}$.

Table 1.2 Macrolide susceptibilities of *E. coli* W4680AD (Δ*acrAB*, Δ*acrD*) cells carrying plasmids producing MacA along with MacB variants (MIC, μg/mL).

Plasmid	Oleandomycin	Erythromycin
pUC 18	2.44-4.88	1
$MacAB^{WT}$	78	32
$MacAB^{LPL}$	4.88	1-2
$MacAB^{YC}$	9.75-19.5	4
$MacAB^{169}$	2.44-4.88	1

Chapter 2: Investigation of the protein-protein interactions between MacA and MacB.

2.1 Immobilization of MacB and a binding assay development.

There are many well-established *in vitro* and *in vivo* assays to investigate the

interactions between proteins (Date 2007). In this study, we used the surface plasmon resonance (SPR) approach. SPR is an optical technique for exploring protein-protein interactions *in vitro*. It works by measuring the refractive index near the surface of a sensor to which a protein of interest has been immobilized. The advantages of SPR over other biochemical and biophysical techniques include speed, direct monitoring of binding without the need for labeling ligands, direct determination of association and dissociation rates, and small amounts of sample needed. SPR can be used for the affinity analysis, the kinetic analysis, the concentration assay, the binding stoichiometry, the thermodynamic analysis, the study of interaction mechanisms, etc. SPR has been used for the study of the protein-protein interactions between MFP and TolC (Tikhonova, Dastidar et al. 2009) and the complex assembly of AcrAB-TolC (Tikhonova, Yamada et al. 2011). In this study, we decided to use SPR for the investigation of the mechanism of complex assembly of MacAB-TolC.

Previously, we described the construction of several MacB variants, $MacB^{D}$, $MacB^{169}$, $MacB^{LPL}$ and $MacB^{YC}$. All MacB variants have a D643C substitution at the C-terminal end of MacB and $MacB^{YC}$ has an Y14C point mutation at the N-terminal end of MacB. Previous studies showed that these two cysteines in MacB are accessible to thiol-reactive reagents (Kobayashi, Nishino et al. 2003). To test whether the intrinsic and introduced cysteines are accessible to thiol-reactive reagent MP-biotin, we treated $MacB^{WT}$ and MacB variants with MP-biotin and determined the biotinylation of these MacB variants. The biotinylated proteins were separated by 12% SDS-PAGE, transferred onto a PVDF membrane, incubated with streptavidin alkaline phosphatase conjugate and finally visualized by NBT/BCIP (Figure 2.1). $MacB^{WT}$ with all three intrinsic cysteines in

place was not labeled with MP-biotin. Therefore, none of the three cysteines in MacB are accessible to MP-biotin and are unlikely to interfere with the biotinylation and immobilization processes. $MacB^{D}$, $MacB^{169}$, $MacB^{YC}$ and $MacB^{LPL}$ with cysteine on either N-terminus or C-terminus all can be biotinylated and were ready for immobilization.

To develop a binding assay, the fully functional $MacB^{D}$ was biotinylated and immobilized onto a SA chip with two different surface densities 1987 Responses Unit (RU) (D^{high}) and 794 RU (D^{low}). A change in the response signal by 1,000 RU is equivalent to the change in a surface concentration of 1 ng protein/mm^2 or approximately 6-10 mg/mL in a bulk protein. Therefore, about 100 μM and 40 μM concentrations of MacB were immobilized onto the high and low density surfaces, respectively. 0.25 μM purified $MacA^{WT}$ was injected over $MacB^{Dhigh}$, $MacB^{Dlow}$ and the control surfaces simultaneously in HEPES running buffer (pH 7.0) containing 20 mM HEPE-KOH, 150 mM NaCl, 0.2% TX-100 and MES running buffer (pH 6.0) containing 20 mM MES-KOH, 150 mM NaCl, 0.2% TX-100. The binding responses of $MacA^{WT}$ to MacB surfaces were normalized by substracting the binding responeses on the control surface. Even though the binding of $MacA^{WT}$ towards MacB was detected under both conditions, the specific binding response was more than twice higher at pH 6.0 than that at pH 7.0 (Figure 2.2 A). In addition, the binding responses of $MacA^{WT}$ were higher on the high density $MacB^{D}$ surface than those on the low density $MacB^{D}$ surface, indicating that the interaction between $MacA^{WT}$ and MacB is specific (Figure 2.2 B). To detect notable binding signals, we decided to use MES running buffer (pH 6.0) for further study.

In order to investigate whether $MacB^{D}$ in MES running buffer (pH 6.0) is able to

bind nucleotides, we injected 0.25-8 mM Mg-ATP over $MacB^{Dhigh}$ and $MacB^{Dlow}$ surfaces. The binding signals of ATP to $MacB^{D}$ increased with increasing concentrations of ATP (Figure 2.2 C). In addition, the binding of ATP is specific to $MacB^{D}$ because the changes in binding response were proportional to the surface densities of $MacB^{D}$ (Figure 2.2 D).

Since $MgCl_2$ is required for the ATP hydrolysis, we analyzed the effect of $MgCl_2$ to $MacA^{WT}$ binding towards $MacB^{D}$. $MacA^{WT}$ was premixed with increasing concentrations of $MgCl_2$ and injected over $MacB^{D}$ surface (1377 RU) (Figure 2.2 E). With increasing concentrations of $MgCl_2$, the binding of $MacA^{WT}$ to $MacB^{D}$ decreased about 40% and this negative effect remained the same after 8 mM $MgCl_2$. In order to eliminate the effect of $MgCl_2$ to MacA binding, we decided to use MES running buffer (pH 6.0) supplemented with 8mM $MgCl_2$ for binding assay.

In addition, the MacA-MacB complex remained stable under different mild regeneration conditions such as increased pH and salt concentrations or addition of zwitterionic detergents. Therefore after scanning various binding and regeneration buffer, we decided to use MES running buffer (pH 6.0) supplemented with 8 mM $MgCl_2$ as running buffer. Biffer containing 500 mM $MgCl_2$, 20 mM Tris-HCl (pH 8.0), 150 mM NaCl, 0.2% TX-100 were set as the regeneration buffer.

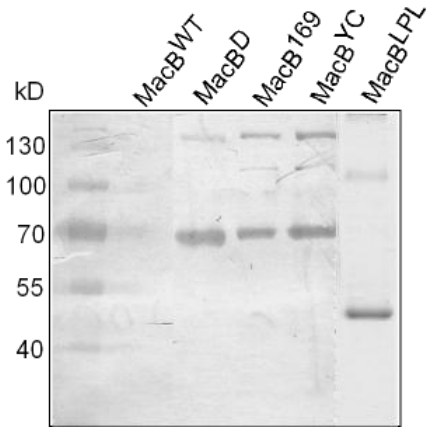


Figure 2.1 Biotinylation of MacB^{WT} and its derivatives. 0.5 μg of each MP-biotin treated protein was separated by 12 % SDS-PAGE, transferred onto a PVDF membrane and incubated with streptavidin alkaline phosphatase. Biotinylated MacB^{D}, MacB^{YC}, MacB^{169} and MacB^{LPL} were visualized by NBT/BCIP.

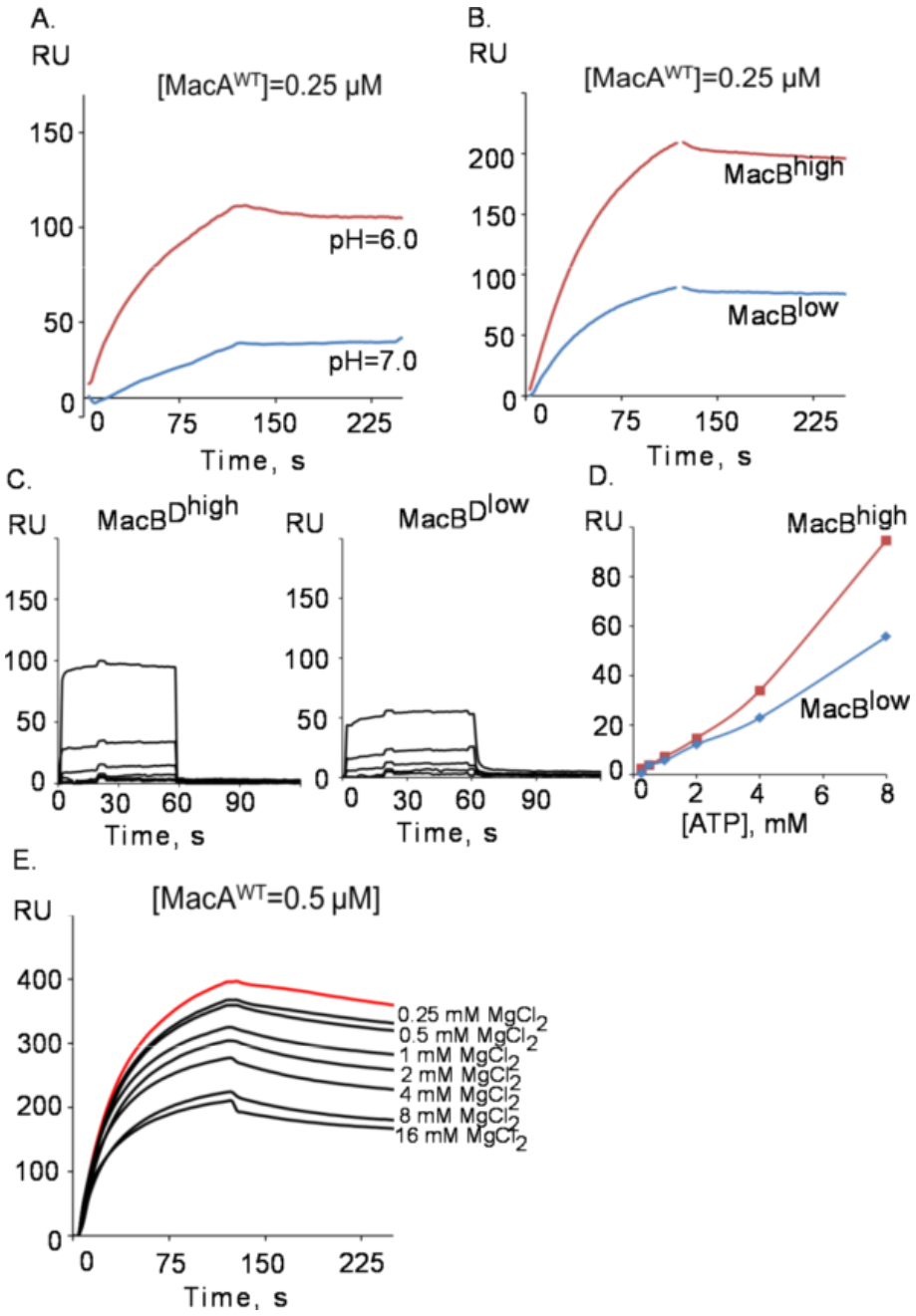


Figure 2.2 Development of a binding assay. A. Binding of 0.25 µM $MacA^{WT}$ to $MacB^{D}$ (998 RU) surface in MES (pH 6.0) and HEPES (pH 7.0) running buffers. In all experiments, $MacA^{WT}$ was injected at a constant rate of 50 mL min^{-1}. The binding responses of $MacA^{WT}$ to MacB surfaces were normalized by subtracting the binding responses on the control surface. B. Binding of 0.25 µM $MacA^{WT}$ to $MacB^{Dlow}$ (794 RU)

and $MacB^{Dhigh}$ (1978 RU) surfaces. C. Sensorgrams of ATP binding to $MacB^{D}$ surfaces. 0.25-8 mM of ATP were injected over $MacB^{Dhigh}$ (1978 RU) and $MacB^{Dlow}$ (794 RU) surfaces in MES running buffer (pH 6.0). D. Equilibrium binding responses of ATP to $MacB^{Dlow}$ (794 RU) and $MacB^{Dhigh}$ (1978 RU) surfaces were plotted as a function of ATP concentrations. E. Binding of MacA to MacB in the presence of increasing concentrations of $MgCl_2$. 0.5 μM $MacA^{WT}$ were premixed with 0.25-16 mM $MgCl_2$ and injected over $MacB^{D}$ (1377 RU) surface. Sensorgrams were normalized by subtracting the binding responses of increasing concentrations of $MgCl_2$ and running buffer as double reference. $MacA^{WT}$ injected alone was indicated as a red line.

2.2 Immobilized MacB variants bind nucleotides.

MacB is suggested to function as a dimer (Tikhonova, Devroy et al. 2007; Lin, Bavro et al. 2009). To confirm that the purified MacB retains its structure in detergent, we analyzed purified MacB by size exclusion chromatography (SEC). We self-packed a 1 mL Sephacryl™ S-300 gel filtration column and equilibrated it with MES (pH 6.0) running buffer in the presence or absence of 8 mM $MgCl_2$. 5-10 μg of purified MacB was pre-mixed with the size standard containing BSA (66 kD), alcohol dehydrogenase (150 kD) and ferritin (440 kD) and loaded onto the column. Fractions were collected and analyzed using 12% SDS-PAGE followed by silver staining. Figure 2.3 shows the quantitated intensity of protein bonds plotted as a function of the fraction number. MacB, with 145 kD MW for a dimer, eluted as a single peak, which overlapped with the peak of alcohol dehydrogenase (AD, 150 kD). From the gel filtration results, we can conclude

that in MES running buffer (pH 6.0) purified MacB is a stable homogeneous dimer.

For kinetic studies, we immobilized biotinylated $MacB^{D}$, $MacB^{169}$, $MacB^{YC}$ and $MacB^{LPL}$ onto the surfaces with 1377 RU, 1462 RU, 1340 RU and 800 RU surface densities, respectively. To determine whether immobilized MacB variants were capable of binding nucleotides and further compare their affinities towards nucleotides, two-fold dilutions of 0.25 to 8 mM Mg-ATP, Mg-ADP and Mg-AMP-PNP were injected over MacB surfaces and control surface in MES running buffer (pH 6.0) supplemented with 8 mM MgCl2.

The binding of ATP generated the largest responses, implying that ATP may have the highest binding affinity towards $MacB^{D}$. At all nucleotide concentrations, the binding responses reached steady-state rapidly and nucleotides dissociated from $MacB^{D}$ within 5s, indicating that the binding reaction is reversible (Figure 2.4 A). The binding curves of ATP and ADP to $MacB^{D}$ surfaces were similar and the absolute binding responses (Figure 2.4 B) were also comparable between ATP and ADP. The binding responses of AMP-PNP were much lower than those of ATP and ADP at the same concentrations, which might be explained by the structure dissimilarity of AMP-PNP. We could not fit the nucleotide binding curves into any available kinetic models. The shapes of the curves suggest the presence of at least two binding steps, the high-affinity step in the range of 0.5-2.0 mM nucleotides and the low affinity step in a high millimolar range. The K_M value of MacB 1.7-2.5 mM (Table 1.1) is in the range of the high affinity step. The nucleotide binding signals increased non-monotonously at nucleotide concentrations more than 4 mM, which could come from the contribution of additional factors, such as chemical or conformational changes of MacB or low non-specific interactions.

Despite the inactivation of MacB^{169} ATPase, MacB^{169} was able to bind nucleotides with comparable affinity to that of MacB^{D}, indicating that the inactivation of the catalytic site of MacB^{169} has no effect on nucleotides binding.

On the other hand, the binding responses of ATP and ADP on MacB^{YC} surface were approximately two times less than those of MacB^{D} and MacB^{169}. Furthermore, MacB^{YC} did not bind AMP-PNP. These results suggest that MacB^{YC}, adopting a different conformation, is defective in nucleotides binding.

As described in Chapter 1.1, we find that at pH 6.0 MacB^{LPL} can hydrolyze ATP with the same efficiency as MacB^{D} at pH 6.0. In agreement, immobilized MacB^{LPL} has binding affinity towards nucleotides similar to that of MacB^{D}, indicating that deletion of periplasmic loop does not affect the nucleotide binding by MacB.

Taken together, MacB^{169} and MacB^{LPL} can bind nucleotides with the same affinity as MacB^{WT}, whereas MacB^{YC} is defective in nucleotide binding.

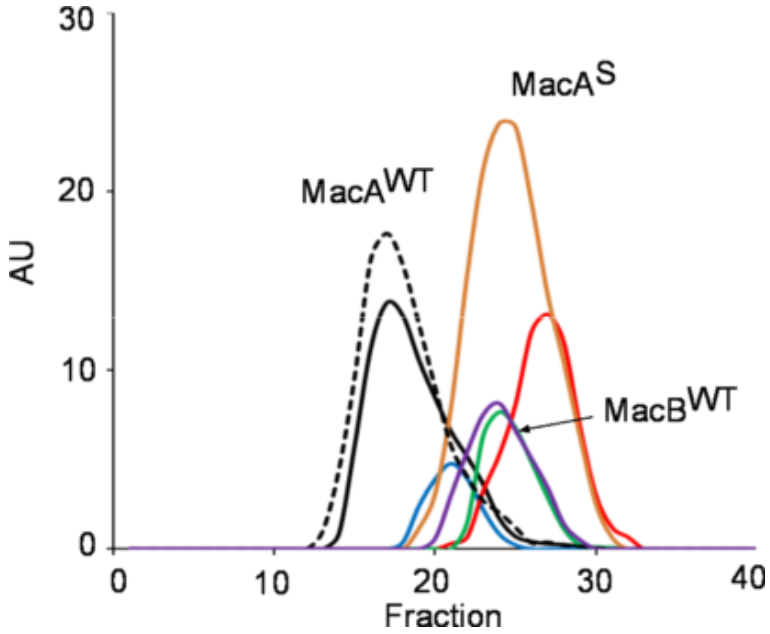
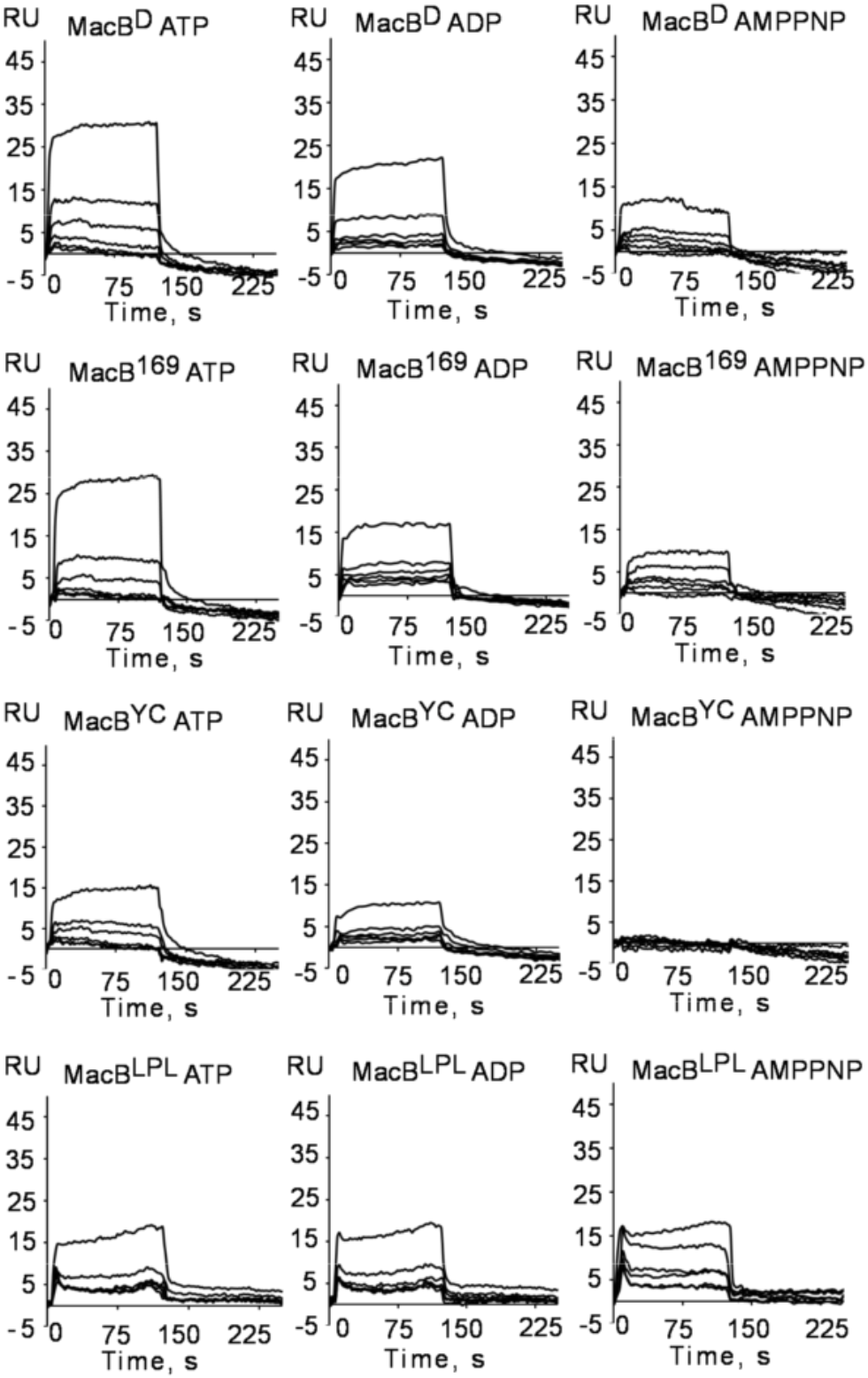


Figure 2.3 Gel filtration analysis of MacB^{D}, MacA^{S} and MacA^{WT}. Purified MacB^{D}

(purple line), $MacA^{WT}$ (solid and dash black line) and $MacA^{S}$ (orange line) 5-10 μg each were pre-mixed with a similar amount of the size standard containing BSA (66 kD, red line), alcohol dehydrogenase (150 kD, green line) and ferritin (440 kD, blue line). The mixture were loaded onto a self-packed 1 mL Sephacryl™ S-300 column equilibrated with MES running buffer (pH 6.0) in the presence or absence of 8 mM $MgCl_2$. Fractions were collected and then analyzed using 12% SDS-PAGE followed by silver staining. The intensity of protein bands on SDS-PAGE was further analyzed by Image J and plotted as a function of the fraction number.

A.


RU
MacB^D ATP
MacB^D ADP
MacB^D AMPPNP
MacB^169 ATP
MacB^169 ADP
MacB^169 AMPPNP
MacB^YC ATP
MacB^YC ADP
MacB^YC AMPPNP
MacB^LPL ATP
MacB^LPL ADP
MacB^LPL AMPPNP
45
35
25
15
5
-5
0
75
150
225
Time, s

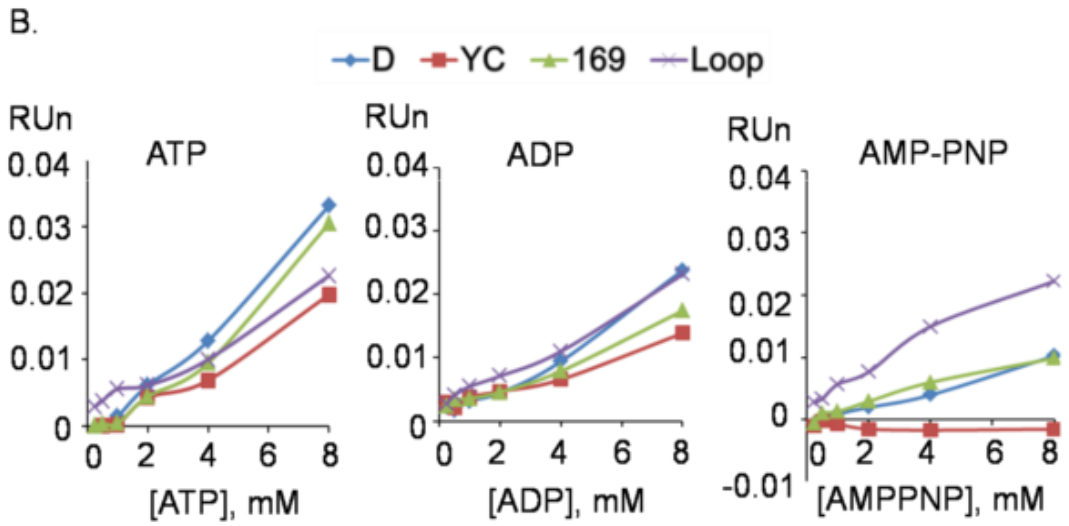


Figure 2.4 Immobilized MacB binds ATP, ADP and AMP-PNP. A. Sensorgrams of two-fold dilutions of 0.25-8 mM indicated nucleotides injected over $MacB^{D}$ (1377 RU), $MacB^{169}$ (1462RU), $MacB^{YC}$ (1340 RU) and $MacB^{LPL}$ (800 RU) surfaces in MES running buffer (pH 6.0) supplemented with 8 mM $MgCl_2$ B. Equilibrium binding responses of nucleotides from sensorgrams of A were plotted as a function of nucleotide concentrations. Binding responses were normalized to differences in surface densities and molecular masses of MacB variants.

2.3 $MacA^{WT}$ forms oligomer in solution.

In general, affinity and kinetic measurement of protein interactions require that each analyte molecule stays in a monovalent and homogeneous manner. The heterogeneity of analytes makes kinetics studies ambiguous. Thus, it is essential to ensure the homogeneity of analytes which is mostly achieved from purifying the monomeric peak by size exclusion chromatography (SEC) immediately before SPR. $MacA^{S}$ exists as a

monomer in solution but forms heterogeneous oligomers at high concentrations (Tikhonova, Dastidar et al. 2009; Yum, Xu et al. 2009). $MacA^{WT}$ is suggested to exit as a hexamer (Xu, Sim et al. 2009; Yum, Xu et al. 2009). Before the kinetic study of MacA and MacB interactions, we wanted to determine the oligomeric state of $MacA^{S}$ and $MacA^{WT}$ in MES running buffer (pH 6.0).

We self-packed a 1 mL Sephacryl^{TM} S-300 gel filtration column and equilibrated it with MES running buffer (pH 6.0) with or without 8 mM $MgCl_2$. $MacA^{WT}$ and $MacA^{S}$ were pre-mixed with a similar amount of the size standard containing BSA (66 kD), alcohol dehydrogenase (150 kD) and ferritin (440 kD) and loaded onto the column. $MacA^{WT}$ was eluted as a single symmetric peak (Figure 2.3) with the apparent molecular weight higher than that of 440 kD ferritin. The size of $MacA^{WT}$ was the same in MES running buffer (pH 6.0) in the presence or absence of 8 mM $MgCl_2$. Therefore, $MacA^{WT}$ forms stable, homogenous oligomer and $MgCl_2$ had no effect on the oligomeric state of $MacA^{WT}$.

$MacA^{S}$ was eluted as a single peak between 66 kD BSA and 150 kD AD with an apparent MW about 80 kD. This result suggests that in MES running buffer (pH 6.0) $MacA^{S}$ has a lower oligomeric level than that of $MacA^{WT}$ which is most likely to be in a monomeric form.

2.4 $MacA^{WT}$ binds MacB with nanomolar affinity.

As described in Section II.2, we constructed MacB variants with defects in ATP binding, ATP hydrolysis and MacA-dependent stimulation. Our next question is how the

ability of binding or hydrolyzing ATP of MacB affects the binding kinetics between MacA-MacB. To characterize the kinetics of MacA-MacB association, two-fold dilutions of $MacA^{WT}$ were injected over MacB variant surfaces in MES running buffer (pH 6.0) supplemented with 8 mM $MgCl_2$ (Figure 2.5). $MacA^{WT}$ generated a robust binding response on $MacB^{D}$ surface even at low nanomolar concentrations of $MacA^{WT}$ (Figure 2.5 A).

Quantitative analysis of the binding curves revealed that double-exponential rate equations could be used to approximate the association and dissociation phase of $MacA^{WT}$, indicating multiple binding events. We tried to fit the binding curves of MacA to MacB into different kinetic models such as 1:1 binding model, sequential binding model, and two state model (TS). The best kinetic model for $MacA^{WT}$-$MacB^{D}$ binding curves was TS model that assumes that $MacA^{WT}$ binds $MacB^{D}$ first and this association induces further conformational changes in MacB. The on-rate of MacA-$MacB^{D}$ association was about 10^{4} $M^{-4}s^{-1}$ (Table 2.1). The 10^{-2} s^{-1} off-rate, representing the complex stability, exceeded the turnover number of $MacB^{D}$ ATPase (Table 1.1) about ten folds, suggesting that the MacA-MacB complex remains stable during ATP hydrolysis process. The equilibrium dissociation constant was calculated from the kinetic parameters in Table 2.1 $MacA^{WT}$ binds MacB with a high affinity around 10^{-8} M.

Immobilized $MacB^{169}$, $MacB^{YC}$ and $MacB^{LPL}$ bind $MacA^{WT}$ with similar affinities and kinetics to that of $MacB^{D}$ (Figure 2.5 B-D). Even though the normalized binding responses of $MacA^{WT}$ differed among MacB variants, the kinetics of $MacA^{WT}$-MacB association was quite similar with all rate constants and equilibrium dissociation constants varied within 30%. Therefore, neither the periplasmic loop, catalytic activity

nor the correct NBDs conformation of MacB is required for the binding of $MacA^{WT}$ to MacB. All this results further suggest that the interactions between TM domains of MacA and MacB contribute significantly to the high affinity binding of MacA to MacB.

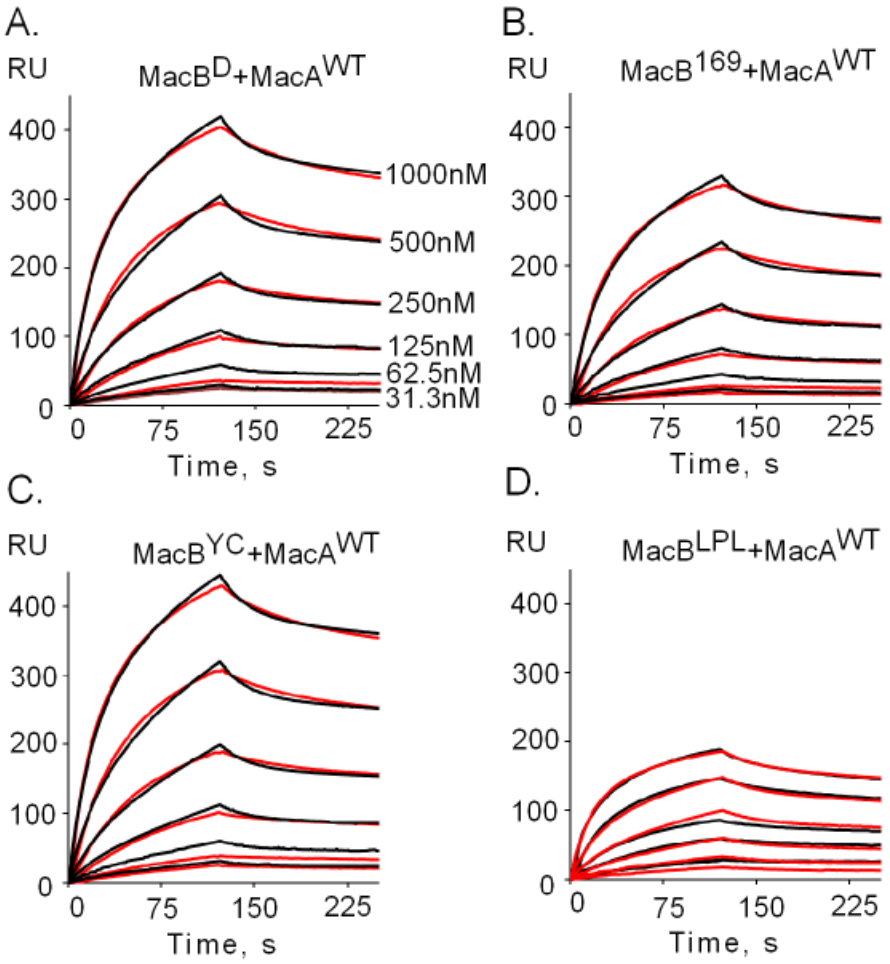


Figure 2.5 $MacA^{WT}$ binds MacB variants. Sensorgrams (red lines) of two-fold dilutions of 31.3-1000 nM $MacA^{WT}$ injected over $MacB^{D}$ (1377 RU) (A), $MacB^{169}$ (1462 RU) (B), $MacB^{YC}$ (1340 RU) (C) and $MacB^{LPL}$ (800 RU) (D) surfaces in MES running buffer (pH 6.0) supplemented with 8 mM $MgCl_2$. Sensorgrams are fit globally into TS model (black lines).

Table 2.1 Kinetic parameters of MacA-MacB interactions in the presence of nucleotides

Surface	$k_{a1}(M^{-1}\ s^{-1})$	$k_{d1}(s^{-1})$	k_{a2} (s^{-1})	$k_{d2}(s^{-1})$	K_D (M)	Chi
$MacB^{D}$	$(2.97\pm0.08)\times10^{4}$	$(2.95\pm2.40)\times10^{-2}$	$(2.06\pm0.13)\times10^{-2}$	$(10.7\pm1.86)\times10^{-4}$	5.18×10^{-8}	53.9
$MacB^{D}$+ATP	$(4.17\pm0.12)\times10^{4}$	$(3.56\pm0.26)\times10^{-2}$	$(1.89\pm0.11)\times10^{-2}$	$(3.55\pm3.55)\times10^{-4}$	1.61×10^{-8}	58.5
$MacB^{D}$+ADP	$(2.79\pm0.11)\times10^{4}$	$(2.79\pm0.37)\times10^{-2}$	$(2.28\pm0.24)\times10^{-2}$	$(9.29\pm2.93)\times10^{-4}$	4.07×10^{-8}	44.3
$MacB^{D}$+AMPPNP	$(2.8\pm0.11)\times10^{4}$	$(2.64\pm0.37)\times10^{-2}$	$(2.18\pm0.23)\times10^{-2}$	$(8.54\pm2.84)\times10^{-4}$	3.6×10^{-8}	68.4
$MacB^{YC}$	$(2.69\pm0.01)\times10^{4}$	$(2.59\pm0.15)\times10^{-2}$	$(1.9\pm0.10)\times10^{-2}$	$(8.21\pm1.85)\times10^{-4}$	4.17×10^{-8}	52.4
$MacB^{YC}$+ATP	$(3.64\pm0.09)\times10^{4}$	$(2.92\pm0.20)\times10^{-2}$	$(1.85\pm0.10)\times10^{-2}$	$(4.34\pm1.6)\times10^{-4}$	1.88×10^{-8}	62.4
$MacB^{YC}$+ADP	$(2.32\pm0.08)\times10^{4}$	$(1.91\pm0.27)\times10^{-2}$	$(2.2\pm0.25)\times10^{-2}$	$(11.9\pm2.56)\times10^{-4}$	4.46×10^{-8}	37.5
$MacB^{YC}$+AMPPNP	$(2.54\pm0.10)\times10^{4}$	$(2.43\pm0.37)\times10^{-2}$	$(2.32\pm0.27)\times10^{-2}$	$(9.36\pm3.08)\times10^{-4}$	3.86×10^{-8}	74.3
$MacB^{D169N}$	$(2.5\pm0.06)\times10^{4}$	$(2.48\pm0.24)\times10^{-2}$	$(1.86\pm0.14)\times10^{-2}$	$(7.4\pm2.35)\times10^{-4}$	3.94×10^{-8}	35.3
$MacB^{D169N}$+ATP	$(3.56\pm0.10)\times10^{4}$	$(2.84\pm0.24)\times10^{-2}$	$(1.9\pm0.13)\times10^{-2}$	$(4.25\pm2.07)\times10^{-4}$	1.78×10^{-8}	40.8
$MacB^{D169N}$+ADP	$(2.33\pm0.10)\times10^{4}$	$(2.15\pm0.37)\times10^{-2}$	$(2.24\pm0.31)\times10^{-2}$	$(9.48\pm3.68)\times10^{-4}$	3.89×10^{-8}	26.3
$MacB^{D169N}$+AMPPNP	$(2.99\pm0.06)\times10^{4}$	$(3.68\pm0.15)\times10^{-2}$	$(2.61\pm0.08)\times10^{-2}$	$(9.29\pm1.02)\times10^{-4}$	4.37×10^{-8}	46.8
$MacB^{LPL}$	$(3.96\pm0.05)\times10^{4}$	$(2.27\pm0.12)\times10^{-2}$	$(1.82\pm0.17)\times10^{-2}$	$(15.3\pm3.93)\times10^{-4}$	4.81×10^{-8}	35.7
$MacB^{LPL}$+ATP	$(8.86\pm0.12)\times10^{4}$	$(4.64\pm0.16)\times10^{-2}$	$(1.97\pm0.09)\times10^{-2}$	$(9.2\pm1.67)\times10^{-4}$	2.44×10^{-8}	26.9
$MacB^{LPL}$+ADP	$(5.17\pm0.01)\times10^{4}$	$(2.90\pm0.004)\times10^{-2}$	$(3.31\pm0.15)\times10^{-2}$	$(26.3\pm2.50)\times10^{-4}$	4.41×10^{-8}	21.9
$MacB^{LPL}$+AMPPNP	$(5.07\pm0.09)\times10^{4}$	$(4.79\pm0.06)\times10^{-2}$	$(2.27\pm0.05)\times10^{-2}$	$(11.5\pm0.21)\times10^{-4}$	4.80×10^{-8}	48.3

Data were fit globally using the TS model. k_{-1}, k_{-2}, k_1 and k_2 are microscopic rate constants. Equilibrium dissociation constants (K_D) were calculated from the ratio of the dissociation and association rate constants.

2.5

2.5 MacA^{S} binds MacB but with lower affinity comparing with MacA^{WT}.

MacA^{S} has no TM domain and exists as a monomer in solution (Figure 2.3). To investigate how the removal of TM domain of MacA affects the interactions between MacA and MacB, increasing concentrations of MacA^{S} were injected over MacB surfaces in MES running buffer (pH 6.0) supplemented with 8 mM $MgCl_2$. MacA^{S} bound all MacB variants (Figure 2.6). However, more than ten-fold more MacA^{S} were needed to reach the same binding responses as that of MacA^{WT}, indicating that the TM domain of MacA contributes significantly to the binding affinity between MacA and MacB. The binding curves of MacA^{S}-MacB were fit into various kinetic models, but experimental data showed a systematic deviation from all the models. Since MacA^{S} has no TM domain, it is possible that the binding of MacA^{S} and MacA^{WT} trigger different binding events towards MacB. In addition, the oligomerization of MacA^{S} on the surface and in the solution can also cause this deviation.

Previous results showed that MacA^{S} cannot simulate the ATPase activity of MacB (Tikhonova, Devroy et al. 2007). The defect of MacA^{S} in binding to MacB can be one of the reasons for the lack of MacA-dependent stimulation of MacB ATPase.

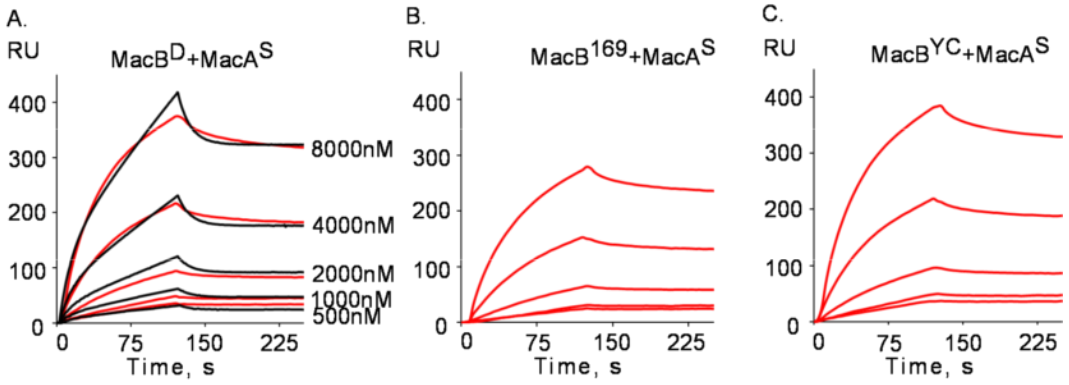


Figure 2.6 MacA^{S} binds MacB variants. Sensorgrams (red lines) of two-fold dilutions of 500-8000 nM MacA^{S} injected over MacB^{D} (1377 RU) (A), MacB^{169} (1462 RU) (B) and MacB^{YC} (1340 RU) (C) surfaces in MES running buffer supplemented with 8 mM $MgCl_2$ (pH 6.0). Sensorgrams of MacB^{D} surface were fit globally into TS model (black line)

.

2.6 ATP binding increases MacA-MacB affinity.

To investigate how the binding and hydrolysis of ATP affect the kinetic association between MacA and MacB, 0.5 μM MacA^{WT} was pre-mixed with two-fold dilutions of 0.25-8 mM Mg-ATP, Mg-ADP or Mg-AMP-PNP in MES running buffer (pH 6.0) supplemented with 8 mM $MgCl_2$ and injected over MacB^{D}, MacB^{169}, MacB^{YC} and MacB^{LPL} surfaces. To determine how nucleotides affect MacA binding to MacB, the responses from nucleotides alone were subtracted from the binding responses of MacA^{WT} plus nucleotides. The normalized binding curves were fitted locally to obtain a k_{obs} value, which represents both the on- and off- rates in binding reactions. The k_{obs} values were then plotted as a function of nucleotide concentrations as shown in Figure 2.7. With increasing concentrations of ADP, the value of k_{obs} decreased about 15% at 1 mM ADP and remained the same for up to 8 mM ADP. On the contrary, the k_{obs} values increased when ATP was injected together with MacA^{WT}. At 0.25 mM to 1 mM ATP concentration, the k_{obs} values increased gradually about 30% and then slightly decreased with higher concentrations of ATP. No changes in k_{obs} were observed in the presence of AMP-PNP, indicating that MacA-MacB interaction isn't affected by AMP-PNP. Even though MacB

variants showed variable binding responses, the changes in k_{obs} caused by different nucleotides remained the same.

Since MacB variants differ in their abilities to hydrolyze ATP, the same changes in k_{obs} suggest that the changes in $MacA^{WT}$ binding are caused by ATP binding not ATP hydrolysis.

To further characterize the kinetics of MacA-MacB association in the presence of nucleotides, increasing concentrations of $MacA^{WT}$ were pre-mixed with constant 4 mM concentration of Mg-ATP, Mg-ADP and Mg-AMP-PNP and injected over MacB surfaces. Quantitative analysis of the binding curves revealed complex binding events that could be fit into by double-exponential rate equations. The best fitting model for $MacA^{WT}$-MacB binding in the presence of nucleotides was also the TS model, which assumes a conformational change of MacB upon MacA-MacB association (Figure 2.8). However, some deviations from this model could be seen in curve alignments, indicating that the reaction could be more complex. The calculated equilibrium dissociation constants given in Table 2.1 yield the same high 10^{-8} M affinity for $MacA^{WT}$ complex with all MacB variants in the presence of nucleotides. Interestingly, the binding affinity of $MacA^{WT}$-MacB in the presence of 4 mM ATP was up to three fold higher than that in the absence nucleotides. This effect could be seen only in the presence of ATP but not in other nucleotides and all the MacA-MacB complexes were affected by ATP. We conclude that it is ATP binding not hydrolysis that enhances the affinity of $MacA^{WT}$-MacB association. In Chapter 1.3, we suggested that the binding of nucleotides to MacB promotes the closed conformation of MacB NBD. Therefore taken together, this result further suggests that $MacA^{WT}$ has a higher affinity to the ATP-bound state of MacB.

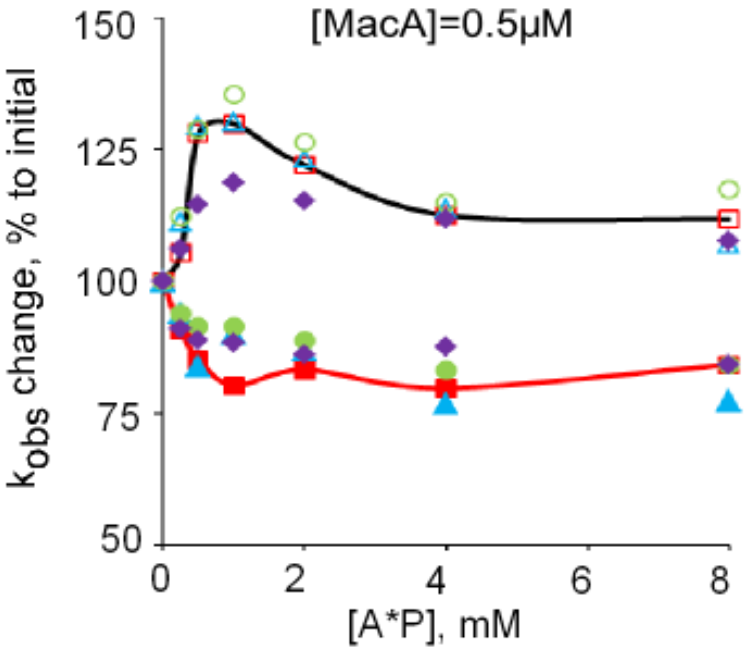


Figure 2.7 Dependence of k_{obs} of MacA on the concentrations of nucleotides. 0.5 μM MacA^{WT} was pre-mixed with two-fold dilutions of 0.25-8 mM Mg-ATP (open symbols) or Mg-ADP (closed symbols) and injected over MacB^{D} (1377 RU, triangles), MacB^{169} (1462 RU, circles), MacB^{YC} (1340 RU, squares) and MacB^{LPL} (800 RU, diamonds) surfaces in MES running buffer supplemented with 8 mM $MgCl_2$ (pH 6.0). The sensorgrams were fit locally and the change in k_{obs} values are plotted as a function of nucleotide concentrations.

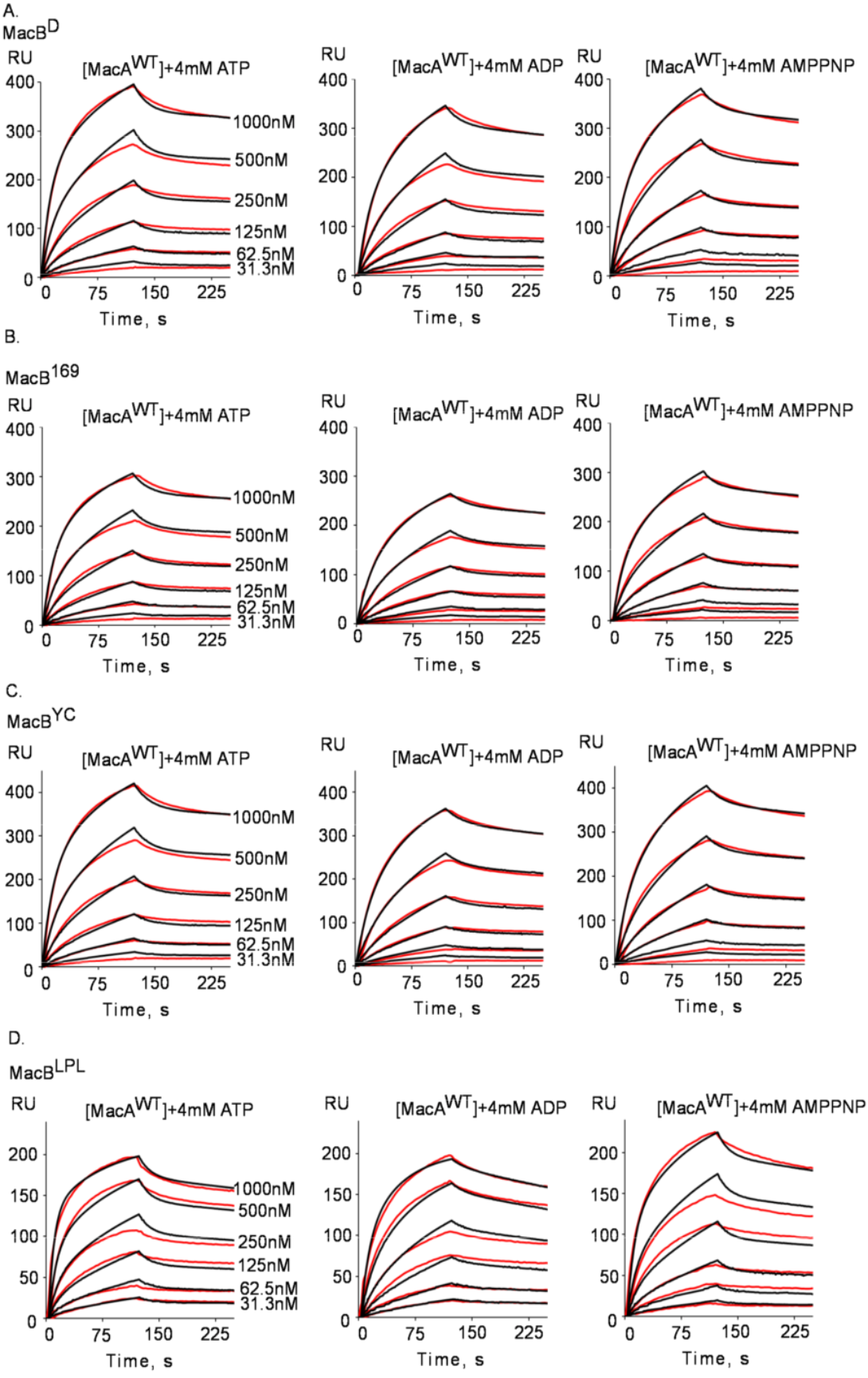

A.
MacB^D
RU
[MacA^WT]+4mM ATP
[MacA^WT]+4mM ADP
[MacA^WT]+4mM AMPPNP
1000nM
500nM
250nM
125nM
62.5nM
31.3nM
Time, s
B.
MacB^169
C.
MacB^YC
D.
MacB^LPL

Figure 2.8 MacA^{WT} binds MacB in the presence of nucleotides. A. Sensorgrams (red lines) of two-fold dilutions of 31.3-1000 nM MacA^{WT} pre-mixed with 4 mM indicated nucleotides and injected over MacB^{D} (1377 RU) surface in MES running buffer supplemented with 8 mM $MgCl_2$ (pH 6.0). Sensorgrams were fit globally into TS model (black lines). B. The same as A but injected over MacB^{169} (1462 RU) surface. C. The same as B but injected over MacB^{YC} (1340 RU) surface. D. The same as B but injected over MacB^{LPL} (800 RU) surface.

Chapter 3: Investigation of the protein-protein interactions between MacAB and TolC.

3.1 Immobilized TolC binds MacA^{S} and MacA^{WT}.

TolC, a versatile outer membrane channel, forms complex with MacAB to conduct the transportation of macrolides. Previous studies show that TolC can form complex with MacA^{WT} with a high nanomolar affinity (Tikhonova, Dastidar et al. 2009). However, whether MacB and TolC could directly interact with each other is unknown. The crystal structure of MacB PCD reveals some structural similarities to the periplasmic domain of RND-type transporter AcrB (Xu, Sim et al. 2009). The periplasmic portion of AcrB is 70Å in length and can interact with TolC directly (Murakami, Nakashima et al. 2002; Tikhonova, Yamada et al. 2011). The PCD of MacB is much smaller than that of AcrB, so it may not be large enough to contact TolC in the periplasm cell membranes. In order to investigate the mechanism of complex assembly of MacAB-TolC, our first task was to

determine whether MacB can interact directly with TolC. For this purpose, we immobilized $TolC^{A269C}$ onto biochip using thiol-coupling procedure. Since A269 is located in the extracellular loop at the top end of the β-strands of TolC, $TolC^{A269C}$ can be immobilized onto the surface with an upside down orientation. This arrangement makes the periplasmic coiled-coil domains of TolC available for the interactions with MacB and MacA.

In order to confirm that TolC maintain its functionality after immobilization, increasing concentrations of $MacA^{S}$ and $MacA^{WT}$ in MES running buffer (pH 6.0) supplemented with 8 mM $MgCl_2$ were injected over $TolC^{A269C}$ surface. $MacA^{WT}$ was able to bind TolC, indicating that the immobilized TolC retains its functionality and can be used for further analysis (Figure 3.1 B). On the other hand, $MacA^{S}$ could bind TolC but higher concentrations were needed to detect this binding (Figure 3.1 A). One possible reason for the binding defect of $MacA^{S}$ is that $MacA^{WT}$ and $MacA^{S}$ adopt different conformation in solution. In chapter 2.3, we conclude that $MacA^{WT}$ and $MacA^{S}$ stay in hexamer and monomer forms in solution respectively. In addition, in previous studies (Xu, Lee et al. 2011), the α-helical hairpin domains of MacA are suggested to be the docking site for the periplasmic coiled coil domain of TolC. Thus, another possible reason for the defect of $MacA^{S}$ binding towards TolC is that the monomer form of $MacA^{S}$ cannot provide enough docking sites for TolC binding.

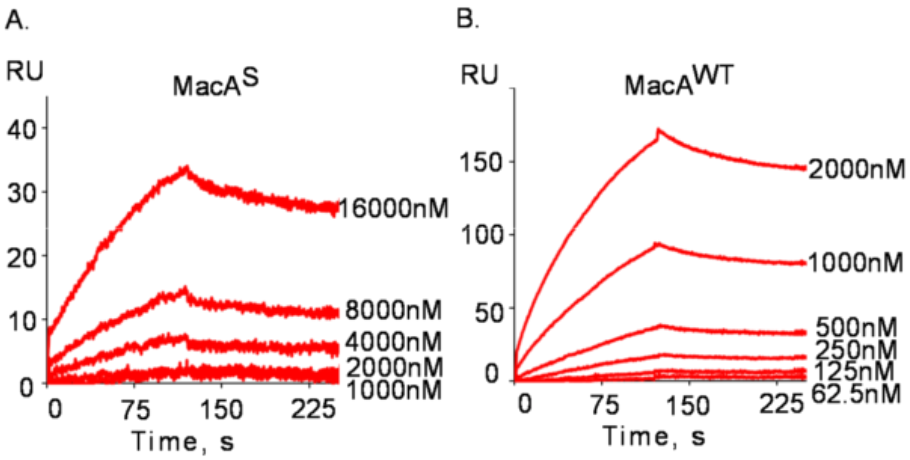


Figure 3.1 Immobilized TolC binds MacA^{S} and MacA^{WT}. A. Sensorgrams of two-fold dilutions of 1000-16000 nM MacA^{S} injected over TolC (790 RU) surface in MES running buffer supplemented with 8 mM $MgCl_2$ (pH 6.0). B. Sensorgrams of two-fold dilutions of 62.5-2000 nM MacA^{WT} injected over TolC (790 RU) surface in MES running buffer (pH 6.0) supplemented with 8 mM $MgCl_2$.

3.2 TolC does not directly interact with MacB.

To investigate the interaction between MacB and TolC, increasing concentrations of MacB^{WT} and MacB^{LPL} were injected over TolC surface in MES running buffer (pH 6.0) supplemented with 8 mM $MgCl_2$. No binding responses were detected on TolC surface (Figure 3.2). Thus, both MacB^{WT} and MacB^{LPL} cannot interact with immobilized TolC. To confirm the results, in the reverse assay, increasing concentrations of TolC^{WT} were injected over MacB^{D} (RU 1600) and MacB^{LPL} (RU 800) surfaces. Since MacB^{LPL} mutant does not contain the periplamic loop domain, which is thought to be the site of TolC

interaction, no TolC binding is expected on $MacB^{LPL}$ surface. However, some binding responses generated by increasing concentrations of $TolC^{WT}$ can be detected on both MacB surfaces. These binding signals are most likely a result of non-specific interactions between α-helices of MacB and streptavidin or mismatch in buffer composition, rather than binding (Figure 3.3 A). We also investigated the binding of $TolC^{\Delta Loop}$ mutant to MacB surfaces. This $TolC^{\Delta Loop}$ has simultaneous alteration of the four residues of $_{147}GLVA_{150}$ to AGSG, which are located in the turn region between the outer helices H3 and H4 of TolC. These mutations inactivated efflux activity without affecting cross-linkable interactions between TolC and AcrA or TolC and AcrB (Weeks, Celaya-Kolb et al. 2010). As in the case with $TolC^{WT}$, the sensorgrams of $TolC^{\Delta Loop}$ binding also suggest non-specific interactions between MacB and TolC (Figure 3.3 B). Taken together, these results suggest that MacB does not interact with TolC directly.

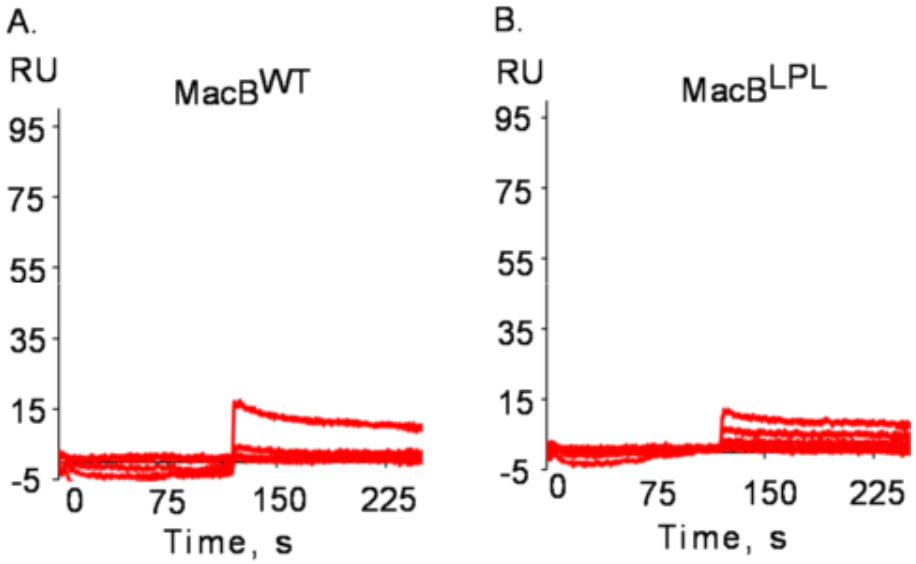


Figure 3.2 Immobilized TolC cannot bind MacB. Sensorgrams of two-fold dilutions of 62.5-1000 nM $MacB^{WT}$ (A) or $MacB^{LPL}$ (B) injected over TolC (790 RU) surface in MES

running buffer (pH 6.0) supplemented with 8 mM $MgCl_2$.

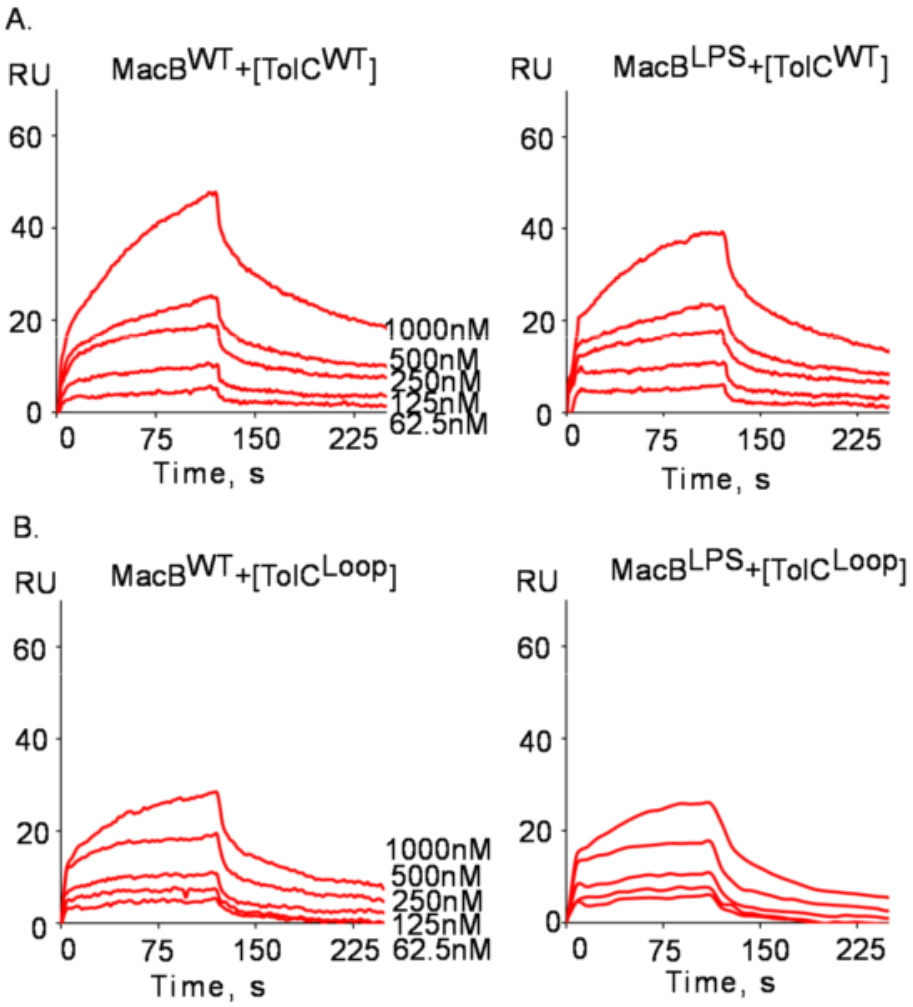


Figure 3.3 TolC^{WT} and TolC$^{\Delta Loop}$ cannot bind MacB. A. Sensorgrams of two-fold dilutions of 62.5-1000 nM TolC^{WT} injected over MacB^{D} (1600 RU) and MacB^{LPL} (800 RU) surfaces as indicated in MES running buffer (pH 6.0) supplemented with 8 mM $MgCl_2$. B. Sensorgrams of two-fold dilutions of 62.5-1000 nM TolC$^{\Delta Loop}$ injected over MacB^{D} (1600 RU) and MacB^{LPL} (800 RU) surfaces as indicated in MES running buffer (pH 6.0) supplemented with 8 mM $MgCl_2$.

3.3 MacB is essential for the recruitment of TolC.

In order to couple the energy generated by ATP hydrolysis to substrate transport across the outer membrane through TolC channel, MacAB is believed to go through conformational changes favorable for the recruitment of TolC and the formation of functional complexes. MacA is thought to play a significant role in this assembly process. Previous studies show that MacAB-TolC complexes can be detected and co-purified *in vivo* (Tikhonova, Devroy et al. 2007; Modali and Zgurskaya 2011). To investigate how the ATP hydrolysis state of MacB affects the recruitment of TolC by MacA, we purified $MacA^{WT}$ expressed alone or together with MacB variants from *E. coli* W4680AD (Δ*acrAB,* Δ*acrD*) cells. The purified proteins were separated by 12% SDS-PAGE, transferred onto the PVDF membrane, incubated with anti-MacB, anti-MacA or anti-TolC rabbit polyclonal antibodies followed by alkaline- phosphatase-conjugated anti-rabbit IgG antibody and visualized by BCIP and NBT (Figure 3.4). Results showed that TolC can be co-purified with $MacA^{WT}$ alone and $MacA^{WT}$-$MacB^{WT}$ but not with MacB alone, indicating that $MacA^{WT}$ is required for the recruitment of TolC to form MacAB-TolC complexes. The amounts of co-purified TolC remained the same in MacA-$MacB^{169}$ and MacA-$MacB^{YC}$ samples, suggesting that the defect in MacB ATPase does not significantly affect the complex formation. Surprisingly, no TolC was co-purified with MacA-$MacB^{LPL}$. In contrast, TolC is pulled down by $MacA^{WT}$ alone but not in the complex with $MacB^{LPL}$. These results demonstrate that the periplasmic loop of MacB is not only essential for the MacA-dependent stimulation of MacB ATPase but also for the proper assembly of MacAB-TolC complexes.

To investigate the role of MacB LPL domain in the complex assembly of

MacAB-TolC, we pre-assembled MacA-MacB^{WT} and MacA-MacB^{LPL} complexes with different MacB to MacA stoichiometries and then injected the complexes over the TolC surface. Previously no MacB^{WT} or MacB^{LPL} binding were detected on TolC surface (Figure 3.1). If pre-assembled MacA-MacB complexes can be recruited onto TolC surface by MacA, the binding response of complexes should be higher than that of MacA alone, indicating that MacB is retained on TolC surface through MacA. On the contrary, a lower binding response for pre-assembled MacA-MacB complexes suggests that the presence of MacB interferes with MacA-TolC interaction. Figure 3.5 showed that the binding responses of MacA-MacB^{WT} complexes were increased compared to those of MacA^{WT} alone. On the other hand, MacB^{LPL} prevented MacA^{WT} from binding to TolC. This result supports the previous conclusion that the larger periplasmic loop of MacB is not only required for MacA-dependent stimulation of MacB ATPase activity of but is also involved in the assembly of MacAB-TolC complex.

Taken together, these results further suggest that the MacA-dependent stimulation of MacB ATPase is coupled with TolC recruitment.

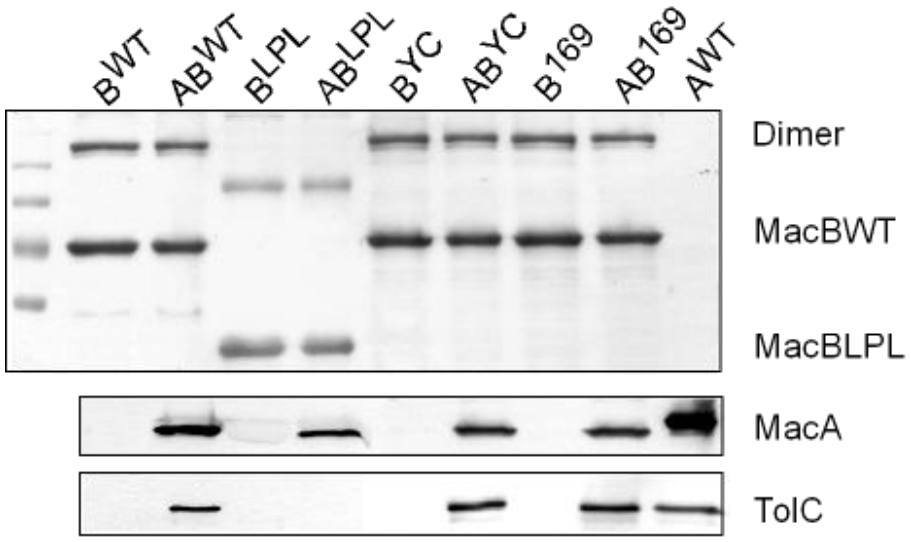


Figure 3.4 Co-purification of MacA and TolC with MacB^{WT} and its derivatives. 6-his-tagged MacB^{WT} or its derivatives were purified from *E. coli* W4680AD (Δ*acrAB*, Δ*acrD*) cells carrying plasmids that co-express MacB variants along with MacA^{WT}. The co-purification of MacA and TolC with MacB was analyzed by 12 % SDS-PAGE and immunoblotting with anti-MacB, anti-MacA and anti-TolC polyclonal antibodies.

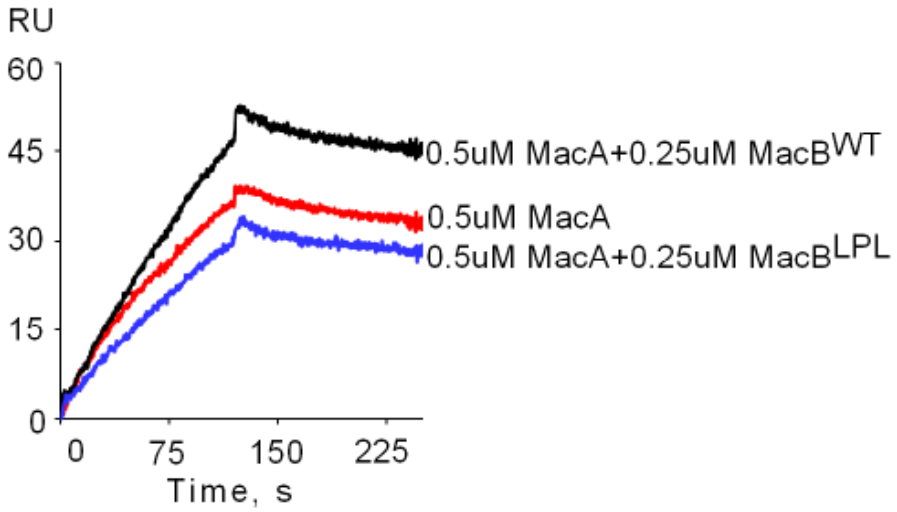


Figure 3.5 MacB^{LPL} fails to recruit TolC. 0.5 μM MacA^{WT} alone (red line) and 0.5 μM

$MacA^{WT}$ pre-mixed with 0.25 μM $MacB^{WT}$ (black line) or $MacB^{LPL}$ (blue line) were injected over TolC (790 RU) surface in MES running buffer (pH 6.0) supplemented with 8 mM $MgCl_2$.

Chapter 4: Reconstitution of MacAB-TolC into nanodiscs.

4.1 Construction and purification of tag-less ApoA-I.

All three components of MacAB-TolC complex are membrane proteins and they are insoluble in aqueous buffer solutions. Therefore, to study the biological and physiological functions of these proteins, detergent and reconstituted proteoliposomes were used. In detergent, MacB can hydrolyze ATP, but the stimulation of MacB ATPase by MacA is not more than 50% (Tikhonova, Devroy et al. 2007). In detergents, MacB may exhibit a conformation different from that in the native environment. Furthermore, the interactions between MacA and MacB may be disrupted by detergent micelle. In contrary, MacA significantly stimulates the MacB ATPase when reconstituted together with MacB into proteoliposomes (Tikhonova, Devroy et al. 2007). However, the limitation of reconstituted proteoliposomes is that only on side of the protein is accessible to aqueous environment. Due to this character of proteoliposomes, we cannot investigate the nucleotide binding and complex assembly simultaneously. Thus, in order to create a membrane like environment for the study of functional tripartite complexes *in vitro*, we decided to reconstitute MacAB-TolC complexes into lipid nanodiscs.

Nanodiscs are reconstituted high-density lipoprotein (rHDL), composed of a planar

bilayer of phospholipids surrounded by a dimer form of apolipoprotein A-I (apoA-I) (Figure 4.1 A). This reconstitution system has been elegantly adopted by laboratories to incorporate various membrane proteins into the phospholipid bilayer (Whorton, Jastrzebska et al. 2008) and functional studies based on this reconstituted system have been reported from numerous laboratories (Tsukamoto, Sinha et al. 2010). We expect that MacB reconstituted into nanodiscs will be accessible to nucleotides, substrates, MacA and TolC simultaneously. Therefore, this reconstituted system could help us to recreate a complete event for the macrolide transport through MacAB-TolC complex (Figure 4.1 B).

In order to establish a reconstitution system, we purified 6-His-tagged ApoA-I as described in (Ryan, Forte et al. 2003) and then optimized the reconstitution conditions using different phospholipids, detergents and protein compositions. Even though all tested recombination resulted in the formation of nanodiscs, to best mimic the lipid environment of *E. coli*, *E. coli* polar lipid extracts were used as the phospholipid source. Previous studies demonstrated that MacB is a functional ATPase in TX-100 (Tikhonova, Devroy et al. 2007). Thus, TX-100 was selected to solubilize lipid and MacB. In contrary, TolC was unstable in TX-100/lipid mixture and tended to aggregate. Thus, DDM was used instead of TX-100 for the reconstitution of TolC nanodiscs. The finalized reconstitution procedure was described in Experimental Procedures II.8.

In order to further purify MacB and TolC nanodiscs using the 6 His-tag at the C terminal ends of MacB and TolC, respectively, we decided to remove the 6 his-tag from ApoA-I and fused an N-terminal intein-tag to apoA-I (Figure 4.1 C). The intein-tag can be self-cleaved from ApoA-I after DTT treatment, generating a tag less ApoA-I protein.

The *ApoA-I* gene fragment was cloned into a pTYB11 vector result in the fusion of the Intein-CDB tag to the N-terminal of ApoA-I (Figure 4.1 C). After several round optimizations of the expression and purification conditions, the expression temperature of intein-ApoA-I was set at 12 ℃. Before the separation of cytoplasmic fractions, cell lyste was treated with 0.5% TX-100 to release membrane associated intein-ApoA-I. The self-cleavage of Intein-tag from ApoA-I was carried out at RT for more than 16 hrs. A reasonable amount of tag-less ApoA-I protein with a MW around 27 kD can be purified as shown in Figure 4.1 D. This tag-less ApoA-I was used for the reconstitution of nanodiscs in the further studies.

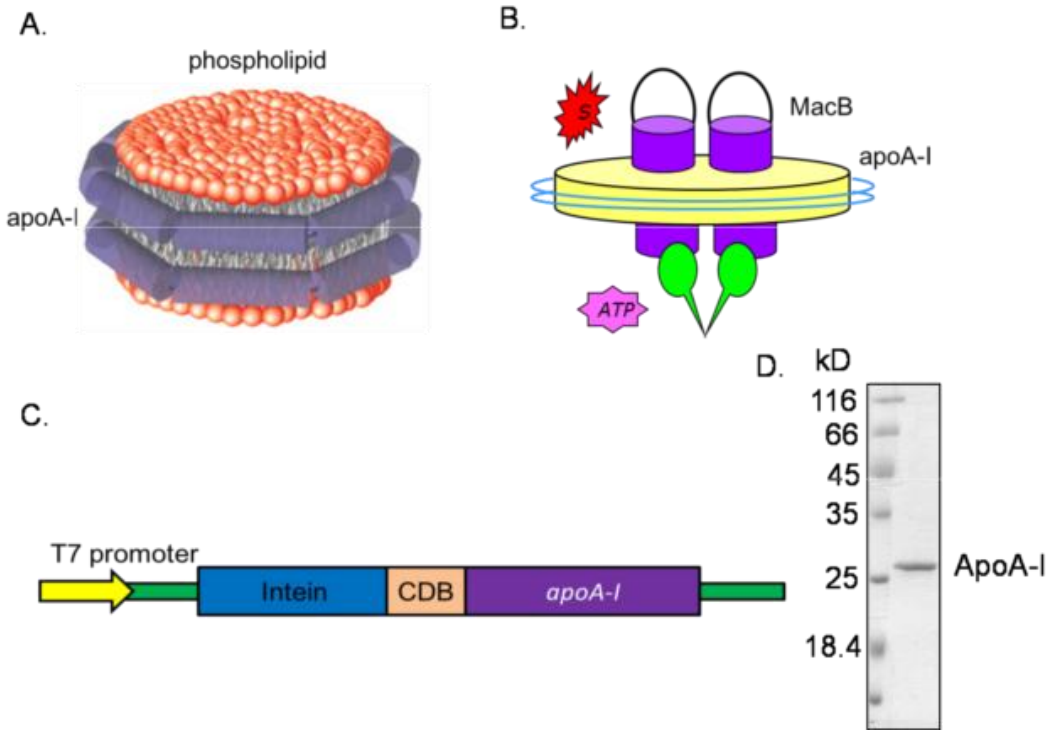


Figure 4.1 Reconstituion of nanodiscs. A. Diagram of a nanodisc with two copies of a membrane scaffold protein surrounding the hydrocarbon side chains of a lipid bilayer (Boldog, Grimme et al. 2006). B. Diagram of MacB nanodiscs with a substrate and ATP

accessible to both sides of MacB. C. The *apoA-I* gene was cloned into a pTYB11 vector and the arrangement of the insertion is indicated. D. 0.5 μg of purified ApoA-I protein was separated by 12 % SDS-PAGE and visualized by CBB staining.

4.2 MacB and TolC can be reconstituted into nanodiscs.

To investigate the protein-protein interactions of MacAB-TolC *in vitro*, we reconstituted both the inner membrane transporter MacB and the outer membrane channel TolC into nanodiscs. After reconstitution procedures, to purify protein associated nanodiscs, samples were loaded onto Ni^{2+}-charged NTA column equilibrated buffer containing 20 mM Tris-HCl (pH 8.0), 100 mM NaCl. The MacB or TolC nanodiscs were eluted by buffer supplemented with 500 mM imidezole. The protein component in fractions was verified using 12% SDS-PAGE followed by silver staining (Figure 4.2 A). Non-MacB/TolC associated particles cannot be retained on the column as shown in the fractions of flow through and wash. The co-elution of MacB and TolC with ApoA-I could be detected in the fractions of 500 mM imidezole. Furthermore, the presense of lipids in these fractions were confirmed by measuring the lipid concnetrations.

The 500 mM imidezole samples contained all MacB/TolC associated particles, which could be the mixtures of MacB/TolC containing nanodiscs and proteoliposomes. To further purify the protein containing nanodiscs, the samples were loaded onto YMC-Pack Diol-300 size exclusion column equilibrated in buffer containing 20 mM Tris-HCl (pH 8.0), 100 mM NaCl. The flow rate was set at 1 mL/min and the fractions were collected 0.5 min each. The presence of proteins was monitored by the absorbance

at 280 nm. Nanodiscs were eluted later than proteoliposomes or other lipid containing vesicles due to the small sizes. Furthermore, to confirm the homogenicity of nanodiscs, the fractions corresponding to nanodiscs were reloaded onto a size exclusion column with a flow rate at 0.1 mL/min. The flow rate set here as considerably slow in oder to reveal the differences in sizes more precisely. Both empty and MacB nanodiscs eluted as single symmetric peaks with elution times of 72.14 min and 70.55 min, respectively, indicating that the reconstituted nanoidscs are homogeneous in sizes (Figure 4.2 B). The sizes of MacB nanodiscs were slightly larger than those of empty nanodiscs probably due to the insertion of MacB.

To further verify the formation of nanodiscs, transmission eletron microscopy was utilized. The fractions collected from the peaks of empty and MacB nanodiscs were adsorbed onto carbon-coated copper grids at RT for 2 min. Then the grids were washed with double distilled water and stained with 2% phosphotungstic acid (PTA) (pH 7.1). The images of emty nanodiscs and MacB nanodiscs are shown (Figure 4.2 B). In agreement with previous studies (Chen, Ren et al. 2009), the nanodiscs are white and circular with diameters around 10 nm.

Taken together, it is concluded that we have reconstituted empty nanodiscs and MacB/TolC containing nanodiscs.

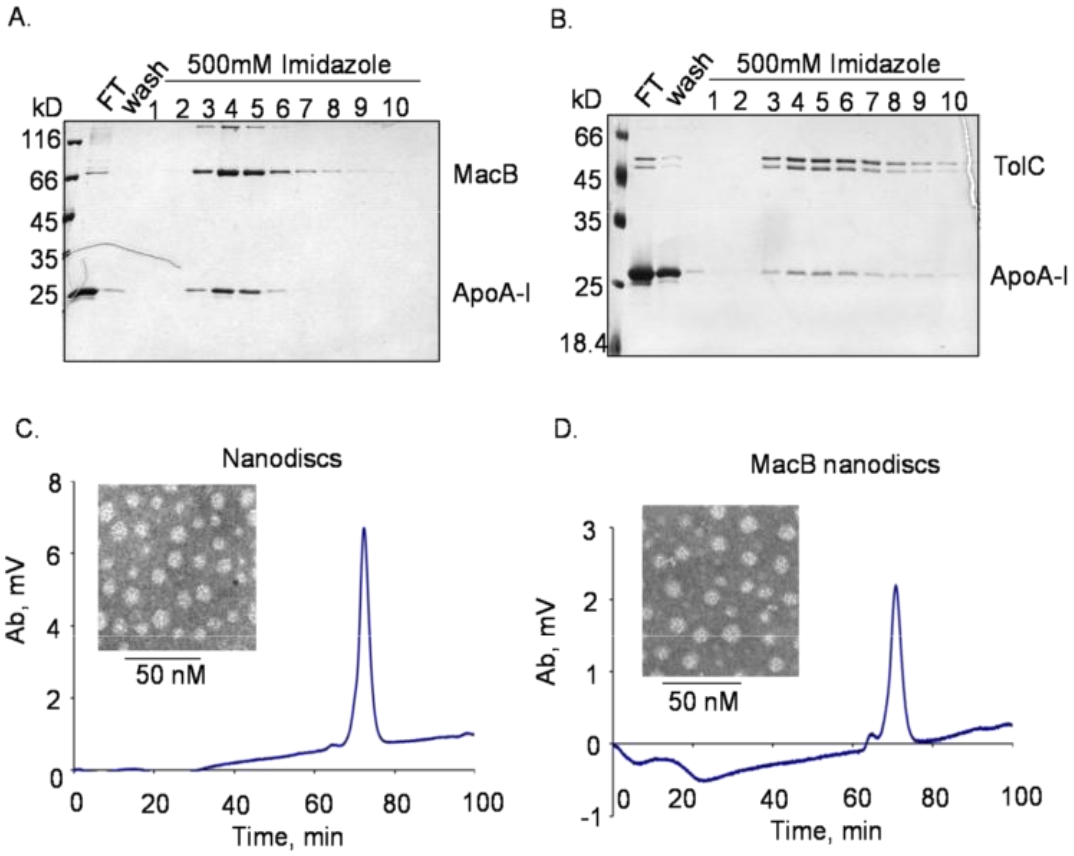


Figure 4.2 MacB and TolC can be reconstituted into nanodiscs. A. Purification of MacB and TolC nanodiscs, respectively. Samples after reconstitution procedures were loaded onto Ni^{2+}-charged NTA column equilibrated with buffer containing 20 mM Tris-HCl (pH 8.0), 100 mM NaCl. MacB or TolC nanodiscs were eluted by buffer supplemented with 500 mM Imidazole. B. Size exclusion chromatography (SEC) of nanodiscs. The flow rate was set at 0.1 mL/min. The presence of proteins was monitored by the absorbance at 280 nm and plotted as a function of the elution time. Insert: TEM images of nanodiscs or MacB nanodiscs.

4.3 MacB reconstituted into nanodiscs can hydrolyze ATP.

In Chapter 1.1, we demonstrate that purified MacB can hydrolyze ATP in detergent

TX-100 and in reconstituted proteoliposomes (Figure 1.1). In order to investigate the functionality of MacB in nanodiscs and how reconstitution of MacB into lipid bilayer affects the activity of MacB, we measured the specific ATPase activity of MacB in nanodiscs in the combination with TolC nanodiscs and $MacA^{S}$. The reactions contained 0.42 μM MacB in nanodiscs and 1 mM Mg-ATP and were carried out in HEPES buffer (pH 7.0) without 0.2% TX-100 at 37℃ (Figure 4.3). $MacB^{WT}$ in nanodiscs could hydrolyze ATP with a comparable activity to that of $MacB^{WT}$ in detergent, suggesting that $MacB^{WT}$ is functional in nanodiscs. TolC nanodiscs, empty nanodiscs, lipid itself and purified ApoA-I showed no activity towards ATP, indicating that only MacB contributes to the ATPase activity of MacB nanodiscs. Addition of TolC nanodiscs, $MacA^{S}$ or the combination of these two into the reactions did not stimulate MacB ATPase. In agreement with previous studies (Tikhonova, Devroy et al. 2007), this result suggests that the presence of TMs of MacA is required for the MacA-dependent stimulation of MacB ATPase. Furthermore, TolC did not contribute to the ATPase activity of MacB. Surprisingly, $MacB^{C56A/D643C}$, which lost 60% ATPase activity compared to $MacB^{WT}$ in detergent (Figure 1.1), regained ATPase activity after reconstituted into nanodiscs. This result strongly suggests that reconstitution of $MacB^{C56A/D643C}$ into lipid nanodiscs compensates the loss of $MacB^{C56A/D643C}$ ATPase by providing a more native environment for MacB function. Therefore, this functional $MacB^{C56A/D643C}$ in nanodiscs can be used for immobilization and kinetic study.

For immobilization purposes, $MacB^{C56A/D643C}$ was biotinylated and then reconstituted into nanodiscs. To investigate the effect of biotinylation to MacB ATPase, we measured the specific ATPase activity of biotinylated $MacB^{C56A/D643C}$ in detergent and

in nanodiscs (Figure 4.2). Biotinylated MacB$^{C56A/D643C}$ could hydrolyze ATP with a similar efficiency to that of unlabeled MacB$^{C56A/D643C}$, indicating that biotinylation procedure does not affect the functionality of MacB. Furthermore, reconstitution of biotinylated MacB$^{C56A/D643C}$ into nanodiscs rescued the loss of MacB ATPase to the level of MacB^{WT}.

Taken together, MacB^{WT} and MacB$^{C56A/D643C}$ in nanodiscs are functional ATPases. This further suggests that reconstitution of MacB into nanodiscs provides us a more natural way to investigate the complex formation of MacAB-TolC.

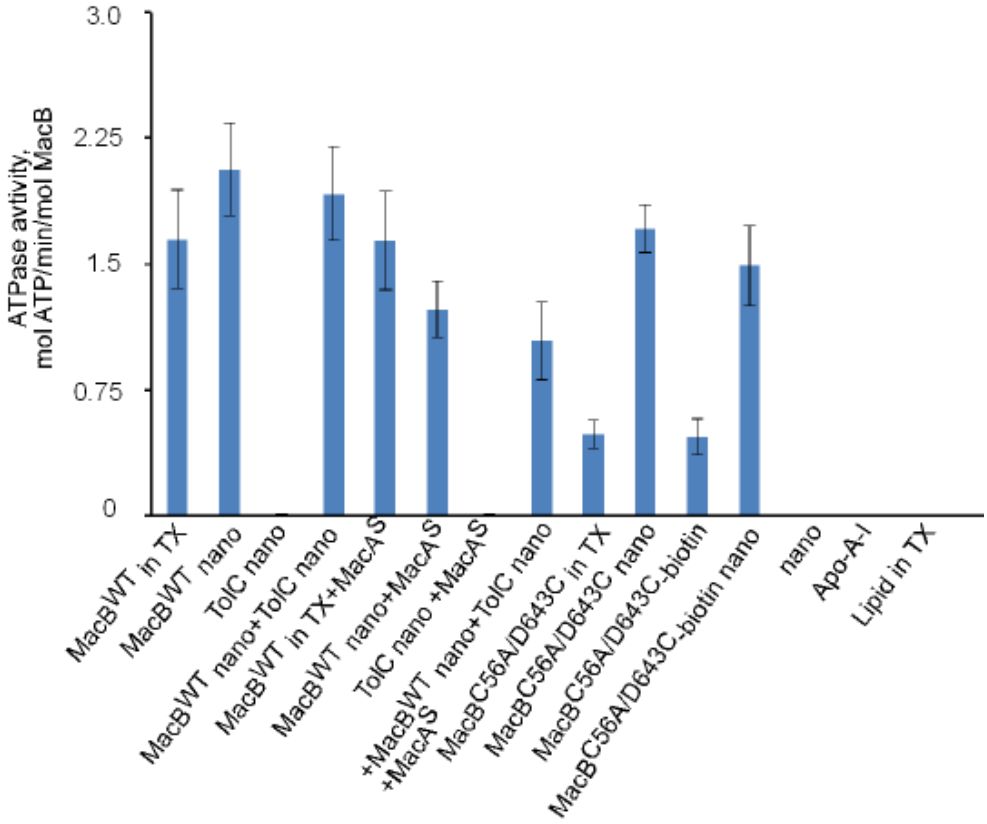


Figure 4.3 Specific ATPase activity of nanodiscs. Specific activity of MacB^{WT} and MacB$^{C56A/D643C}$ in detergent or reconstitutied into nanodiscs in the precence of MacA^{S} and TolC associated nanodiscs (MacB: TolC: MacA^{S} molar ratio 2:3:3). Reactions

contained 0.42 μM MacB in nanodiscs and were carried out in the presence of 1mM Mg-ATP at 37 ℃. Error bars are SDs (n = 3).

4.4 Immobilized MacB nanodiscs bind ATP.

In Chapter 2.2, we show that Immobilized $MacB^{WT}$ and its derivatives are capable of binding ATP in MES (pH 6.0) running buffer. Therefore, we wanted to investigate whether $MacB^{C56A/D643C}$ nanodiscs could bind ATP and how the binding of ATP to MacB was affected upon reconstitution. For this purpose, empty and MacB nanodiscs were immobilized onto a SA chip as described in Chapter 2.1 with and 2551 RU and 2783 RU surface densities, respectively. Increasing concentrations of ATP were injected over MacB nanodiscs surface, the empty nanodiscs surface and THE protein free surface simultaneously in MES running buffer (pH 6.0) and HEPES running buffer (pH 7.4) without TX-100. Binding responses were normalized by subtracting the responses from the protein free surface (Figure 4.4). The shape of ATP binding curves of $MacB^{C56A/D643C}$ in nanodiscs looked similar to those of $MacB^{D}$ in detergent, implying that the binding kinetic of ATP to MacB is probably the same in detergent and in nanodiscs. The response curves reached steady-state rapidly and ATP dissociated from MacB surfaces within 5 sec, suggesting that the binding reaction is reversible. On the other hand, no binding responses were detected on empty nanodiscs surface, indicating that the binding of ATP is specific to MacB but not to phospholipids or ApoA-I proteins. In addition, the binding signals of ATP were more notable in MES running buffer (pH 6.0) compared to those in HEPES running buffer (pH 7.4). Therefore, MES running buffer (pH 6.0) will be used in

further studies.

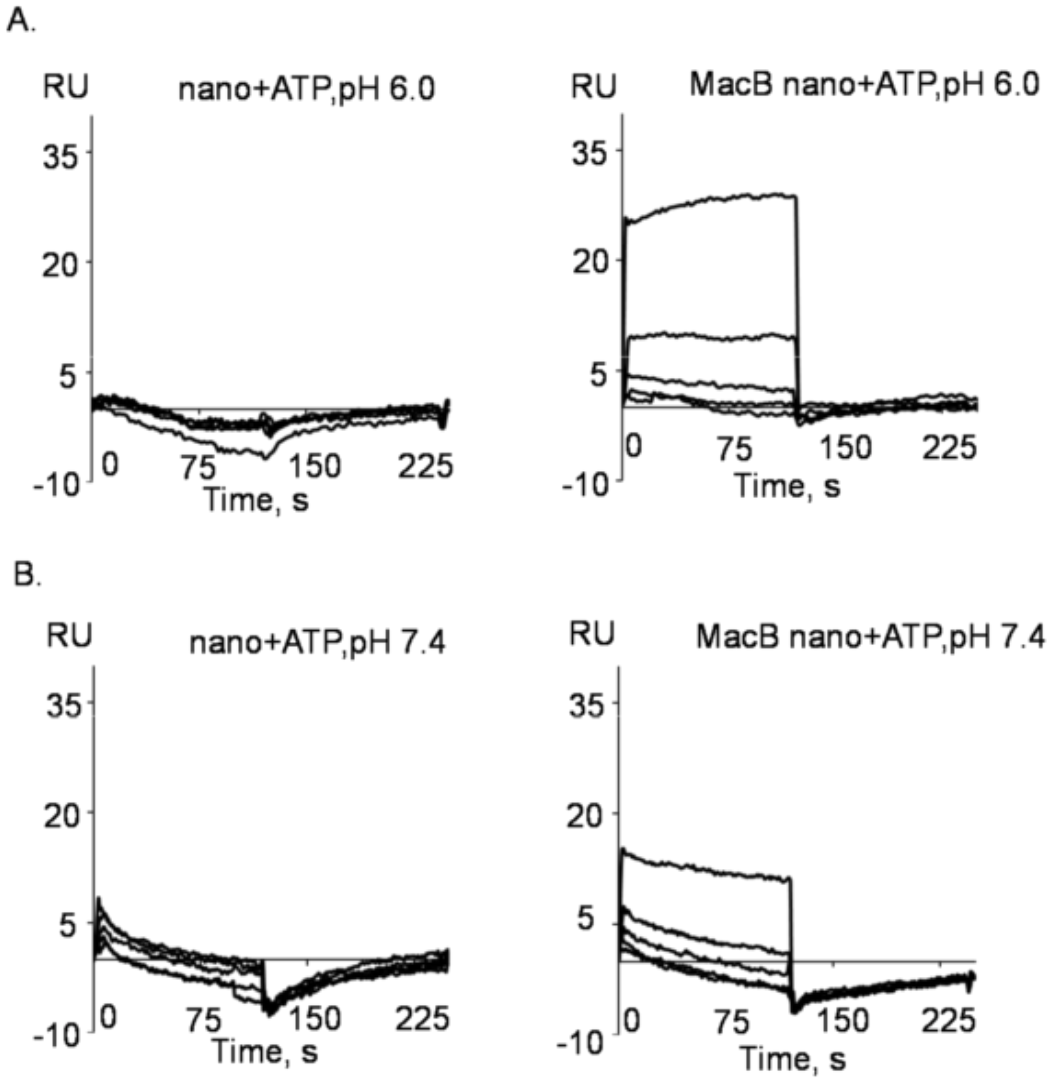


Figure 4.4 Immobilized MacB nanodiscs bind ATP. Sensorgrams of two-fold dilutions of 0.25-8 mM Mg-ATP injected over MacB nanodiscs (2783 RU) surface and nanodiscs (2551 RU) surface in MES running buffer (pH 6.0) without TX-100 (A) or HEPES running buffer (pH 7.4) without TX-100 (B).

4.5 MacA^S binds MacB nanodiscs.

To investigate the interaction between MacA and MacB, increasing concentrations of MacA^S were injected over MacB nanodiscs surface and empty nanodiscs surface in MES running buffer (pH 6.0) without TX-100. MacA^S bound MacB nanodiscs (Figure 4.5). However, the binding responses were also detected on nanodiscs surface but the signal was very low. At this point, it is difficult to conclude that MacA^S can interact with MacB in nanodiscs. More investigations need to be done in the future.

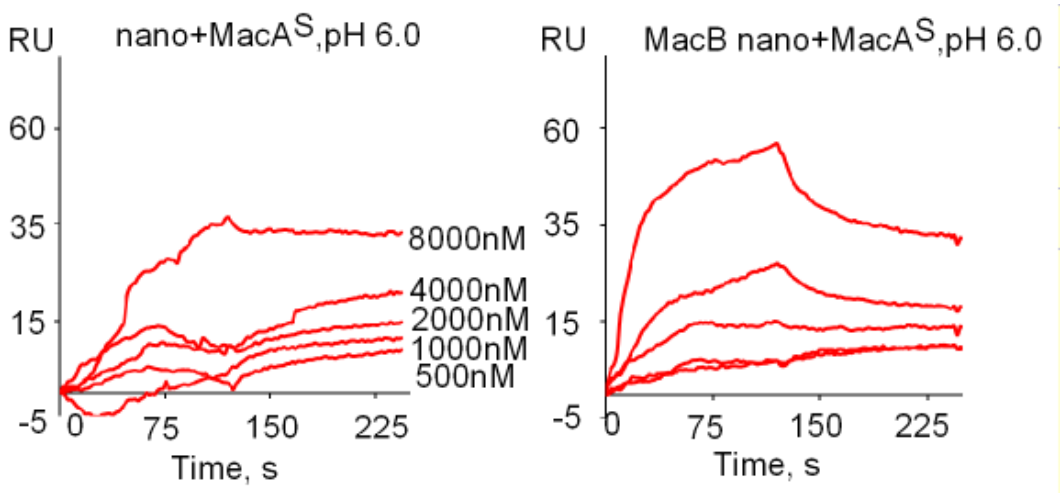


Figure 4.5 Immobilized MacB nanodiscs bind MacA^S. Sensorgrams of two-fold dilutions of 500-8000 nM MacA^S injected over MacB nanodiscs (2783 RU) surface and nanodiscs (2551 RU) surface in MES running buffer (pH 6.0) without TX-100.

III. Discussion.

One of the reasons why Gram-negative bacteria are more resistant to antibiotics than Gram-positive bacteria is the distinctive structural feature of their cell wall. It is composed of two membranes: the inner (IM) and the outer (OM) membrane. The outer membrane contributes to the intrinsic resistance by acting as an efficient permeability barrier (Nikaido 1998). The second key factor for the high level of resistance of Gram-negative bacteria towards antibiotics is the expression of multidrug efflux systems located in the cell envelope. Due to the double membrane arrangement, in Gram-negative bacteria the MDR efflux pumps form tripartite complexes for the direct translocation of diverse substrates from the cytoplasm or cytoplasmic membrane into the extracellular medium. These tripartite complexes are composed of an inner membrane transporter, a periplasmic membrane fusion (MFP) and an outer membrane channel.

In *E. coli*, MacAB-TolC is the first experimentally described ATP-driven tripartite efflux pump which is involved in the extrusion of macrolides and enterotoxin (Kobayashi, Nishino et al. 2001; Yamanaka, Kobayashi et al. 2008). In this complex, MacA is a MFP, inserted into the inner membrane with one transmembrane (TM) segment. MacB is the inner membrane ABC-type transporter which uses ATP hydrolysis to energize the transport reaction. MacA and MacB together form the macrolide-specific efflux pump which required the third component, TolC, to efflux drugs out the cell. TolC is an outer membrane (OM) protein and is also an important component in other MDR efflux pumps. MacB functions as a dimer and purified MacB displays ATPase activity. MacA has a dual role: it acts as the physical linker between MacB and TolC and stimulates the ATPase activity of MacB (Tikhonova, Devroy et al. 2007). The molecular mechanism of such

stimulation remains unclear. It has been shown that MacA could function as a switch in coupling the energy consumption by transporter to the efflux of substrates (Modali and Zgurskaya 2011). TolC does not modulate the ATPase activities of MacB or MacAB complex. However, the function of MacAB depends on the association of TolC *in vivo.* How MacAB-TolC complex is assembled and whether or not ATP plays a significant role in this process remain unknown.

In this study, we elucidated the mechanism of complex assembly of MacAB-TolC. The interaction between MacA and MacB is stimulated by ATP binding but remains unchanged during ATP hydrolysis cycle. We also found that the large periplasmic loop of MacB is required for MacA-dependent stimulation of MacB ATPase and contributes to recruitment of TolC into the tripartite complex. Furthermore, we successfully reconstituted MacB and TolC into lipid nanodiscs and intend to use them for the study of the biological and physiological functions of MacAB-TolC complex.

III.1 The interaction between MacA and MacB is not sensitive to either ATP hydrolysis or conformational changes of MacB.

In this study, we developed a real-time assay to monitor the protein interaction using the surface plasmon resonance approach. SPR is a more sensitive and quantitative technique for the investigation of protein-protein interactions comparing with the traditional approaches, such as isothermal calorimetry (ITC), immuno-precipitation et al. This technique has been used extensively in the past decade for studies of soluble proteins. Recently, scientists start to apply this method to the investigation of membrane proteins (de Keyzer, van der Does et al. 2003; Lewinson, Lee et al. 2010; Tikhonova,

Yamada et al. 2011).

First, we investigated the kinetics of MacA and MacB interactions using the SPR approach. We find that $MacA^{WT}$ forms a stable hexameric structure and binds functional active $MacB^{D}$ with nanomolar affinity (Figure 2.3 & Table 2.1). In addition, the $MacA^{WT}$-MacB complex remains stable during the entire ATP hydrolysis cycle. In previous studies (Tikhonova, Dastidar et al. 2009), a similar nanomolar affinity of MacA-TolC interaction was detected. These results suggest that the MacA can form stable complexes with MacB and TolC independently.

In *E. coli*, AcrB together with AcrA and TolC functions as the major MDR pump. This tripartite complex translocates a wide variety of toxic compounds outside the cell using a proton gradient across the membrane (Zgurskaya and Nikaido 1999). MacAB-TolC only confers resistance to macrolides when overproduced in the cells lacking AcrAB-TolC (Kobayashi, Nishino et al. 2001). Recent studies on AcrAB-TolC tripartite complex revealed that the periplasmic MFP AcrA also assembles high affinity complexes with AcrB and TolC independently (Tikhonova, Dastidar et al. 2009; Tikhonova, Yamada et al. 2011). Since AcrAB-TolC and MacAB-TolC share the same outer membrane channel TolC and the stabilities of MFP-TolC complexes are similar, it is likely that the MFPs share a common role in the recruitment of TolC. However, the inner membrane transporter MacB and AcrB exhibit different structural and functional characters and they can have significantly distinctive effects on the recruitment of TolC upon binding to MFPs.

Second, we investigated the involvement of ATP hydrolysis in MacA-MacB interactions. We constructed several MacB variants with substitutions affecting different

ATP hydrolysis stages. $MacB^{YC}$ is defective in ATP hydrolysis and $MacB^{169}$ is a completely inactive ATPase (Figure 1.1). Moreover, $MacB^{YC}$ shows defect in binding nucleotides and exhibits a conformation different from that of $MacB^{D}$ and $MacB^{169}$ (Figure 1.2). Surprisingly, despite the differences in the catalytic activity of MacB, $MacA^{WT}$ binds MacB variants with similar nanomolar affinity (Table 2.1). We conclude that the interaction between MacA and MacB is not sensitive to either the ATP hydrolysis or the conformational changes of MacB. Our SPR results reveal that $MacA^{S}$ binds $MacB^{D}$ with a significantly lower affinity compared to $MacA^{WT}$ (Figure 2.6). In addition, $MacA^{WT}$ has similar affinities towards $MacB^{D}$ and $MacB^{LPL}$ lacking the large periplasmic loop (Figure 2.5). Therefore, in agreement with previous studies (Tikhonova, Devroy et al. 2007), the TM segment of MacA plays a dominant role in the interaction between MacA and MacB. The interaction between the TMs of MacB and MacA make the major contribution to the MacA-MacB interaction captured on the surface. Since the amino acid residues Y14 and C56 are located in the NBDs of MacB, the conformational changes of $MacB^{YC}$ could only occur in the NBDs leaving the alignment of $MacB^{YC}$ TMs unchanged. Thus, MacA associates with MacB in the same manner and the same affinity as long as the TMs of MacA and MacB are in position.

III.2 TolC cannot directly interact with MacB.

The crystal structure of MacB periplasmic core domain (PCD) reveals some structural similarities to the periplamic domains of the RND-type multidrug efflux transporter AcrB (Yum, Xu et al. 2009). AcrB is a homotrimer and each monomer has two large periplasmic loops between TM1 and TM2, and TM7 and TM8 (Murakami,

Nakashima et al. 2002). The periplasmic loops of AcrB from each protomer together form the porter domain and the TolC-docking domain, which function as a substrate binding pocket and a substrate exit domain, respectively. AcrB binds TolC directly and probably contributes to the opening of TolC channel (Zgurskaya, Krishnamoorthy et al. 2011).

Even though MacB and AcrB share the same outer membrane channel TolC and there are structural similarities in the periplasmic domains of MacB and AcrB, our SPR result demonstrates that there is no interaction between MacB and TolC *in vitro* (Figure 3.2 & 3.3). In addition, in agreement with previous *in vivo* studies (Modali and Zgurskaya 2011), TolC cannot be co-purified by MacB alone (Figure 3.4). These results strongly suggest that TolC cannot directly interact with MacB.

Previous studies showed conflicting results about MacB-TolC interaction (Lin, Bavro et al. 2009; Yum, Xu et al. 2009). Our studies suggest that TolC cannot interact directly with MacB. The structural study of MacB PCD revealed that the homotrimeric TolC is unlikely to bind the homodimeric MacB because of lack of a geometric fit between the two proteins (Yum, Xu et al. 2009). In addition, the extended length of MacB PCD protruding into the periplasm may not be long enough for the docking with the TolC tip. However, we cannot rule out a possibility that MacB can undergo conformational changes during the transport process and interact with TolC at some point suring transport process.

III.3 The periplasmic loop of MacB is not required for MacA binding but is essential for MacA-mediated stimulation of MacB ATPase.

If direct interaction between MacB and TolC is impossible, the MFP MacA must act

as the structural linker for the assembly of tripartite complexes and the functional transmitter for the translocation of substrates. MacA can interact with MacB on both sides of the membrane and within the membrane (Tikhonova, Devroy et al. 2007). The large periplasmic loop (LPL) of MacB is proposed to be the periplasmic site of interactions with MacA. To investigate the functional role of MacB LPL in MacA-MacB interaction, we deleted the LPL from MacB. We find that the LPL domain of MacB is not crucial for the interaction between MacA-MacB. However, the direct contact between the MP domain of MacA and the LPL domain of MacB is required for the MacA-dependent stimulation of MacB ATPase.

ABC-type transporters can be classified into two categories based on the transport directions of substrates: i) importers, catalyzing the uptake of essential nutrients from the environment, ii) exporters, facilitating the extrusion of diverse compounds from the cytoplasm or lipid membrane. Even though these two types of ABC transporters exhibit different structural and functional characters, they are proposed to share a common transport mechanism. In this transport process, the nucleotide-dependent conformational transitions in NBDs drive the conformational changes in the TMDs (Rees, Johnson et al. 2009). Since the LPL is connected to the TM1 and TM2 of MacB, the conformational changes in TMs can also trigger the changes in MacB LPL domain. These sequential changes in MacB conformation can alter the MacB interaction with MacA and lead to the MacA-dependent stimulation of MacB ATPase. However, MacB lacking the LPL cannot integrate these events into ATP hydrolysis, which causes the deficiency in the MacA-stimulation. Moreover, unlike most of the ABC transporters which normally consist of six TM segments, a C-terminal NBD and a very small periplasmic region

(Davidson, Dassa et al. 2008), MacB has four TM segments, an N-terminal NBD and a large periplasmic loop. This unique LPL domain of MacB may have some distinctive effects on MacB function and the complex assembly of MacAB-TolC, which need to be explored in the future.

III.4 The binding of ATP increases the affinity of MacA-MacB complex.

The ATP hydrolysis and substrate transport of MacB are significantly affected by MFP MacA (Lin, Bavro et al. 2009; Modali and Zgurskaya 2011). Previous studies suggested that MacA and ATP act synergistically on MacB and induce the closed conformation of MacB NBDs (Modali and Zgurskaya 2011). Figure 2.4 and 2.5 demonstrate that MacA and nucleotides bind MacB independently. Our SPR results further reveal that the binding affinities of MacA to all MacB variants in the presence of nucleotides are in the nanomolar range. However, a three-fold increase in MacA-MacB binding affinity is observed only in the presence of ATP and all the MacA and MacB complexes are affected by ATP. Thus, we conclude that it is ATP binding not ATP hydrolysis that enhances the affinity of MacA towards MacB. The best kinetic models for $MacA^{WT}$-MacB interaction in the presence or absence of ATP are all two-state models that $MacA^{WT}$ binds $MacB^{D}$ first and this association induces further conformational changes in MacB. Even though we cannot fit the binding of ATP into any model because of the fast on- and off-rate, it is likely that the association rate of ATP to MacB is faster than that of MacA to MacB. Therefore, ATP binds MacB and causes the dimerization of MacB. Sequentially, MacA form complex with the ATP-bound state of MacB with a higher affinity. Ultimately, the binding of MacA to MacB induces the closed

conformation of MacB NBDs.

However, some deviations from TS model can be seen in curve fittings (Figure 2.5), indicating that the reaction could be more complex.

The structures of several ABC-type exporters reveal a common coupling mechanism. Upon binding of nucleotides, TMs of exporters undergo a twisting motion for the transition from the inward-facing conformation to the outward-facing conformation. Furthermore, the canonical NBDs in the closed dimer requires a sliding motion along NBD interfaces (Dawson, Hollenstein et al. 2007; Oldham, Davidson et al. 2008). On the other hand, previous studies demonstrated that during the assembly of the transport complex the association with MacB induced conformational changes in MacA (Modali and Zgurskaya 2011). Therefore, the deviation of binding curves from the standard TS mode can be the combined actions of MacA and MacB. In addition, MacB is a structurally unique ABC-type transporter and MacA is the first MFP that is found to stimulate an ABC-type drug efflux transporte. The interaction between MacB and MacA in the presence of ATP could represent a unique mechanism, different from other transport systems. Furthermore, the binding curves of MacA to $MacB^{LPL}$ show more systematic deviation from the TS model, suggesting that MacB lacking the LPL domain may go through a different conformation transition in the presence of ATP and MacA.

Taken together, MacA has a higher affinity to MacB-ATP bound state. In detergent MacA and nucleotides only show modest effects towards MacB. However, the MacB ATPase was stimulated significantly by MacA in reconstituted proteoliposomes. It is possible that the effect of nucleotides on MacA-MacB interactions may be amplified tremendously in a lipid environment.

III.5 The mechanism of complex assembly of MacAB.

Membrane fusion protein-dependent transporters are broadly represented in both Gram-negative and Gram-positive bacteria. These transporters exhibit different structures and biochemical mechanisms (Zgurskaya, Yamada et al. 2009). However, despite the mechanistic diversity of these transporters, all MFPs are thought to stimulate the activity of transporters for the transportation of substrates (Eswaran, Koronakis et al. 2004; Touze, Eswaran et al. 2004; Mikolosko, Bobyk et al. 2006) . The molecular mechanism of such stimulation remains unknown.

Previous studies indicate that MP domain of MacA is required for the MacA facilitation of MacB function (Modali and Zgurskaya 2011) through the interaction with MacB LPL region. Our results suggest that the interaction between the MacB LPL domain and MacA is needed for the productive recruitment of TolC by MacA (Figure III.18&19). This result further imply that the MacA-dependent stimulation of MacB ATPase is coupled to the recruitment of TolC by MacA through the interactions between MacA and the large periplasmic loop of MacB.

In summary we propose a mechanism of MacAB-TolC (Figure III.1). In the mechanism, MacB adopts a catalytic cycle similar to other ABC transporters with at least four steps: i) binding of ATP and substrate, ii) transport of substrate, iii) hydrolysis of ATP, and iv) release of ADP and Pi. Binding of ATP to MacB causes the dimerization of NBDs. MacA binds ATP-bound state of MacB with a higher affinity and promotes the closed conformation of MacB NBDs for ATP hydrolysis. Subsequently, the binding of TolC to MacA changes the conformation of the MP domain of MacA (Modali and Zgurskaya 2011). The MP domain of MacA then interacts with the LPL domain of MacB

and stimulated the MacB ATPase.

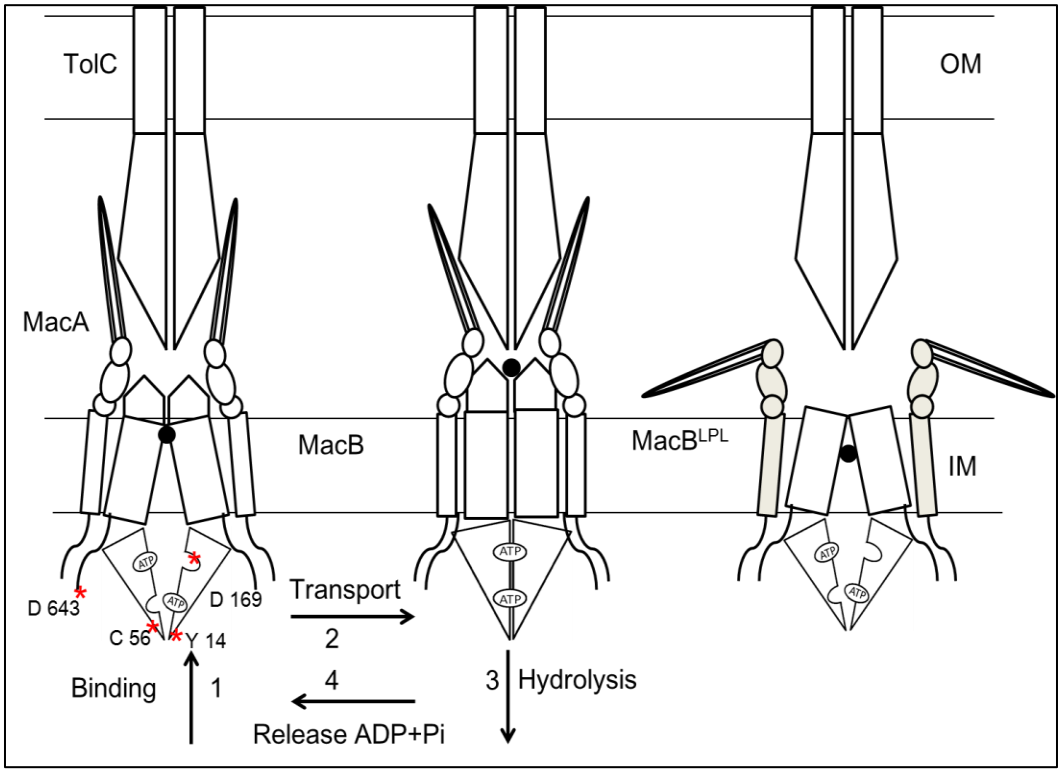


Figure III. 1 A proposed transport mechanism of MacAB–TolC.

III.6 Reconstitution of membrane proteins into lipid nanodiscs can be used to study MacAB-TolC system.

All living organisms share one common feature that the cells are surrounded by at least one bilayer of membranes composed of phospholipids and proteins. Proteins inserted in the membrane bilayers are called membrane proteins. A major challenge for the study of membrane proteins is to obtain functionally active, water-soluble and monodisperse form of proteins (Borch and Hamann 2009). Historically, membrane

proteins have to be solubilized by detergents. But this treatment of proteins often tends to affect the activity of proteins and destabilizes the proteins and their interactions (Popot, Berry et al. 2003). In addition, some membrane protein systems need to associate with phospholipids to maintain their activities. Therefore, protein reconstituted into liposomes are used for biochemical studies of membrane proteins. However, liposomes are large, heterogeneous and can be prone to aggregation upon storage. Furthermore, liposomes are sensitive to changes in osmotic pressure.

To overcome the difficulties in handling and studying membrane proteins, a method that can maintain membrane proteins monomerically in a native-like bilayer and simultaneously in solution is needed (Nath, Atkins et al. 2007). Nanodisc technology offers a solution to some of these challenges. Nanodiscs are soluble nanoscale phospholipid bilayers which can integrate membrane proteins into membrane bilayer by self-assembly (Bayburt, Grinkova et al. 2006). Nanodiscs are homogeneous, stable, and accessible to both sides of the phospholipid bilayer. These features of nanodiscs offer advantages over liposomes and detergent micelles (Bayburt and Sligar 2010). So far a number of membrane proteins were incorporated into nanodiscs for biochemical studies (Whorton, Bokoch et al. 2007; Lewinson, Lee et al. 2010). In the previous studies, MacB showed basal ATPase activity in TX-100 and this activity is either diminished by DDM or inhibited upon reconstitution into proteoliposomes (Tikhonova, Devroy et al. 2007). In order to fully understand the functionality of MacB and the mechanism of the complex assembly of MacAB-TolC in native environment, we reconstituted MacAB-TolC into lipid nanodiscs. This approach could overcome the negative effects of detergent micelles and liposomes and allow studying the complex in native environment.

$MacB^{WT}$ in nanodiscs display basal ATPase activity as in TX-100. The inhibitory effect of lipid towards MacB ATPase in proteoliposomes does not exist in lipid nanodiscs, indicating that nanodiscs provide a more native environment for MacB functions. Intriguingly, $MacB^{C56A/D643C}$, which lost at least 40% activity in TX-100, showed comparable ATPase with $MacB^{WT}$ upon reconstituted into nanodiscs. This result is the most persuasive evidence to support the idea that MacB behaves more natively when reconstituted into nanodiscs. This $MacB^{C56A/D643C}$ associated nanodiscs were able to bind ATP (Figure III.23), further suggesting that MacB in nanodiscs is functional. Even though more experiments need to be done to gain a complete insight about how this reconstituted system works, we believe that this system can be used to study MacAB-TolC complex.

One of the potential problems with this reconstituted system is that we could only use $MacA^{S}$ as the linker protein for the complex assembly which cannot stimulate the MacB ATPase. In the proposed transport mechanism of MacAB-TolC complex (Figure IV.1), MacA facilitates the closure of MacB NBDs in ATP-bound state and stimulates MacB ATPase upon TolC recruitment. All these functions of MacA require the presence of TMS domain, which is absent in $MacA^{S}$. Therefore, $MacA^{S}$ in this reconstituted system could be one of the major drawbacks. Thus, reconstitution of MacAB together into lipid nanodiscs can possibly provide more information about the MacA-dependent stimulation of MacB ATPase and the MacA-mediated complex assembly. This will be our next task to achieve in the future.

Reference

Akama, H., T. Matsuura, et al. (2004). "Crystal structure of the membrane fusion protein, MexA, of the multidrug transporter in Pseudomonas aeruginosa." J Biol Chem **279**(25): 25939-25942.

Alekshun, M. N. and S. B. Levy (2007). "Molecular mechanisms of antibacterial multidrug resistance." Cell **128**(6): 1037-1050.

Andersen, C. (2003). "Channel-tunnels: outer membrane components of type I secretion systems and multidrug efflux pumps of Gram-negative bacteria." Rev Physiol Biochem Pharmacol **147**: 122-165.

Andersen, C., E. Koronakis, et al. (2002). "Transition to the open state of the TolC periplasmic tunnel entrance." Proc Natl Acad Sci U S A **99**(17): 11103-11108.

Bayburt, T. H., Y. V. Grinkova, et al. (2006). "Assembly of single bacteriorhodopsin trimers in bilayer nanodiscs." Arch Biochem Biophys **450**(2): 215-222.

Bayburt, T. H. and S. G. Sligar (2010). "Membrane protein assembly into Nanodiscs." FEBS Lett **584**(9): 1721-1727.

Boldog, T., S. Grimme, et al. (2006). "Nanodiscs separate chemoreceptor oligomeric states and reveal their signaling properties." Proc Natl Acad Sci U S A **103**(31): 11509-11514.

Borch, J. and T. Hamann (2009). "The nanodisc: a novel tool for membrane protein studies." Biol Chem **390**(8): 805-814.

Borges-Walmsley, M. I., K. S. McKeegan, et al. (2003). "Structure and function of efflux pumps that confer resistance to drugs." Biochemical Journal **376**: 313-338.

Carrier, I., I. L. Urbatsch, et al. (2007). "Mutational analysis of conserved aromatic residues in the A-loop of the ABC transporter ABCB1A (mouse Mdr3)." FEBS Lett **581**(2): 301-308.

Chen, B., X. Ren, et al. (2009). "Apolipoprotein AI tertiary structures determine stability and phospholipid-binding activity of discoidal high-density lipoprotein particles of different sizes." Protein Sci **18**(5): 921-935.

Chen, P. S., T. Y. Toribara, et al. (1956). "Microdetermination of Phosphorus." Anal Chem **28**(11): 1756-1758.

Date, S. V. (2007). "Estimating protein function using protein-protein relationships." Methods Mol Biol **408**: 109-127.

Davidson, A. L., E. Dassa, et al. (2008). "Structure, function, and evolution of bacterial ATP-binding cassette systems." Microbiol Mol Biol Rev **72**(2): 317-364, table of contents.

Dawson, R. J., K. Hollenstein, et al. (2007). "Uptake or extrusion: crystal structures of full ABC transporters suggest a common mechanism." Mol Microbiol **65**(2): 250-257.

de Keyzer, J., C. van der Does, et al. (2003). "Direct demonstration of ATP-dependent release of SecA from a translocating preprotein by surface plasmon resonance." J Biol Chem **278**(32): 29581-29586.

Deininger, K. N., A. Horikawa, et al. (2011). "A requirement of TolC and MDR efflux pumps for acid adaptation and GadAB induction in Escherichia coli." PLoS One **6**(4): e18960.

Dhamdhere, G. and H. I. Zgurskaya (2010). "Metabolic shutdown in Escherichia coli

cells lacking the outer membrane channel TolC." Mol Microbiol **77**(3): 743-754.
Dubern, J. F., E. R. Coppoolse, et al. (2008). "Genetic and functional characterization of the gene cluster directing the biosynthesis of putisolvin I and II in Pseudomonas putida strain PCL1445." Microbiology **154**(Pt 7): 2070-2083.
Eswaran, J., E. Koronakis, et al. (2004). "Three's company: component structures bring a closer view of tripartite drug efflux pumps." Curr Opin Struct Biol **14**(6): 741-747.
Fiske, C. H. and Y. Subbarow (1925). "The colorimetric determination of phosphorus." Journal of Biological Chemistry **66**(2): 375-400.
Ge, Q., Y. Yamada, et al. (2009). "The C-terminal domain of AcrA is essential for the assembly and function of the multidrug efflux pump AcrAB-TolC." J Bacteriol **191**(13): 4365-4371.
Geourjon, C., C. Orelle, et al. (2001). "A common mechanism for ATP hydrolysis in ABC transporter and helicase superfamilies." Trends Biochem Sci **26**(9): 539-544.
German, G. J. and R. Misra (2001). "The TolC protein of Escherichia coli serves as a cell-surface receptor for the newly characterized TLS bacteriophage." J Mol Biol **308**(4): 579-585.
Hantke, K., K. Winkler, et al. (2011). "Escherichia coli exports cyclic AMP via TolC." J Bacteriol **193**(5): 1086-1089.
Higgins, C. F. (2001). "ABC transporters: physiology, structure and mechanism--an overview." Res Microbiol **152**(3-4): 205-210.
Higgins, C. F. (2007). "Multiple molecular mechanisms for multidrug resistance transporters." Nature **446**(7137): 749-757.
Higgins, M. K., E. Bokma, et al. (2004). "Structure of the periplasmic component of a bacterial drug efflux pump." Proc Natl Acad Sci U S A **101**(27): 9994-9999.
Holland, I. B. and M. A. Blight (1999). "ABC-ATPases, adaptable energy generators fuelling transmembrane movement of a variety of molecules in organisms from bacteria to humans." J Mol Biol **293**(2): 381-399.
Jack, D. L., N. M. Yang, et al. (2001). "The drug/metabolite transporter superfamily." Eur J Biochem **268**(13): 3620-3639.
Kobayashi, N., K. Nishino, et al. (2003). "Membrane topology of ABC-type macrolide antibiotic exporter MacB in Escherichia coli." FEBS Lett **546**(2-3): 241-246.
Kobayashi, N., K. Nishino, et al. (2001). "Novel macrolide-specific ABC-type efflux transporter in Escherichia coli." J Bacteriol **183**(19): 5639-5644.
Koronakis, V., J. Eswaran, et al. (2004). "Structure and function of TolC: the bacterial exit duct for proteins and drugs." Annu Rev Biochem **73**: 467-489.
Koronakis, V., A. Sharff, et al. (2000). "Crystal structure of the bacterial membrane protein TolC central to multidrug efflux and protein export." Nature **405**(6789): 914-919.
Levy, S. B. and B. Marshall (2004). "Antibacterial resistance worldwide: causes, challenges and responses." Nat Med **10**(12 Suppl): S122-129.
Lewinson, O., A. T. Lee, et al. (2010). "A distinct mechanism for the ABC transporter BtuCD-BtuF revealed by the dynamics of complex formation." Nat Struct Mol Biol **17**(3): 332-338.
Li, X. Z. and H. Nikaido (2004). "Efflux-mediated drug resistance in bacteria." Drugs **64**(2): 159-204.

Li, X. Z. and H. Nikaido (2009). "Efflux-mediated drug resistance in bacteria: an update." Drugs **69**(12): 1555-1623.

Lin, H. T., V. N. Bavro, et al. (2009). "MacB ABC transporter is a dimer whose ATPase activity and macrolide-binding capacity are regulated by the membrane fusion protein MacA." J Biol Chem **284**(2): 1145-1154.

Lubelski, J., W. N. Konings, et al. (2007). "Distribution and physiology of ABC-type transporters contributing to multidrug resistance in bacteria." Microbiol Mol Biol Rev **71**(3): 463-476.

Mao, W., M. S. Warren, et al. (2002). "On the mechanism of substrate specificity by resistance nodulation division (RND)-type multidrug resistance pumps: the large periplasmic loops of MexD from Pseudomonas aeruginosa are involved in substrate recognition." Mol Microbiol **46**(3): 889-901.

Mikolosko, J., K. Bobyk, et al. (2006). "Conformational flexibility in the multidrug efflux system protein AcrA." Structure **14**(3): 577-587.

Modali, S. D. and H. I. Zgurskaya (2011). "The periplasmic membrane proximal domain of MacA acts as a switch in stimulation of ATP hydrolysis by MacB transporter." Mol Microbiol **81**(4): 937-951.

Murakami, S., R. Nakashima, et al. (2002). "Crystal structure of bacterial multidrug efflux transporter AcrB." Nature **419**(6907): 587-593.

Nath, A., W. M. Atkins, et al. (2007). "Applications of phospholipid bilayer nanodiscs in the study of membranes and membrane proteins." Biochemistry **46**(8): 2059-2069.

Nikaido, H. (1996). "Multidrug efflux pumps of gram-negative bacteria." J Bacteriol **178**(20): 5853-5859.

Nikaido, H. (1998). "Antibiotic resistance caused by gram-negative multidrug efflux pumps." Clin Infect Dis **27 Suppl 1**: S32-41.

Nikaido, H. (2009). "Multidrug resistance in bacteria." Annu Rev Biochem **78**: 119-146.

Nikaido, H. and J. M. Pages (2012). "Broad-specificity efflux pumps and their role in multidrug resistance of Gram-negative bacteria." FEMS Microbiol Rev **36**(2): 340-363.

Oldham, M. L., A. L. Davidson, et al. (2008). "Structural insights into ABC transporter mechanism." Curr Opin Struct Biol **18**(6): 726-733.

Pao, S. S., I. T. Paulsen, et al. (1998). "Major facilitator superfamily." Microbiol Mol Biol Rev **62**(1): 1-34.

Paulsen, I. T. (2003). "Multidrug efflux pumps and resistance: regulation and evolution." Curr Opin Microbiol **6**(5): 446-451.

Paulsen, I. T., M. H. Brown, et al. (1996). "Proton-dependent multidrug efflux systems." Microbiol Rev **60**(4): 575-608.

Paulsen, I. T. and K. Lewis (2001). "Microbial multidrug efflux: introduction." J Mol Microbiol Biotechnol **3**(2): 143-144.

Pautsch, A. and G. E. Schulz (1998). "Structure of the outer membrane protein A transmembrane domain." Nat Struct Biol **5**(11): 1013-1017.

Piddock, L. J. V. (2006). "Multidrug-resistance efflux pumps - not just for resistance." Nature Reviews Microbiology **4**(8): 629-636.

Popot, J. L., E. A. Berry, et al. (2003). "Amphipols: polymeric surfactants for membrane biology research." Cell Mol Life Sci **60**(8): 1559-1574.

Rees, D. C., E. Johnson, et al. (2009). "ABC transporters: the power to change." Nat Rev Mol Cell Biol **10**(3): 218-227.
Ryan, R. O., T. M. Forte, et al. (2003). "Optimized bacterial expression of human apolipoprotein A-I." Protein Expr Purif **27**(1): 98-103.
Saier, M. H., Jr., J. T. Beatty, et al. (1999). "The major facilitator superfamily." J Mol Microbiol Biotechnol **1**(2): 257-279.
Schmitz, G., T. Langmann, et al. (2001). "Role of ABCG1 and other ABCG family members in lipid metabolism." J Lipid Res **42**(10): 1513-1520.
Sharma, R., C. L. Sharma, et al. (2005). "Antibacterial resistance: current problems and possible solutions." Indian J Med Sci **59**(3): 120-129.
Sulavik, M. C., C. Houseweart, et al. (2001). "Antibiotic susceptibility profiles of Escherichia coli strains lacking multidrug efflux pump genes." Antimicrob Agents Chemother **45**(4): 1126-1136.
Tenson, T., M. Lovmar, et al. (2003). "The mechanism of action of macrolides, lincosamides and streptogramin B reveals the nascent peptide exit path in the ribosome." J Mol Biol **330**(5): 1005-1014.
Tikhonova, E. B., V. Dastidar, et al. (2009). "Kinetic control of TolC recruitment by multidrug efflux complexes." Proc Natl Acad Sci U S A **106**(38): 16416-16421.
Tikhonova, E. B., V. K. Devroy, et al. (2007). "Reconstitution of the Escherichia coli macrolide transporter: the periplasmic membrane fusion protein MacA stimulates the ATPase activity of MacB." Mol Microbiol **63**(3): 895-910.
Tikhonova, E. B., Y. Yamada, et al. (2011). "Sequential mechanism of assembly of multidrug efflux pump AcrAB-TolC." Chem Biol **18**(4): 454-463.
Tikhonova, E. B. and H. I. Zgurskaya (2004). "AcrA, AcrB, and TolC of Escherichia coli Form a Stable Intermembrane Multidrug Efflux Complex." J Biol Chem **279**(31): 32116-32124.
Touze, T., J. Eswaran, et al. (2004). "Interactions underlying assembly of the Escherichia coli AcrAB-TolC multidrug efflux system." Mol Microbiol **53**(2): 697-706.
Tsukamoto, H., A. Sinha, et al. (2010). "Monomeric Rhodopsin Is the Minimal Functional Unit Required for Arrestin Binding." J Mol Biol **399**(3): 501-511.
Van Bambeke, F., E. Balzi, et al. (2000). "Antibiotic efflux pumps." Biochem Pharmacol **60**(4): 457-470.
Webber, M. A. and L. J. Piddock (2003). "The importance of efflux pumps in bacterial antibiotic resistance." J Antimicrob Chemother **51**(1): 9-11.
Weeks, J. W., T. Celaya-Kolb, et al. (2010). "AcrA suppressor alterations reverse the drug hypersensitivity phenotype of a TolC mutant by inducing TolC aperture opening." Mol Microbiol **75**(6): 1468-1483.
Whorton, M. R., M. P. Bokoch, et al. (2007). "A monomeric G protein-coupled receptor isolated in a high-density lipoprotein particle efficiently activates its G protein." Proc Natl Acad Sci U S A **104**(18): 7682-7687.
Whorton, M. R., B. Jastrzebska, et al. (2008). "Efficient coupling of transducin to monomeric rhodopsin in a phospholipid bilayer." J Biol Chem **283**(7): 4387-4394.
Xu, Y., M. Lee, et al. (2011). "Funnel-like hexameric assembly of the periplasmic adapter protein in the tripartite multidrug efflux pump in gram-negative bacteria." J Biol Chem **286**(20): 17910-17920.
Xu, Y., S. H. Sim, et al. (2009). "Crystal structure of the periplasmic region of MacB, a

noncanonic ABC transporter." Biochemistry **48**(23): 5218-5225.
Xu, Y., S. Song, et al. (2011). "Functional Implications of an Intermeshing Cogwheel-like Interaction between TolC and MacA in the Action of Macrolide-specific Efflux Pump MacAB-TolC." Journal of Biological Chemistry **286**(15): 13541-13549.
Yamanaka, H., H. Kobayashi, et al. (2008). "MacAB Is Involved in the Secretion of Escherichia coli Heat-Stable Enterotoxin II." J Bacteriol **190**(23): 7693-7698.
Yoneyama, H., A. Ocaktan, et al. (1998). "Subunit swapping in the Mex-Extrusion pumps in Pseudomonas aeruginosa." Biochem Biophys Res Commun **244**(3): 898-902.
Yum, S., Y. Xu, et al. (2009). "Crystal structure of the periplasmic component of a tripartite macrolide-specific efflux pump." J Mol Biol **387**(5): 1286-1297.
Zgurskaya, H. I., G. Krishnamoorthy, et al. (2011). "Mechanism and Function of the Outer Membrane Channel TolC in Multidrug Resistance and Physiology of Enterobacteria." Front Microbiol **2**: 189.
Zgurskaya, H. I. and H. Nikaido (1999). "AcrA is a highly asymmetric protein capable of spanning the periplasm." J Mol Biol **285**(1): 409-420.
Zgurskaya, H. I. and H. Nikaido (1999). "Bypassing the periplasm: reconstitution of the AcrAB multidrug efflux pump of Escherichia coli." Proc Natl Acad Sci U S A **96**(13): 7190-7195.
Zgurskaya, H. I. and H. Nikaido (2000). "Multidrug resistance mechanisms: drug efflux across two membranes." Mol Microbiol **37**(2): 219-225.
Zgurskaya, H. I., Y. Yamada, et al. (2009). "Structural and functional diversity of bacterial membrane fusion proteins." Biochim Biophys Acta **1794**(5): 794-807.

Appendix A. List of strains and plasmids

	Relevant genotype or description	**Source or reference**
DH5α	*supE44* D*lacU169 hsdR17 recA1 endA1 gyrA96 thi-1 relA1*	
BL21(DE3)	F⁻*ompT hsdS*$_B$(r_B^- m_B^-)*gal dcm*	Novagen
ET103	BW25113 but *ompT*::kan	(Tikhonova, Devroy et al. 2007)
ECM2112	MC4100 but ΔacrAB::*k an tolC*::*Tn10*	O. Lomovskaya
W4680AD	K-12 but Δ*acrAB* Δ*acrD*	(Tikhonova, Devroy et al. 2007)
Plasmids		
pBAD/MycHis-C	Cloning vector, Amp^r	Invitrogen
pBA^{His}	pBAD/MycHis-C carrying *macA-6His*, Amp^r	(Tikhonova, Devroy et al. 2007)
pBBHis	pBAD/MycHis-C carrying *macB-6His*, Amp^r	(Tikhonova, Devroy et al. 2007)
pBBD169N^{His}	pBB^{His} expressing MacB-6His with D169N, Amp^r	(Tikhonova, Devroy et al. 2007)
pBBC56A^{His}	pBB^{His} expressing MacB-6His with C56A, Amp^r	(Tikhonova, Devroy et al. 2007)
pBBY14C/C56A^{His}	pBB^{His} expressing MacB-6His with Y14C/C56A, Amp^r	(Tikhonova, Devroy et al. 2007)
pBBC56A/D643C^{His}	pBB^{His} expressing MacB-6His with C56A/D643C, Amp^r	(Tikhonova, Devroy et al. 2007)
pBBD643C^{His}	pBB^{His} expressing MacB-6His with D643C, Amp^r	This study
pBBLPL^{His}	pBB^{His} expressing MacB-6His lacking periplasmic loop , Amp^r	This study
pBAB^{His}	pBAD/MycHis-C carrying *macAB-6His*, Amp^r	(Tikhonova, Devroy et al. 2007)

pBABD643C^{His}	pBAB^{His} expressing MacB-6His with D643C, Amp^{r}	This study
pBABD169N^{His}	pBAB^{His} expressing MacB-6His with D169N, Amp^{r}	This study
pBABY14C/C56A^{His}	pBAB^{His} expressing MacB-6His with Y14C/C56A, Amp^{r}	This study
pBABLPL^{His}	pBAB^{His} expressing MacB-6His lacking the periplasmic loop , Amp^{r}	This study
pUC18	Cloning vector, Amp^{r}	
pUMacAB	pUC18 carrying *macAB,* Amp^{r}	(Tikhonova, Devroy et al. 2007)
pUMacABD643C	pUMacAB expressing MacB D643C mutant , Amp^{r}	This study
pUMacABY14C/C56A	pUMacAB expressing MacB Y14C/C56A mutant , Amp^{r}	This study
pUMacABD169N	pUMacAB expressing MacB D169N mutant , Amp^{r}	This study
pUMacABLPL	pUMacAB expressing MacB lacking the periplasmic loop , Amp^{r}	This study
pTolC^{His}	pTrc99A carrying *tolC-6His,* Amp^{r}	(Tikhonova and Zgurskaya 2004)
pUAΔN^{His}	pUZ11 expressing MacAΔN-6His fusion protein	(Tikhonova, Devroy et al. 2007)
pTYB11	Cloning vector, Amp^{r}	NEW ENGLAND Biolabs
pTYB-ApoA-I	pTYB11 carrying *Intein-apoA-I*, Amp^{r}	This study
pNFXex	pET20b^{+} carrying apoA-I, Amp^{r}	(Ryan, Forte et al. 2003)

Appendix B. List of primers

Primer name	Primer sequence (5' TO 3')	reference
apoA-I F	GGTGGTACTAGTGATCCGCCGCAGAG	Forward primer for amplifying *apoA-I* gene from pNFXex plasmid, with SpeI site
apoA-I R	GGTGGTGCGGCCGCCTCACTGGGTGTTAAGCTTCTTCTTAG	Reverse primer for amplifying *apoA-I* gene from pNFXex plasmid, with NotI site
MacBD643C F	ACGACTGGATCCAGTATGTGCTCTGGCACGAGAGCTCTCGTGCCAGAGCACATACTGGATCCAGTCGT	Forward primer for introducing D643C mutation into *macB* in pBBHis plasmid
MacBD643C R	CTCTCGTGCCAGAGCACATACTGTGGATCCAGTCGT	Reverse primer for introducing D643C mutation into *macB* in pBBHis plasmid
pBAD promter	CCTACCTGACGCTTTTTATCGC	Forward primer for amplifying *macB* gene in pBB^{His} palsmid
MacB LPL up	GCCAAACAAATGGTGGCGACACGTACTTTACAACTG	Reverse primer for amplifying 1-301 aa of macB in $pBBD643C^{His}$ plasmid
MacB LPL down	CAGTTGTAAAGTACGTGTCGCCAGCACCATTTGTTTGGC	Forward primer for amplifying 518-648 aa of macB in $pBBD643C^{His}$ plasmid
MacAB F	GCTAGGGTACCTACATGGGGTCGATTTC	Forward primer for amplifying *macAB* gene in pUCMacAB plasmid, with NcoI site

MacAB R	GCTAGCTGCACCTCATTGTGTACATCC	Reverse primer for amplifying *macAB* gene in pUCMacAB plasmid, with PstI site
MacBY14C F	GATATTCGTCGCAGCTGTCCTGCCGGTGATG	Forward primer for introducing Y14C mutation into *macB* in pBABHis plasmid
MacBY14C R	CATCACCGGCAGGACAGCTGCGACGAATATC	Forward primer for introducing Y14C mutation into *macB* in pBABHis plasmid